INTERACTIONS BETWEEN REACTIVE NITROGEN AND MANGANESE: IMPLICATIONS FOR MARINE NITROUS OXIDE CYCLING

A Dissertation
Presented to
The Academic Faculty

by

Amanda Rae Cavazos

In Partial Fulfillment
of the Requirements for the Degree
of PhD in the
School of Earth and Atmospheric Sciences

Georgia Institute of Technology
May 2020

INTERACTIONS BETWEEN REACTIVE NITROGEN AND MANGANESE: IMPLICATIONS FOR MARINE NITROUS OXIDE CYCLING

Approved by:

Dr. Jennifer Glass, Advisor
School of Earth & Atmospheric Sciences
Georgia Institute of Technology

Dr. Joel Kostka
School of Biological Sciences
Georgia Institute of Technology

Dr. Martial Taillefert
School of Earth & Atmospheric Sciences
Georgia Institute of Technology

Dr. Jay Brandes
Skidaway Institute of Oceanography
University of Georgia

Dr. Yuanzhi Tang
School of Earth & Atmospheric Sciences
Georgia Institute of Technology

Date Approved: March 6, 2020

This thesis is dedicated in loving memory of my best friend and lab husband,

Zachariah (Zach) Isaac Badaoui.

ACKNOWLEDGEMENTS

I would like to thank my advisor Dr. Jennifer Glass for all her guidance, mentorship, and support throughout this journey. I would also like to thank my entire thesis committee, Dr. Martial Taillefert, Dr. Yuanzhi Tang, Dr. Joel Kostka, and Dr. Jay Brandes, for all their guidance and assistance. I especially want to thank my parents and my sister for all their love and support. I also want to thank all my friends, near and far, old and new, for all their moral support along the way. Thank you to Emily Saad, Keaton Belli, Shiliang Zhao, and David Tavakoli for technical assistance during the development of Chapter 2 and Lisa Stein and Jessica Kozlowski for helpful discussion during the writing of Chapter 2. Thank you to Marcus Bray for providing *E. coli* sample, to Maxim Kolton for providing SYBR Green for experiments, and to Laura Bristow and Katharina Kitzinger for providing Gulf of Mexico samples for analysis for Chapter 3. Additionally, I want thank Nadia Szeinbaum for providing Mn^{2+}-oxidizing cultures and assistance with microbial cultivation during experimentation and to Brad Tebo for helpful discussions about Mn^{2+}-oxidizing bacteria in Chapter 3. I want to thank Lily Sandler for being an amazing undergrad mentee and for her amazing work in Chapter 4. I would also like to acknowledge my various funding sources, including the National Science Foundation Graduate Research Fellowship Program #DGE-1148903, the Goizueta Fellowship and President's Fellowship at Georgia Tech, and a Geological Society of America Graduate Research Grant.

TABLE OF CONTENTS

LIST OF TABLES

LIST OF FIGURES

LIST OF SYMBOLS AND ABBREVIATIONS

AOA	Ammonia-oxidizing archaea
AOB	Ammonia-oxidizing bacteria
Amo	Ammonia monooxygenase
ATP	Adenosine triphosphate
DIC	Dissolved inorganic carbon
FAS	Ferric ammonium sulfate
Fe	Iron
$FeNH_4$	Ferric ammonium
GC-ECD	Gas chromatography with electron-capture detector
H^+	Hydrogen proton
Hao	Hydroxylamine monooxygenase
HNO	Nitroxyl
k_{obs}	Observed rate constant
MCO	Multicopper oxidase
$Mn(III/IV)O_x$	Manganese oxides
Mn	Manganese
MnO_2	Birnessite
N	Nitrogen
N_2	Dinitrogen
Nar	Nitrate reductase
NH_3	Ammonia
NO	Nitric oxide

N_2O	Nitrous oxide
NH_2OH	Hydroxylamine
Nir(k)	Nitrite reductase
NO_2^-	Nitrite
NO_3^-	Nitrate
Nor	Nitric oxide reductase
Nos	Nitrous oxide reductase
O_2	Oxygen
OMZ	Oxygen minimum zone
R	Rate constant
ROS	Reactive oxygen species

SUMMARY

Nitrous oxide (N_2O) is a potent greenhouse gas that can destroy stratospheric ozone. Production and consumption of N_2O has long been assumed to be controlled solely by nitrogen-metabolizing microbes. It has recently been shown, however, that intermediate metabolites from these microbes can potentially leak out of cells and react with metal oxides to produce N_2O. Typically, these interactions are assumed to occur with iron (Fe) oxides. Recent studies have shown that biotic-abiotic coupling can also occur with manganese (Mn) oxides, especially when reduced by the nitrification intermediate hydroxylamine (NH_2OH). Like Fe oxides, Mn oxides are ubiquitous in sediments and at redox interfaces. Nitrous oxide production from NH_2OH oxidation occurs more rapidly with Mn oxides than with Fe oxides, yet little is known about the mechanisms or relevance of these interactions in marine systems. To better constrain the importance of nitrogenous intermediates-Mn interactions in the oceans, it is essential to characterize the spatial and temporal nature of N-Mn oxide interactions.

This dissertation aims to constrain the importance of coupled biotic/abiotic interactions between reactive nitrogenous intermediates and manganese oxides in marine systems by (1) characterizing the kinetics of NH_2OH oxidation by an environmentally-relevant Mn oxide (Ch. 2), (2) developing a rapid, readily-available, and cost-effective method to visualize associations of microbes and manganese oxide particles (Ch. 3), and (3) developing a method to more rapidly and accurately measure NH_2OH in water samples (Ch. 4).

Previous studies characterized NH_2OH oxidation by high oxidation state Mn oxides in conditions that could not be considered relevant to natural environments. My research has focused on developing rate laws and constants relevant for N_2O emission models. First, I characterized the kinetics of NH_2OH chemo-oxidation, or the abiotic oxidation of NH_2OH, by birnessite, a Mn oxide commonly found in the environment. Hydroxylamine was found to rapidly and completely chemo-oxidize to N_2O in synthetic ocean water at circumneutral pH ($6.2 < pH < 8.3$) (Ch. 2). Complete conversion of NH_2OH to N_2O occurred within 3 min in all experimental runs. The reaction was overall first order with a rate constant of 0.01 s^{-1}. I propose that N_2O is produced via a two electron transfer from NH_2OH to a Mn(IV) center, forming aminoxyl radical during the first electron transfer and nitroxyl (HNO) during the second transfer. The adsorption of HNO on the excess birnessite surface is predicted to slow the rate of HNO dimerization to N_2O, making it the rate-limiting step. Thus, the experimentally derived rate law suggests that NH_2OH chemo-oxidation could be a relevant source of marine N_2O emissions and should be included in future studies.

Building on my finding that NH_2OH chemo-oxidation completely and rapidly produces N_2O, I then developed a rapid, cost-effective, and readily available method that determines the possibility of NH_2OH chemo-oxidation occurring in natural environments. There remains uncertainty as to whether ammonia-oxidizing microbes, which produce NH_2OH, associate with Mn oxides in marine or any environments. Current methods that determine the co-localization of microbes with minerals are either not readily available, are expensive, require extensive sample preparation, or require long wait times for equipment use. In Chapter 3, I present a novel method that uses differential interference contrast (DIC)

and epifluorescent microscopy in tandem to determine the co-localization of microbes with Mn(III/IV) oxide particles on filtered environmental samples on white filters. Filters are stained with the Mn-specific stain leucoberbelin blue (LBB) to create characteristic blue haloes or imprints around Mn oxide particles followed by staining with the fluorescent nucleic acid stain SYBR Green. Mn oxide particles are imaged using DIC microscopy and cells are then imaged using a fluorescent SYBR Green (excitation: 395 nm/emission: 509 nm) light set. Manganese oxide identification and overlay of SYBR Green image is done using the image software ImageJ using color threshold and overlay functions. This method was successfully applied to laboratory and environmental samples and has the potential to be used as a rapid, cost-effective "pre-screen" to determine which samples are worth the time and money for higher resolution imaging. Thus, the significance of Mn oxides in marine biogeochemical cycles can be quickly and effectively studied.

While the role of NH_2OH in terrestrial N_2O emissions has been studied in recent years, measurements in marine systems are lacking. The difficulty of accurately measuring NH_2OH in water samples severely limits studies. Current spectrophotometric methods have detection limits that are well above concentrations in most natural waters. The most common method to measure NH_2OH is oxidation to N_2O by ferric ammonium sulfate (FAS) in acidic conditions and measurement of N_2O via gas chromatography. While this method has a detection limit that is suitable for measuring NH_2OH concentrations in natural waters (< 200 nM), the conversion of NH_2OH to N_2O is often incomplete, has a significant reaction time (≥ 3 hrs), and requires a recovery curve. Given the reaction rate and efficiency of NH_2OH oxidation to N_2O by Mn oxides, I present an alternative to this method by using a commercially available Mn oxide, pyrolusite, in place of FAS (Chapter 4). This reaction

occurs readily at circumneutral pH and goes to completion in about an hour, eliminating the need for sample acidification, reducing analysis time, and removing the need for a recovery curve.

In addition to the three core datasets in this dissertation, I conducted additional related studies on high-resolution profiles of N_2O in continental shelf sediments (App. A), abiotic oxidation of NH_3 by Mn(III) pyrophosphate (App. B), and NH_2OH oxidation by Fe(III) (App. C). In shelf sediments off Cape Hatteras, NC, N_2O peaks when O_2 is depleted and when Fe^{2+} concentrations peak, implying the possibility of chemo-denitrification. Abiotic incubations with NH_3 and soluble Mn(III) pyrophosphate did not produce N_2O, confirming a biotic source of N_2O. I measured rates of N_2O production by Fe(III) and found the reaction to be very slow compared to oxidation by Mn(III/IV).

In summary, this dissertation addresses knowledge gaps in the role that NH_2OH and Mn(III/IV)O_x play in marine N_2O emissions by providing environmentally relevant rate laws and constants for NH_2OH chemo-oxidation and methods to better characterize the biogeochemistry of NH_2OH. Using real-time kinetics, cost-effective spatial analysis via microscopy, and a new rapid measurement of NH_2OH, this dissertation presents preliminary evidence that NH_2OH chemo-oxidation is environmentally relevant in marine systems. Additionally, the methods developed in this dissertation can be used to further build our understanding of N-Mn coupled biogeochemistry in marine systems. Future studies can accurately and rapidly measure marine NH_2OH and other reactive intermediates to better constrain the biogeochemical role of coupled biotic-abiotic and N-Mn interactions.

INTRODUCTION

This chapter is based on original contributions to the review published in *Biogeochemistry* Volume 126, pg: 251-267, 2015 under the title "The importance of abiotic reactions for nitrous oxide production," by Xia Zhu-Barker, Amanda R. Cavazos, Nathaniel E. Ostrom, William R. Horwath, and Jennifer B. Glass.

1.1 Nitrogen intermediates and their implications for N_2O emissions

1.1.1 *Nitrous oxide as a greenhouse gas*

Nitrous oxide (N_2O) is a potent greenhouse gas with nearly 300 times the warming potential of carbon dioxide (IPCC, 2014) and the major source of stratospheric ozone depletion (Ravishankara et al., 2009). There is concern about anthropogenic sources and contribution to atmospheric N_2O, which has been increasing at a rate of about 0.73 ppb yr^{-1} (IPCC, 2014). Globally, present anthropogenic N_2O emissions are estimated to be 5.6-8.9 Tg N_2O-N yr^{-1} (de Vries et al., 2016) compared to 10-12 Tg N_2O-N yr^{-1} from natural sources (Davidson and Kanter, 2014). Nearly 60% of natural emissions are from unaltered terrestrial environments (Davidson and Kanter, 2014). Agriculture constitutes the majority of anthropogenic N_2O emissions (Davidson and Kanter, 2014; de Vries et al., 2016). Agricultural N_2O emissions are a result of increased inputs of reactive N via fertilizers, which are made via the Haber-Bosch process. Ammonia and nitrate (NO_3^-) from fertilizers is used by microbes in the soil and emit N_2O through different metabolisms (Section 1.2). N_2O emissions from fertilizer use is considered a "necessary evil", as it helps crops grow in areas that would normally be unable to support human populations.

Oceans contribute significant amounts of naturally produced N_2O (~2.8 Tg N_2O-N yr^{-1}; ~25-30% of natural emissions). Estimates of marine N_2O emission range from 1.7-4.4 Tg N_2O-N yr^{-1} (Ji et al., 2018). Low oxygen (O_2) zones tend to be N_2O hot spots, producing upwards of 1.3 Tg N_2O-N yr^{-1} (Babbin et al., 2015) and could account for 5-22% of marine N_2O emissions (Arévalo-Martínez et al., 2015). The large range of uncertainty in these models comes from the difficulty in constraining the production and consumption of N_2O in different oceanic conditions. Across all environments, N_2O production and consumption is typically believed to be driven solely by microbial processes.

1.2 Known biotic pathways of N_2O

1.2.1 *Denitrification*

Denitrification is the microbial process that reduces nitrate (NO_3^-) to dinitrogen gas (N_2; complete denitrification) or N_2O (incomplete denitrification) in low-O_2 environments. The first step, which reduces NO_3^- to nitrite (NO_2^-), is mediated by various nitrate reductases (Nar) can be carried out by all three domains of life (Kuyper et al., 2018). The produced NO_2^- is then reduced to nitric oxide (NO) via the nitrite reductase (Nir) enzyme, and NO is reduced to N_2O via nitric oxide reductase (Nor). The reduction of N_2O to N_2 via nitrous oxide reductase (Nos) is the main sink for N_2O and final step in classical denitrification. Numerous bacteria and archaea use Nos, which does not contribute directly to energy conservation (Kuyper et al., 2018). Nos is inhibited by O_2 at levels around 205 nM O_2 (Dalsgaard et al., 2014) and results in incomplete denitrification.

Denitrification is believed to be the main source of oceanic N_2O, particularly in oxygen minimum zones (OMZs). OMZs are characterized by waters where O_2 levels is

undetectable by conventional sensors (< 1 µM detection limit). The depth range over which O_2 rapidly declines is the oxycline, and it is where most oceanic N_2O is produced. Increased anthropogenic N inputs could expand OMZs and thus increase oceanic N_2O emissions (Babbin et al., 2015; Naqvi et al., 2000). Elucidation of the role that incomplete denitrification plays in marine N_2O turnover has been improved due to isotopic tracer studies of *in situ* incubations, but the role of other N_2O-producing microbial metabolisms remains elusive.

1.2.2 *Nitrification*

Classical nitrification is the step-wise oxidation of ammonia (NH_3) to NO_3^-. In both ammonia oxidizing bacteria (AOB) and archaea (AOA), NH_3 is oxidized to hydroxylamine (NH_2OH) via ammonia monooxygenase (Amo). In AOB, NH_2OH was long thought to be oxidized to NO_2^- in oxic conditions via hydroxylamine dehydrogenase (Hao; Hooper et al., 2004), but it was recently shown that NH_2OH is oxidized to NO instead (Caranto and Lancaster, 2017; Lancaster et al., 2018). Thereafter, NO is either abiotically oxidized to NO_2^- in oxic conditions (Ford et al., 1993), or enzymatically oxidized to NO_2^- by a proposed NO oxidoreductase (Lancaster et al., 2018). While N_2O is not an obligatory intermediate or an expected product of nitrification, N_2O has been measured in cultures of AOB (Caranto et al., 2016; Goreau et al., 1980; Hooper and Terry, 1979; Kozlowski et al., 2016b; Kozlowski et al., 2014; Stein, 2019) and AOA (Kozlowski et al., 2016b; Santoro et al., 2011; Steiglmeier et al., 2014; Stein, 2019).

The pathways for N_2O production differ in AOB and AOA. In AOB, it was initially thought that N_2O was produced when NH_2OH was oxidized by Hao and formed free

nitroxyl (HNO) as an intermediate, which then dimerized to form N_2O (Hooper and Terry, 1979). More recently, N_2O and NO were found to be produced by anaerobic oxidation of NH_2OH by cytochrome P_{460} (Caranto et al., 2016). Cytochrome P_{460} was later found to produce NO, with N_2O production occurring when NH_2OH reacts with an iron-NO enzymatic intermediate (Vilbert et al., 2018). Isotope tracing in nitrifier cultures elucidated the origin of N_2O from nitrifier cultures. The isotopic signature of N_2O from natural and laboratory studies shows that most N_2O originates from NO_2^- reduction via denitrification, not NH_2OH oxidation (Ostrom et al., 2010; Stein, 2011). Additionally, metagenomic analysis revealed that AOB encode and express the enzymes that allow them to perform nitrifier denitrification.

1.2.3 *Nitrifier denitrification*

Nitrifier denitrification is the heterotrophic oxidation of NH_3 to NO_2^-, followed by the reduction of NO_2^- to N_2O or N_2 (Wrage et al., 2001). Most cultivated AOB encode and express NirK and NorB, which reduce NO_2^- and NO to N_2O, respectively (Stein, 2019). Nitrifier denitrification becomes a significant source of N_2O when O_2 is low. In laboratory cultures of nitrifying bacteria, ^{15}N isotope tracer experiments showed that $^{15}N_2O$ was produced from nitrifier denitrification, but only in O_2 limited conditions (Poth and Focht, 1985; Sutka et al., 2006). Nitrifier denitrification by AOB can be a major source of N_2O in environments with fluctuating O_2 and NH_3 (Frame and Casciotti, 2010), such as agricultural soils (Zhu et al., 2013). In environments with lower NH_3, such as the oceans, AOA tend to contribute more to N_2O emissions (Francis et al., 2005; Hollibaugh et al., 2011; Ji and Ward, 2017; Löscher et al., 2012; Martens-Habbena et al., 2009), but the mechanism of N_2O production for AOA differs from AOB.

1.2.4 *Ammonia-oxidizing archaea nitrosation*

Unlike AOB, AOA do not possess genes for nitrifier denitrification (Hollibaugh et al., 2011; Stein, 2019). Although a NirK-like homologue has been found in AOA genomes (Walker et al., 2010), there is no evidence that AOA are capable of nitrifier denitrification. In cultures and incubations, N_2O production does not increase with decreasing O_2 concentrations (Steiglmeier et al., 2014). Additionally, isotopic analysis of N_2O produced from AOA cultures and environmental incubations show N_2O with a site preference typically seen in ammonia oxidation, not nitrifier denitrification (Santoro et al., 2011; Walker et al., 2010). Although the exact mechanism remains elusive, AOA produce N_2O when NO from NH_3 oxidation reacts with NH_2OH (nitrosation) produced by a Amo (Kozlowski et al., 2016b; Martens-Habbena et al., 2014). The coupling of biotic and abiotic interactions to produce N_2O has gained interest recently, and our understanding of how reactive intermediates play a role in these interactions has greatly improved.

1.3 Rethinking the nitrogen cycle: intermediates

Reactive nitrogenous intermediates such as NH_2OH, HNO, NO, and NO_2^- are typically present in low (nM) concentrations in natural environments due to their high reactivity and necessity in microbial metabolisms. NH_2OH and NO are obligate intermediates of nitrification react with other nitrogenous intermediates through nitrosation (Soler-Jofra et al., 2016), the process of transferring a NO^+ group from a nitrous-acid-derived compound to a nucleophilic center, or with reactive metals such as manganese (Mn) oxides (Hansel et al., 2015) to produce N_2O. While HNO was thought to be an intermediate of nitrification (Hooper and Terry, 1979), it has been shown to be an

intermediate of NH_2OH-NO nitrosation (Bonner et al., 1978). NO_2^- is the product of NH_3 oxidation and is used in NO_2^- oxidation, the last step of nitrification, and can undergo nitrosation with NH_2OH to form N_2O (Terada et al., 2017). Additionally, intermediates such as NH_2OH, NO_2^-, and NO can react with metals to produce N_2O or other nitrogenous products. Iron (Fe) was previously thought to be a major driver of these "cryptic" reactions, but reactions of N intermediates and Mn are more thermodynamically favorable (Luther, 2010).

Reactions involving NH_2OH tend to be fast, making its role in geochemical cycling difficult to constrain. Autoxidation of NH_2OH occurs rapidly, especially in the presence of copper (Anderson, 1964). The quick turnover of NH_2OH in cells and its high chemical reactivity led most to conclude that NH_2OH could not accumulate in the environment. However, cells release NH_2OH into the environment when conditions are optimal (Liu et al., 2017b) and during periods of high nitrification (Schweiger et al., 2007). It is thought that any accumulated NH_2OH will rapidly auto-oxidize in the presence of O_2. However, NH_2OH can also rapidly react with redox-active metals, such as Mn, resulting in the production of N_2O.

1.4 Manganese geochemistry and biological cycling

1.4.1 *Microbially -mediated Mn cycling*

Manganese is ubiquitous in marine environments (water column, sediments, ferromanganese nodules, hydrothermal vent plumes, fjords, to name a few) and is typically cycled among three oxidation states: II, III, and IV (Hansel, 2017; Tebo et al., 2005). The lowest oxidation state is Mn^{2+}, which is soluble and is the most dominant species in surface

marine waters (Hansel, 2017). Because the abiotic oxidation of Mn^{2+} to Mn^{3+} is kinetically slow (Luther III et al., 2018), it is assumed that microbes are the main drivers of Mn^{2+} oxidation. Additionally, Mn^{2+} oxidation to Mn^{3+} can be mediated by the bacterial production of superoxides (Learman et al., 2011a). Mn^{3+} can be bound either by organic ligands or within solid mineral phases. The highest oxidation state of Mn in nature is Mn(IV), which is insoluble and precipitates as oxide minerals, usually with Mn^{3+} ($Mn(III/IV)O_x$). $Mn(III/IV)O_x$ minerals are reduced by certain microbes back to Mn^{2+} through a two electron transfer, providing energy if environmental conditions are favorable.

1.4.2 *Microbial manganese cycling for energy generation*

Reduction of $Mn(III/IV)O_x$ is thermodynamically favorable and yields more energy than iron or sulphate reduction. The high energy yield makes reduction of $Mn(III/IV)O_x$ an important electron acceptor for carbon oxidation in anoxic, Mn-rich coastal sediments, attributing between 25-99% of carbon oxidation (Aller, 1990; Canfield et al., 1993a; Canfield et al., 1993b; Nickel et al., 2008; Thamdrup et al., 2000; Vandieken et al., 2014). Mn-reducing microbes have also been shown to couple organic-bound Mn(III) reduction to the oxidation of organic carbon (Hui et al., 2012; Kostka et al., 1995). Microbes capable of Mn reduction are found within delta-, epsilon-, and gamma-proteobacteria and can usually use various electron acceptors (Burdige and Nealson, 1986; Hui et al., 2012; Kostka et al., 1995; Lovley et al., 1993; Lovley and Phillips, 1988; Lovley et al., 1989; Myers and Nealson, 1988; Nealson et al., 1991; Thamdrup, 2000; Vandieken et al., 2014). Microbes use various methods to extracellularly reduce $Mn(III/IV)O_x$, many of which are similar to those that are used to reduce Fe oxides (Boone et al., 1995; Burdige and Nealson, 1986;

DiChristina, 1992; Lovley et al., 2004; Myers and Nealson, 1988; Nealson and Saffarini, 1994). Mn reduction is proposed to be a "side reaction" of some fermentative metabolisms, serving as an electron sink instead of a source of energy (Lovley, 1991).

Mn oxidation in marine environments has been attributed to Mn^{2+}-oxidizing bacteria and fungi; it is currently unknown if any archaea oxidize Mn^{2+}. Like microbial Mn(III/IV) reduction, microbial Mn oxidation requires two one-electron transfers, with Mn^{3+} as an intermediate (Luther, 2010; Luther III, 2005; Webb et al., 2005a). ATP synthesis is believed to occur during the second electron transfer, as the activation energy for the oxidation of Mn^{2+} to Mn^{3+} is too high for ATP synthesis (Ehrlich and Newman, 2008). ATP synthesis from Mn oxidation has been shown in two marine gammaproteobacteria: *Pseudoalteromonas* sp. SSW_{22} (Ehrlich, 1983; Ehrlich and Salerno, 1990) and *Alteromonas* sp. BIII45 (Ehrlich, 1976), but despite extensive studies, the biochemical mechanism remains unclear.

1.4.3 *Non-energy generating manganese cycling*

Numerous microbes oxidize Mn^{2+} without gaining energy, using biotic and abiotic processes that produce $Mn(III/IV)O_x$ (Hansel and Learman, 2015; Tebo et al., 2005). Multicopper oxidases (MCO) are the primary enzymes linked to non-energy generating Mn oxidation, and recently animal haem peroxidases and genes involved in a variety of cellular functions (Andeer et al., 2015; Anderson et al., 2009; Brouwers et al., 2000a; Brouwers et al., 1999; Brouwers et al., 2000b; Corstjens et al., 1997; de Vrind et al., 1998; de Vrind et al., 2003; Tebo et al., 2005; Van Waasbergen et al., 1996). Fungal laccases are similar to MCO and have been linked to Mn^{2+} oxidation to Mn^{3+} and even to $Mn(III/IV)O_x$

in some studies (Hofer and Schlosser, 1999; Miyata et al., 2006a; Miyata et al., 2004; Miyata et al., 2006b; Schleper and Hofer, 2002). Another mechanism of non-energetic Mn oxidation is by extracellular reactive oxygen species (ROS; Hansel et al., 2015; Sutherland et al., 2018), which is thermodynamically more favorable than oxidation by O_2 in conditions of most marine waters (Hansard et al., 2011). ROS are produced via aerobic respiration, and superoxide can be released from microbial cells to oxidize Mn^{2+} (Hansel et al., 2015; Rose, 2012). Mn can also be cycled indirectly via other energy generating microbial processes, including through nitrogenous metabolisms.

Mn cycling can be coupled to both nitrification and denitrification. The oxidation of NH_3 to N_2 by Mn(III/IV)O_x (Eq. 1) is thermodynamically favorable from pH 1-14 (Luther et al., 1997). Ammonia can be oxidized to NO_3^- by Mn(III/IV)O_x reduction (Eq. 2), but not at pH > 7.9 (Luther et al., 1997).

$$2\ NH_3 + 3\ MnO_2 + 6\ H^+ \rightarrow 3\ Mn^{2+} + N_2 + 6\ H_2O \quad (1)$$

$$NH_3 + 4\ MnO_2 + 7\ H^+ \rightarrow 4\ Mn^{2+} + NO_3^- + 5\ H_2O \quad (2)$$

Nitrification coupled to Mn(III/IV)O_x reduction has been observed in marine sediments (Fernandes et al., 2015; Hulth et al., 1999; Javanaud et al., 2011; Lin and Taillefert, 2014; Luther et al., 1997). Incubations amended with Mn(III/IV)O_x showed an increase in anaerobic nitrification rates and increased production of N_2 and N_2O (Fernandes et al., 2015). However, coupled nitrification/Mn reduction does not occur in all Mn-rich marine

sediments (Thamdrup and Dalsgaard, 2000). The exact mechanism or microbes that utilize this redox couple have yet to be elucidated.

Denitrification coupled to Mn oxidation is thermodynamically feasible at higher pH (Luther et al., 1997), but direct evidence in nature is still lacking. A few studies have hinted at Mn-coupled denitrification (Luther et al., 1997; Mogollón et al., 2016), but it is predicted to occur in anoxic marine sediments that are organic carbon-limited and Mn-rich (Mogollón et al., 2016).

1.4.4 *Environments that support coupled manganese-nitrogen cycling*

Manganese is ubiquitous in nature and potentially contributes to nitrogen cycling in a variety of environments. In agricultural soils where fertilizer is added in abundance, Mn is present in both oxidized and reduced forms. Agricultural soils represent major sources of anthropogenic N_2O, and Mn plays a role in its production through coupled biotic and abiotic interactions (Bremmer, 1997; Heil et al., 2016). Coastal sediments, estuaries, and bays are also prone to increased N inputs from anthropogenic sources (Naqvi et al., 2000) and Mn-transforming microbes have been isolated from these environments (Bräuer et al., 2011; Cowen and Silver, 1984; Hansel and Francis, 2006; Krumbein, 1971; Moffett, 1997; Tebo and Emerson, 1985; Tebo et al., 1984; Thamdrup, 2000; Thiel, 1925; Vandieken et al., 2014).

Ferromanganese nodules form in deep-sea sediments, presumably formed by Mn-oxidizing microbes (Nitahara et al., 2011; Nitahara et al., 2017; Shiraishi et al., 2016; Tully and Heidelberg, 2013). Interestingly, AOA have been found on ferromanganese nodules (Nitahara et al., 2011; Nitahara et al., 2017; Shiraishi et al., 2016; Wang et al., 2012). AOA

presumably take advantage of the low NH_3 concentrations and accumulated copper, but whether AOA play a role in ferromanganese nodule formation via Mn metabolisms is unknown. Mn-N coupled cycling was thought to be driven strictly by enzymatic processes, but interactions of Mn with reactive N intermediates has gained interest.

1.5 Biotic-abiotic couplings in nitrogen-manganese cycling

Coupling of N-Mn cycling was originally thought to only occur for ATP generation. Nitrogenous intermediates such as NH_2OH and NO_2^- reacting with Fe^{3+} and Fe^{2+} to produce N_2O and NO, respectively, have been studied extensively (Bengtsson, 1973; Bengtsson et al., 2002; Buchwald et al., 2016; Butler and Gordon, 1986; Grabb et al., 2016; Kampschreur et al., 2011; Moraghan and Buresh, 1977; Rue et al., 2018; Soni and Mehrotra, 2003; Zhu-Barker et al., 2015). N-Fe coupled interactions occur when nitrogenous intermediates leak out of microbial cells and accumulate in the environment, generally not contributing to ATP generation. Although N-Fe interactions are thermodynamically favorable, they tend to be kinetically slow (App. C), with reaction rates ranging from hours to more than a week. Additionally, N-Fe interactions occur more rapidly in acidic conditions not representative of oceanic conditions.

Hydroxylamine oxidation by Mn(III/IV) is thermodynamically favorable in circumneutral pH (Eq. 3).

$$2\ NH_2OH + 2\ MnO_2 + 4\ H^+ \rightarrow N_2O + 2\ Mn^{2+} + 5\ H_2O,\ \Delta G^{\circ\prime} = -106.2\ \text{kJ mol e}^{-1} \quad (3)$$

Previous studies have characterized the kinetics of NH_2OH oxidation by various forms of Mn(III/IV), mostly bound by organic compounds in acidic solutions or ultra-pure water

(Banerjee et al., 2002; Davies and Kustin, 1969; Hynes et al., 1993; Salem, 1995). Compared to NH_2OH oxidation to N_2O by Fe^{3+}, oxidation by $Mn(III/IV)O_x$ (chemo-oxidation) is kinetically faster. The fastest rate of NH_2OH chemo-oxidation observed occurred within milliseconds by using Mn(III) in an acidic perchlorate solution (Davies and Kustin, 1969). In deionized water, $Mn(III/IV)O_x$ oxidizes NH_2OH more rapidly than Fe oxides (Rue et al., 2018), suggesting the importance of NH_2OH chemo-oxidation in natural environments.

In soils, it was originally proposed that N_2O originated from microbial nitrification and denitrification. However, recent studies have shown that N_2O emissions are linked to soil NH_2OH and $Mn(III/IV)O_x$ content (Heil et al., 2015; Liu et al., 2017a; Liu et al., 2016). This correlation was further supported when AOB and AOA were shown to leak NH_2OH from their membranes and contribute to N_2O emission (Liu et al., 2017b). Organic matter content in soil was found to decrease N_2O production from NH_2OH chemo-oxidation by forming oximes with NH_2OH (Bremmer et al., 1980; Heil et al., 2015; Liu et al., 2017a). In cropland soils, NH_2OH chemo-oxidation occurred in about 5 min with approximately 50% conversion (Heil et al., 2015), suggesting that NH_2OH chemo-oxidation could play a significant role in N_2O emissions in other environments.

The importance of NH_2OH chemo-oxidation has yet to be assessed in marine systems, especially where NH_3 oxidizing microbes and $Mn(III/IV)O_x$ possibly associate. Estuary and coastal sediments experience high influxes of both NH_3 (Bernhard et al., 2010) and $Mn(III/IV)O_x$. In OMZs, AOA and $Mn(IIIIV)O_x$ tend to accumulate at oxyclines (Anschutz et al., 2005; Lian and Hunter, 1986; Overnell et al., 2002; Trefry et al., 1984). In deep-sea sediments, AOA have been observed on ferromanganese nodules surfaces

(Nitahara et al., 2011; Nitahara et al., 2017; Shiraishi et al., 2016; Tully and Heidelberg, 2013). Despite the numerous places where NH_2OH chemo-oxidation occurs, little is known about its contribution to global N_2O emissions.

1.6 Research scopes and objectives

This dissertation aims to better constrain the mechanism and relevance of NH_2OH chemo-oxidation by Mn(III/IV)O_x in N_2O production from seawater using geochemical kinetics, light and fluorescent microscopy, and improvement of NH_2OH analyses. Chapter 2 details the chemical kinetics of N_2O production via NH_2OH chemo-oxidation by birnessite (MnO_2), an ubiquitous Mn(III/IV)O_x similar to that produced by microbes. The calculated rate law and constant can be applied to global oceanic models to better predict marine N_2O emissions. Chapter 3 presents a cost-effective, rapid, and readily-available method to roughly estimate microbes and Mn(III/IV)O_x on filters using differential interference contrast (DIC) and fluorescent microscopy in tandem. By using fluorescent nucleic and Mn-specific dyes, acquired images can be used to determine which samples would be worth analysing using more powerful geochemical and co-localisation methods. Finally, Chapter 4 presents an improvement on a method that is widely used for measuring NH_2OH in aquatic samples. Because NH_2OH oxidation by Mn(III/IV)O_x is kinetically rapid, I adjusted the method that originally used Fe and replaced it with pyrolusite, a commercially-available Mn(III/IV)O_x mineral. This improvement removes the need for sample acidification, and the acquisition of a recovery curve, and therefore reduces sample processing time. Finally, in Appendices A, B, and C, I produced high-resolution profiles of N_2O in continental shelf sediments, showed that NH_3 cannot be oxidized to N_2O by

Mn(III) pyrophosphate, and that N_2O production by Fe(III) is significantly slower than by Mn(III/IV)O_x.

KINETICS OF NITROUS OXIDE PRODUCTION FROM HYDROXYLAMINE OXIDATION BY BIRNESSITE IN SEAWATER

This work was published in *Marine Chemistry* Volume 202, pg: 49-57, 2018 under the same title, by Amanda R. Cavazos, Martial Taillefert, Yuanzi Tang, and Jennifer Glass.

1.7 Abstract

This study characterized the kinetics of abiotic production of the greenhouse gas nitrous oxide (N_2O) by chemical oxidation of the nitrification intermediate hydroxylamine (NH_2OH) in seawater at circumneutral pH (6.2-8.3). The oxidant was birnessite, a ubiquitous manganese oxide mineral in a variety of marine environments. Experiments using microsensor electrodes for high-resolution measurements of N_2O production combined with the simultaneous measurements of the removal of NH_2OH using spectrophotometric techniques revealed that the reaction was overall first order with the rate law $d[N_2O]/dt = k[NH_2OH]^{0.9}[MnO_2]^{0.3}[H^+]^0$ where k is 0.01 s^{-1}. Birnessite consistently oxidized 80-100% of NH_2OH to N_2O within 3 minutes. Mass balance on nitrogen indicated rapid formation and disappearance of an intermediate species that was evidently involved in the formation of N_2O. In the presence of a nitroxyl (HNO) scavenger, N_2O production rates and yield were suppressed by 17–59% and ~50%, respectively, suggesting that HNO is an intermediate in NH_2OH oxidation to N_2O. These results support a mechanism wherein Mn(IV) is reduced to Mn(III) with the formation of an aminoxyl radical as the first product of NH_2OH oxidation, which donates a second electron to another Mn(IV) center or reduces

the same Mn(III) to release Mn^{2+} and HNO in solution. The final step is predicted to be HNO dimerization to N_2O given the complete oxidation of NH_2OH to N_2O at steady-state. The experimentally-derived second-order rate constant for the dimerization step suggests that adsorption of HNO onto the excess solid surface controls the rate of N_2O formation. Our findings suggest that abiotic NH_2OH oxidation could be an important source of N_2O in coastal ecosystems such as open oceans and oxygen minimum zones as well as sediment ecosystems wherever nitrification occurs in the presence of particulate metal oxides.

1.8 Introduction

Nitrous oxide (N_2O) is a potent greenhouse gas with over 250 times the warming potential of carbon dioxide per 100 year timescale (IPCC, 2014). Bacterial nitrification ($NH_4^+ \rightarrow NH_2OH \rightarrow NO \rightarrow N_2O$), denitrification ($NO_3^- \rightarrow NO_2^- \rightarrow NO \rightarrow N_2O \rightarrow N_2$), and nitrifier denitrification ($NH_4^+ \rightarrow NH_2OH \rightarrow NO \rightarrow NO_2^- \rightarrow NO \rightarrow N_2O$) all contribute to global N_2O emissions (Caranto and Lancaster, 2017; Stein, 2011), while archaeal nitrification may be an important source of N_2O from the oceans (Santoro et al., 2011).

Recent studies have challenged the assumption that N_2O is produced purely by enzymatic pathways, and highlighted the importance of understanding the mechanisms of coupled biotic-abiotic interactions between redox-active nitrogen and metal species (Kozlowski et al., 2016b; Liu et al., 2017a; Luther et al., 1997; Zhu-Barker et al., 2015). One such reaction is hydroxylamine (NH_2OH) oxidation coupled to the reduction of manganese (Mn) oxides such as $Mn(IV)O_2$ (Eq. 3). Hydroxylamine is an intermediate product of both aerobic and anaerobic microbial NH_3 oxidation (Kartal et al., 2011; Oshiki et al., 2016; Vajrala et al., 2013; Yoshida and Alexander, 1964). Birnessite $(Mn(III, IV))O_2$,

hereafter referred to as MnO_2, is a ubiquitous Mn oxide mineral with a layered structure composed of MnO_6 octahedral sheets (Potter and Rossman, 1979) and high redox potential (1.2 V; Zhou et al., 2006), and is capable of oxidizing a wide range of organic and inorganic species (Feng et al., 2015; Remucal and Ginder-Vogel, 2014).

Although NH_2OH oxidation by MnO_2 has been shown to contribute significantly to N_2O emissions in terrestrial soils (Heil et al., 2015), this pathway has not been characterized in marine environments, which contributes to ~1/4 of global N_2O emissions (Davidson et al., 2013). Because Eq. (3) is thermodynamically favorable across a wide pH range (Luther, 2010), it may occur when NH_2OH leaked from nitrifying and anammox microbes encounter marine Mn oxides, such as in marine flocs suspended above oxyclines (Nameroff et al., 2002), at seawater-sediment interfaces (Lin and Taillefert, 2014; Luther et al., 1997), and in ferromanganese nodules in deep sea sediments (Mallik, 1980; Shiraishi et al., 2016). In this study, we characterized the kinetics of NH_2OH oxidation by birnessite in synthetic seawater at circumneutral pH as a first step towards understanding the importance of abiotic N_2O production in marine ecosystems.

1.9 Methods

1.9.1 *Synthetic ocean water preparation*

All chemicals used in the experiments were ACS grade or higher. All experiments were performed at pH above the pK_a of NH_2OH (5.9) to ensure that NH_2OH was present in its unprotonated form. All glass and plastic ware were acid washed in 1.2 N HCl. Synthetic ocean water (SOW) was prepared according to Morel et al. (1979). Nitrogen and trace

metal salts were excluded from the SOW, and pH was adjusted to 7.8 with KCl or KOH for all experiments except the variable pH experiments (see below).

1.9.2 *Birnessite synthesis and characterization*

Birnessite (MnO_2) was prepared according to Villalobos et al. (2003) and was equilibrated in SOW for 2–4 days prior to reaction with NH_2OH (Bargar et al., 2005; Webb et al., 2005b). A portion of the MnO_2 suspension was air-dried, finely ground, and analyzed by X-ray diffraction (XRD) using a PANalytical Empyrean diffractometer with Cu Kα source (initial scan range 10–85° with 0.0130 step size and 44.4 s step time), which confirmed the birnessite phase (**Fig. 1**). The concentration of Mn(III, IV) in the MnO_2-amended SOW (see below) was measured by the leucoberbelin blue colorimetric method (Krumbein and Altmann, 1973) on an UV-Vis spectrophotometer (Genesys 20, Thermo Fischer Scientific).

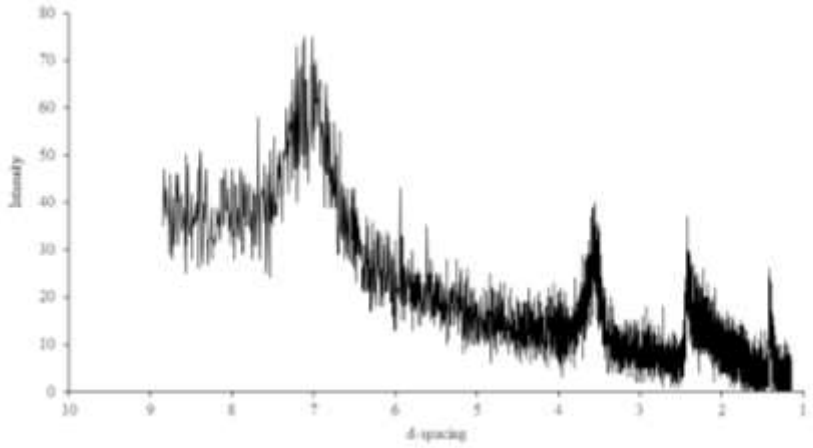

Figure 1. X-ray diffraction pattern of synthesized acid birnessite used in experiments. The characteristic peak of birnessite is observed at 7 Å.

1.9.3 *N_2O production measurement by microelectrode*

Nitrous oxide production was measured with a N_2O microsensor electrode and multimeter (Unisense, Aarhus, Denmark; 1 µM detection limit) while the solution was continuously stirred in 4.5 mL microrespiration chambers with lid ports. The microsensor was calibrated according to the manufacturer's protocol in N_2O saturated solution in SOW (22 mM, using solubility constants from Weiss and Price (1980)) with MnO_2 concentrations corresponding to those in the experiments to correct for potential background noise due to particulates. All experiments were conducted in duplicate. Because NH_2OH is highly reactive, all NH_2OH solutions (as $NH_2OH{\cdot}HCl$, Sigma-Aldrich) were prepared in SOW within 10 min of use. Experiments were initiated by injecting NH_2OH solution into the microrespiration chamber containing SOW with varied concentrations of MnO_2. Nitrous oxide concentrations were quantified every second for ~3 minutes. The isolation method was used to determine the order of the reaction with respect to each reactant, and all experiments were performed in the presence of excess oxidant (MnO_2; 300-1000µM). Initial rates were determined by calculating the slope of N_2O production over the first minute of the reaction using the least squares fit in MatLab (R2015a).

To test whether nitroxyl (HNO) was a reaction intermediate for Eq. (3), we performed another set of experiments in which the HNO scavenger N-acetyl-L-cysteine (Sigma-Aldrich) was added to the microrespiration chamber at 300-900 µM (~3× the NH_2OH concentration). Despite its reactivity towards the NO_2 radical and peroxynitrite, N-acetyl-L-cysteine is typically regarded as an effective HNO scavenger. N-acetyl-L-cysteine donates a thiol group (RSH) to HNO to form a thiol-bound HNO adduct (Samuni et al.,

2013), effectively preventing dimerization to N_2O, though N-acetyl-L-cysteine may also react with the adduct to form NH_2OH as by-product and ultimately enhance formation of N_2O (Samuni et al., 2013). We also performed control experiments with NH_4^+ in place of NH_2OH to determine if N_2O was produced from oxidation of NH_4^+, a possible NH_2OH decomposition product.

1.9.4 *NH_2OH consumption measurement by spectrophotometry*

A parallel set of experiments were performed in 2 mL Eppendorf tubes to quantify NH_2OH consumption and potential production of other dissolved N species. Hydroxylamine (100 µM) was added to SOW containing 0, 300, or 1000 µM MnO_2. Samples were collected every 5-30 s for 3 min and filtered through 0.45 µm cellulose acetate syringe filters (VWR International). Nitrate (NO_3^-) and nitrite (NO_2^-) concentrations were analyzed using the modified Griess method (García-Rodledo et al., 2014). Measurement of NH_4^+ by the phenol hypochlorite method (Solórzano, 1969) was infeasible due the NH_2OH interference (Riley, 1953).

A variety of NH_2OH spectrophotometric analyses were tested to determine the optimal procedure for our experimental conditions. When used with SOW, the reagents in the quinolinol method developed by Frear and Burrell (1955) formed a thick, cloudy precipitate, preventing further use. Instead, we optimized the iodine method, originally described by Fiadeiro et al. (1967) and improved in Strickland and Parsons (1972), for use in small volumes of SOW. Specifically, 1 mL sample was placed in a 2 mL Eppendorf tube, and 40 µL of sulphanilic acid and 20 µL iodine solution were added and allowed to react for 3 min. Then, 20 µL of a sodium arsenite solution was added and allowed to react

for 2 min. Finally, 20 µL of N-(1-Napthyl)-ethylenediamine was added, color was allowed to develop for 15 min, and the absorbance at 543 nm was read by an UV-vis spectrophotometer. Calibration curves were made using filtered MnO_2 solutions in SOW with a 0.45 µm cellulose acetate syringe filter to account for possible interferences from Mn.

1.10 Results

1.10.1 *Mass balance*

To determine the percent of NH_2OH oxidized to N_2O as a function of MnO_2 concentration, we quantified the consumption of NH_2OH (initial concentration 100 µM) and production of N_2O at pH 7.8. No detectable NH_2OH consumption, and no more than 6 µM N_2O (10% yield) production was observed in the absence of MnO_2 (**Fig. 2a**). In the presence of MnO_2, ≥50% NH_2OH was consumed within 5 s of NH_2OH addition, and 97-100% NH_2OH was consumed within 210 s exhibiting a pseudo-first order decay with a half-life of 20-25 s (**Fig. 2b-f**; **Table 1**). NO_x^- production was minimal in all experiments (<5 µM; data not shown). Mass balance indicates that an unknown intermediate species is produced initially, but then consumed over time (**Fig. 2b-f**). After accounting for the 2:1 substrate-to-product ratio, we found that 89–100% of NH_2OH was converted to N_2O at steady-state (**Table 1**), and that N_2O yield from NH_2OH was inversely proportional to the initial NH_2OH concentration (**Table 1, 2**). When HNO scavenger N-acetyl-L-cysteine was added, N_2O production rates decreased by 17–59% (**Fig. 3**) while N_2O production yields decreased by 41–52% (not shown). Minimal N_2O was produced when NH_2OH was replaced with NH_4^+ (**Fig. 3**).

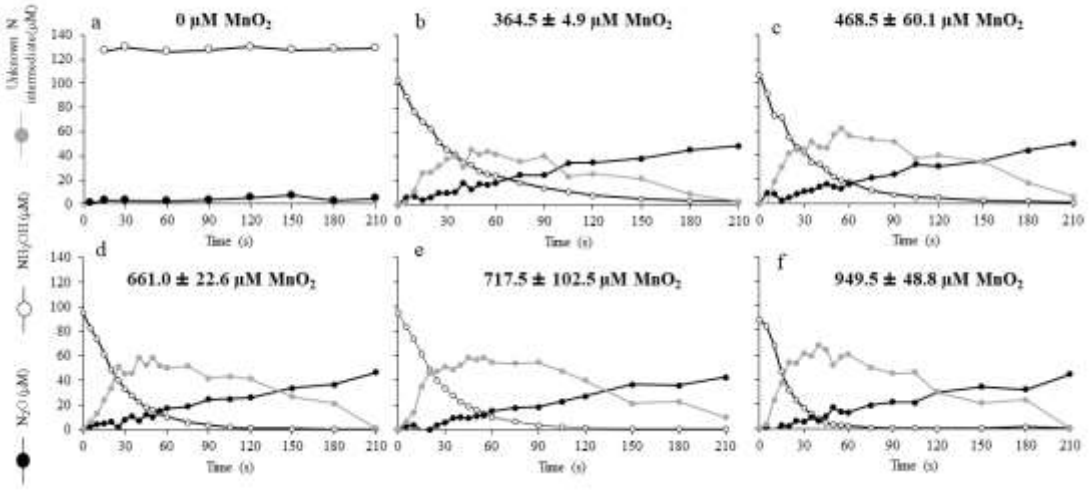

Figure 2. Complete conversion of NH_2OH to N_2O in various experiments. Mass balance conserved between NH_2OH and N_2O from experiments conducted with 100 µM NH_2OH with (a) 0 µM, (b) 364.5 ± 4.9 µM, (c) 468.5 ± 60.1 µM, (d) 661.0 ± 22.6 µM, (e) 717.5 ± 102.5 µM, and (f) 949.5 ± 48.8 µM MnO_2 at pH 7.8. Conversion to N_2O ranged from 89-100%. Symbols represent N species: black, N_2O; white, NH_2OH; gray, unknown N intermediate.

Table 1. Mass balance between NH_2OH and N_2O from the varied MnO_2 experiments. All values represent an average value (n=2).

$[MnO_2]$ (µM)	$[NH_2OH°]$ (µM)	$[NH_2OH_f]$ (µM)	$[N_2O]$ (µM)	% NH_2OH consumption	% NH_2OH conversion to N_2O
364.5 ± 4.9	103.0 ± 16.7	2.6 ± 1.0	48.8 ± 5.4	97.5	97.2
468.5 ± 60.1	107.3 ± 1.7	0.8 ± 0.2	50.2 ± 0.2	99.3	94.3
661.0 ± 22.6	95.5	0.4 ± 0.2	46.9 ± 9.1	99.6	98.6
717.5 ± 102.5	95.5	0.4 ± 0.2	42.5 ± 6.5	99.6	89.4
949.5 ± 48.8	88.6 ± 1.7	0.3 ± 0.3	44.0 ± 13.1	99.7	99.7

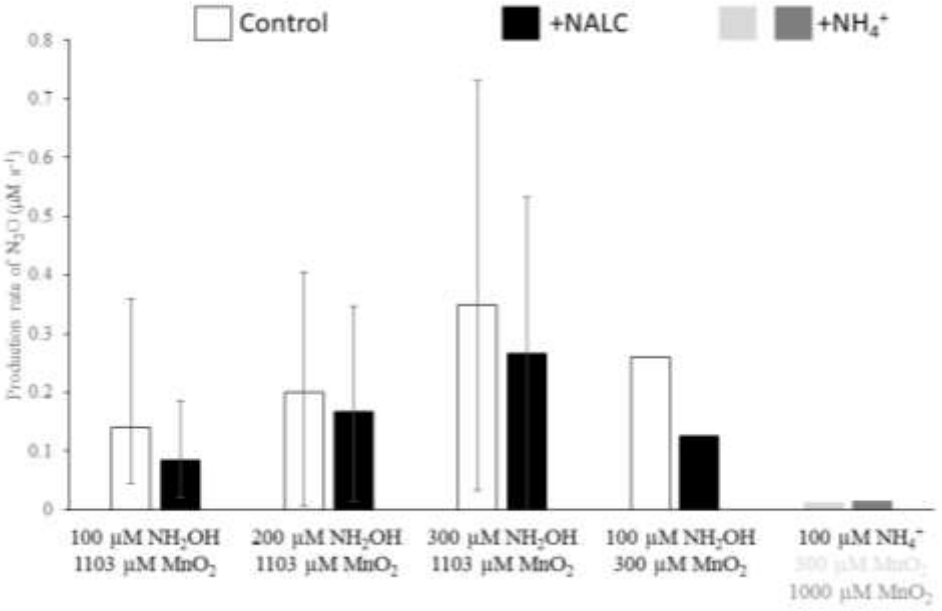

Figure 3. Addition of N-acetyl-L-cysteine decreases N_2O production rates with no noticeable production from NH_4^+. Nitrous oxide production rates decrease with 300-900 µM N-acetyl-L-cysteine addition (3× NH_2OH concentration) at pH 7.8. Error bars, when present, show range of data (n=2, except for 100 µM NH_2OH into 1103 µM MnO_2 where n=3). No error bars represent single experiments (n=1).

Table 2. Nitrous oxide production rates, rate constants, *k* values, and maximum N_2O yield of each experimental condition for each duplicate. Rate constant is first order.

[MnO_2] ($\times10^{-6}$ M)	[NH_2OH] ($\times10^{-6}$ M)	pH	Rate$_{N2O}$ (D1) ($\times10^{-7}$ M s^{-1})	Rate$_{N2O}$ (D2) ($\times10^{-7}$ M s^{-1})	k_{N2O} (D1) ($\times10^{-3}$ s^{-1})	k_{N2O} (D2) ($\times10^{-3}$ s^{-1})	Rate$_{NH2OH}$ (D1) ($\times10^{-7}$ M s^{-1})	Rate$_{NH2OH}$ (D2) ($\times10^{-7}$ M s^{-1})	k_{NH2OH} (D1) ($\times10^{-3}$ s^{-1})	k_{NH2OH} (D2) ($\times10^{-3}$ s^{-1})	Mean yield (%)
790	100	7.8	2.40	2.02	8.14	6.85					91.3
	150		3.21	3.08	7.57	7.25					82.5
	200		3.58	3.86	6.52	7.03					80.4
	250		4.96	5.26	7.38	7.82					80.1
	300		6.05	6.08	7.64	7.68					79.7
					7.45 ± 0.59	**7.33 ± 0.42**					
361	100	7.8	2.20	2.40	9.45	10.3	3.34	4.65	13.9	19.3	100
414			1.95	2.35	8.02	9.70	3.59	4.49	13.0	16.3	92.1
426			2.06	2.43	8.43	9.94	2.87	4.21	10.8	15.8	96.9
677			1.92	2.11	6.82	7.39	2.84	3.17	10.1	11.2	90.5
915			1.76	2.16	5.71	7.01	2.55	2.51	9.1	9.0	92.7
					7.69 ± 1.45	**8.89 ± 1.52**					
300	100	6.2	2.14	2.21	10.1	10.5					100
		6.7	1.99	2.33	9.13	10.7					100
		7.0	2.36	2.26	10.9	10.5					96.9
		7.8	2.18	2.45	9.73	10.9					100
		8.3	2.59	2.28	11.3	9.94					100
					10.2 ± 0.87	**10.5 ± 0.37**					
					8.68 ± 1.60				**12.9 ± 3.5**		

1.10.2 *Kinetic experiments to determine the overall order of the reaction and the rate constant*

To determine the overall order and rate constant of the reaction, a general rate law for NH_2OH oxidation by MnO_2 was developed:

$$\frac{d[NH_2OH]}{dt} = -k[NH_2OH]^a[MnO_2]^b[H^+]^c \quad (4)$$

Where *a, b,* and *c* represent the order of the reaction with respect to each reactant, and *k* is the rate constant.

1.10.2.1 *Order with respect to NH_2OH*

To determine the order with respect to NH_2OH, the isolation method was used, in which initial NH_2OH concentrations were varied while MnO_2 and pH were kept constant, such that Eq. (4) can be rearranged to give:

$$\frac{d[NH_2OH]}{dt} = -k_{obs}[NH_2OH]^a \quad (5)$$

$$where\ k_{obs} = k[MnO_2]^b[H^+]^c \quad (6)$$

If the unknown intermediate species is rapidly produced and consumed, the steady-state hypothesis can be used to relate the rate of NH_2OH consumption to the rate of N_2O production measured by the microsensor such that Eq. 5 becomes:

$$-\frac{d[NH_2OH]}{dt} = 2\frac{d[N_2O]}{dt} = R = k_{obs}[NH_2OH]^a \quad (7)$$

where R is twice the rate of N_2O production. As the rate of N_2O production was linear over most of the reaction (**Fig. 4a**), it was possible to use the initial rate method to obtain *a* after rearranging Eq. 7 to:

$$\log(R) = \log(k_{obs}) + a \times \log([NH_2OH^\circ]) \quad (8)$$

where *$[NH_2OH^\circ]$* is the initial concentration of NH_2OH.

We found that initial N_2O production rates increased linearly with increasing NH_2OH concentration (**Fig. 4a**). The slope of Eq. 8 gives *a*, the order of reaction with respect to NH_2OH, which was found to be first order (a = 0.9 ± 0.07; **Fig. 5a).**

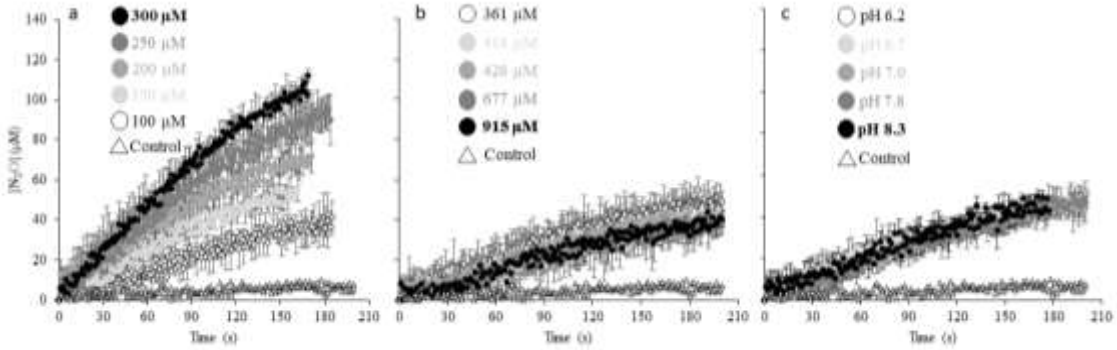

Figure 4. Nitrous oxide production as a function of NH_2OH, MnO_2, and pH. Averaged N_2O production rate from (a) varied initial NH_2OH concentrations into 790 µM MnO_2 at pH 7.8 ± 0.1, (b) 100 µM NH_2OH into varied initial MnO_2 concentrations at pH 7.8 ± 0.1, and (c) 100 µM NH_2OH into 300 µM MnO_2 at varied pH. The control (open triangles) represents 100 µM NH_2OH into SOW with no MnO_2. Slope and standard error of the averaged best fit line (n=2) are shown below varied parameters.

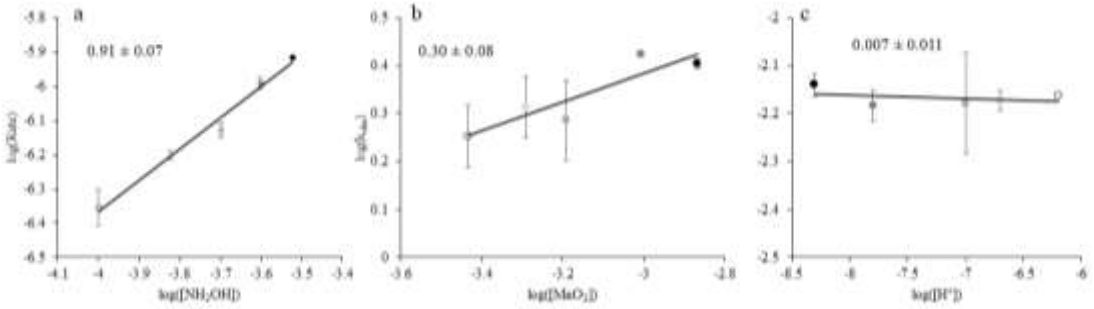

Figure 5. Hydroxylamine oxidation is first order with respect to NH_2OH. Order of reaction with respect to (a) NH_2OH, (b) MnO_2, and (c) pH. Data points represent the average of the duplicates and error bars represent standard deviation between the duplicates. Calculations of k_{obs} are described in section 2.4.2.1 of the text.

1.10.2.2 *Order with respect to MnO_2*

To determine the order of the reaction with respect to MnO_2, experiments were performed by injecting 100 µM NH_2OH into 361, 414, 426, 677, and 915 µM MnO_2 at pH 7.8 and monitoring NH_2OH concentrations as a function of time (**Fig. 2b-f**). Because the order of the reaction with respect to NH_2OH was ~1 (**Fig. 5a**), Eq. 5 can be rearranged to:

$$\frac{d[NH_2OH]}{dt} = k_{obs}[NH_2OH] \quad (9)$$

$$where\ k_{obs} = k[MnO_2]^b[H^+]^c \quad (10)$$

In this case, the initial rate method was used to calculate the k_{obs} from Eq. 9 for each experiment. The order of the reaction, *b*, was then determined from the linearized form of Eq. 10 by representing log k_{obs} at each concentration of MnO_2 as a function of the initial concentration of MnO_2 at fixed pH:

$$\log(k_{obs}) = log(k[H^+]^c) + b \times log[MnO_2] \quad (11)$$

Using this approach, a slope equal to the order of reaction with respect to MnO_2, *b* of 0.3 ± 0.08 was found (**Fig. 5b**).

1.10.2.3 *Order with respect to proton concentration*

To determine the order of reaction with respect to the proton concentration, experiments were carried out by injecting 100 µM NH_2OH into 300 µM MnO_2 at pH 6.2, 6.7, 7.0, 7.8, and 8.3, and monitoring N_2O concentrations as a function of time (**Fig. 4c**). The same method used for determining the order of reaction with respect to MnO_2 was used for determining the order of reaction with respect to the proton concentration. The

slope of the initial rate of N_2O production represented as a function of the initial concentration of NH_2OH (Eq. 9) was used to calculate the pseudo-first order rate constant (k_{obs}) at each pH. The order of the reaction with respect to proton concentration, *c*, was then determined by linearizing Eq. 10 to:

$$logk_{obs} = log([kMnO_2]^b) + c \times log[H^+] \quad (12)$$

The slope of the log of the k_{obs} as a function of the pH (Eq. 12) indicates a zero order reaction with respect to pH ($c = 0.007 \pm 0.011$) at circumneutral pH (**Fig. 5c**).

1.10.3 *Rate law*

The orders of each reactant were substituted into Eq. 4 to give Eq. 13:

$$\frac{dN_2O}{dt} = k[NH_2OH]^{0.9}[MnO_2]^{0.3} \quad (13)$$

When the production rates of N_2O and initial concentrations of NH_2OH and MnO_2 from each experiment (**Table 2**) are substituted into Eq. 13, the overall first order rate constant, *k*, is found to be 0.009 ± 0.002 s^{-1}. When the overall first order rate constant is calculated using NH_2OH oxidation rates, *k* is found to be 0.013 ± 0.004 s^{-1}. The good agreement between these two calculations indicate that the steady-state hypothesis used to calculate the order of the reaction with respect to NH_2OH and proton concentrations was appropriate.

1.11 Discussion

1.11.1 *Mineral effects on NH_2OH reactivity*

To our knowledge, this is the first study that measures the kinetics of NH_2OH oxidation by an environmentally-relevant mineral substrate (MnO_2). In previous studies with enzyme-bound Mn(IV) or ligand-bound Mn(III) in pure water or acidic perchlorate solution (**Table 3**), NH_2OH was suggested to interact with the Mn(III, IV) center by outer-sphere complexation (Banerjee et al., 2002; Salem, 1995). In this study, NH_2OH oxidation takes place at the MnO_2 mineral surface, where high surface area, small particle size, and highly reactive surface sites mediate rapid reaction. In seawater, abundant cations may enter the interlayer region of birnessite and replace water molecules, leading to strong aggregation (Holland and Walker, 1996; Villalobos et al., 2003). Thus, the small decrease in N_2O production rates observed at increasing MnO_2 concentration (**Table 2**) may be due to aggregation.

Table 3. Comparison of NH_2OH oxidation by a variety of Mn species and other relevant reactions under various experimental conditions.

NH_2OH oxidation and other reactions	Solution	Measurement Method	pH	Overall order	Rate Constant	Source
Tri-bridged Mn(IV,IV) dimer	Double-distilled water	Spectrophotometry	4.0-5.3	1	$2.0\text{-}15.0\times10^{3}$ s^{-1}	Banerjee et al. (2002)
Mn(III)	Acidic perchlorate media	Spectrophotometry	-0.5-0.2	2	$1.5\text{-}2.7\times10^{-3}$ M^{-1} s^{-1}	Davies and Kustin (1969)
bis(pentane-2,4-dionato)diaquo manganese(III)	Double-distilled water	Spectrophotometry/ titration	5.02-5.70	1	6.65-158 s^{-1}	Hynes et al. (1993)
Mn(III)-bis(salicylaldimine) complexes	Double-distilled water	Spectrophotometry	5.2-8.4	2	0.16-7.44 M^{-1} s^{-1}	Salem (1995)
Acid birnessite (MnO_2)	Synthetic ocean water	Microsensor/ Spectrophotometry	6.2-8.3	1	$4.09 \pm 0.33\times10^{-4}$ s^{-1}	This study
HNO dimerization	Milli-Q purified water	UV steady-state photolysis	11-14.3	2	$8 \pm 3 \times 10^{6}$ M^{-1} s^{-1}	Shafirovich and Lymar (2002)
HNO reduction by NH_2OH	Deionized water with chelator	Spectrophotometry/ Computational	7.45	2	$4.0 \pm 0.3\times10^{-7}$ M^{-1} s^{-1}	Jackson et al. (2009)
HNO trapping by ligand-bound Mn^{3+} center	0.1 M phosphate buffer with EDTA	Spectroscopy	7 or 10	2	$4\text{-}9\times10^{4}$ M^{-1} s^{-1}	Martí et al. (2005)

1.11.2 *Known competing reactions*

We considered the following abiotic processes to explain the findings reported above.

1.11.2.1 *Nitrosation*

Nitrosation involves the transfer of a NO group from nitrous acid compound to a nitrogenous nucleophilic center. For example, NH_2OH and HNO can react to form N_2:

$$HNO + NH_2OH \rightarrow N_2 + 2H_2O \quad (14)$$

ΔG_r° = -328.78 kJ mol e^{-1} (Latimer, 1952; Shafirovich and Lymar, 2002)

At low pH, NH_2OH may be oxidized by HNO_2 to form N_2O (Hussain et al., 1968; Soler-Jofra et al., 2016):

$$NH_2OH + HNO_2 \rightarrow N_2O + 2H_2O \quad (15)$$

$$NH_3OH^+ + HNO_2 \rightarrow N_2O + H_2O + H_3O^+ \quad (16)$$

Nitroxyl (HNO) may also dimerize to produce N_2O:

$$HNO + HNO \rightarrow N_2O + H_2O \quad (17)$$

The importance of Eq. 14 has been demonstrated at high NH_2OH:$Na_2N_2O_3$ (HNO donor) ratios and may explain the lower N_2O yields with high NH_2OH (**Table 2**), but the reaction is slower than HNO dimerization (Eq. 17; Fehling and Friedrichs, 2011; Shafirovich and Lymar, 2002), and is unlikely to be important in natural waters with low NH_2OH (see below). Equations 15 and 16 are unlikely to have occurred in this study as all experiments

were performed above the pK_a of NH_2OH (5.9) and HNO_2 (2.8), and NO_2^- concentrations did not significantly change during the reaction (data not shown). Together with the fact that the addition of a HNO scavenger decreased rates (**Fig. 3**) and yields (not shown) of N_2O production, these considerations suggest that HNO dimerization is the most likely nitrosation reaction to occur in these experiments.

1.11.2.2 *Hydroxylamine disproportionation*

Hydroxylamine disproportionation (or autoxidation) to NH_4^+, N_2O or N_2 (Bari et al., 2010; Bonner et al., 1978) is described by the following reactions:

$$2NH_2OH + H^+ \rightarrow NH_4^+ + HNO + 3H_2O \quad (18)$$

$$4NH_2OH + 2H^+ \rightarrow N_2O + 2NH_4^+ + 3H_2O \quad (19)$$

$$3NH_2OH + H^+ \rightarrow N_2 + NH_4^+ + 3H_2O \quad (20)$$

These reactions are catalyzed by copper and other reduced metals (Anderson, 1964; Butler and Gordon, 1986; Moews and Audrieth, 1959). However, NH_2OH disproportionation was ruled out in the present system as NH_2OH levels remained constant in the absence of MnO_2, with only background levels of N_2O present (**Fig. 2a**). While NH_4^+ can be oxidized to NO_3^- or NO_2^- by MnO_2 at environmentally relevant pH, mM levels of NH_4^+ are required to produce <10 µM NO_3^- or <100 µM NO_2^- (Boumaiza et al., 2018).

1.11.2.3 *Nitrous oxide reduction by Mn^{2+}*

The reduction of N_2O by Mn^{2+} was considered a possible mechanism for a general decrease in N_2O production rates with increasing MnO_2 concentrations (**Fig. 4b; Table 2**).

In the investigated reaction (Eq. 3), Mn^{2+} would be produced simultaneously with N_2O, and this Mn^{2+} could, in theory, reduce N_2O to N_2:

$$N_2O + Mn^{2+} + H_2O \rightarrow N_2 + MnO_2 + 2H^+ \quad (21)$$

$$\Delta G^\circ = -52.06 \text{ kJ mol } e^{-1}$$

Equation 21 could account for the small fraction of missing N in our mass balance. If N_2 produced by this reaction was the missing N fraction, however, it should have increased as a function of time, as Mn^{2+} was progressively produced during the reduction of MnO_2 by NH_2OH. As the missing N fraction was immediately produced and progressively removed from solution (**Fig. 2**), this reaction was likely not significant in these experiments.

1.11.2.4 *Nitroxyl binding by Mn^{3+}*

A more likely explanation for the increased rates of NH_2OH consumption with increasing MnO_2 without significant change in rates of N_2O production (**Figs. 2, 4b**) may be trapping of the intermediate HNO by mineral-bound Mn(III). Such HNO trapping has been observed using porphyrin-bound Mn^{3+} in solution (Martí et al., 2005). The suppression of N_2O production by the HNO scavengers (**Fig. 3**) suggests that HNO was likely an intermediate in the oxidation of NH_2OH by MnO_2 (Eq. 3). If mineral-bound Mn(III) was present or formed during the reaction, it could bind the HNO intermediate at the mineral surface, thereby preventing HNO dimerization to N_2O (Eq. 17). This pathway requires formation of an aminoxyl radical (Banerjee et al., 2002; Davies and Kustin, 1969; Salem, 1995) that may further reduce a Mn(IV) metal center to Mn(III), and either scavenge HNO or reduce the same Mn(III) intermediate to release both Mn^{2+} and HNO into solution.

Release of HNO to solution is likely followed by dimerization to N_2O. Although these mechanistic details will be difficult to distinguish experimentally, the high N_2O yield at steady-state (**Tables 1 & 2**) indicates the sequestration of HNO onto the solid phase was likely not significant.

1.11.3 *Proposed reaction sequence and mechanisms of NH_2OH oxidation to N_2O by MnO_2*

Here we propose a reaction sequence for the oxidation of NH_2OH to N_2O by MnO_2 consistent with our experimental findings and mass balance. Birnessite is well known to have low zero point charge (e.g. ~2.25) (Balistrieri and Murray, 1982; Murray, 1974), making the surface charge negative across a wide range of pH (including the circumneutral pH values used in this study). This surface property, combined with its high surface area and presence of structural vacancy sites, makes birnessite highly reactive for the sorption of various species, especially positively charged species such as metal cations. On the other hand, the lone electron pair on N in NH_2OH is likely to introduce a polar effect, thus the molecule can be attracted to charged surfaces such as birnessite surface. Though the exact location (e.g. vacancy site vs edge site) and mechanism (e.g. inner-sphere vs outer-sphere) of such interaction is unclear, NH_2OH as a polar molecule can possibly form an adsorbed complex with the birnessite surface, transferring an electron to a Mn(IV) atom (**Fig. 6a**), reducing Mn(IV) to Mn(III), and also resulting in the deprotonation of the hydroxyl group that forms the aminoxyl radical ($H_2NO\cdot$) (**Fig. 6a)**. The electron from the $H_2NO\cdot$ radical can be further transferred to either the produced Mn(III) to produce HNO and dissolved Mn(II) (**Fig. 6b**), or to another Mn(IV) atom to produce another Mn(III) and adsorbed HNO surface complex (**Fig. 6c**). The HNO species produced by these two reactions likely represents the transient intermediate N species derived from mass balance calculations

(**Fig. 2**). As proposed by Fehling and Friedrichs (2011), HNO dimerizes to form *cis*-ON(H)N(H)O, which readily deprotonates to form *cis*-ONN(H)O^- (**Fig. 6d**) and rearranges to the protonated *cis*-HONN(O)H at circumneutral pH (**Fig. 6e**). Deprotonation of this intermediate forms the poorly stable *cis*-hyponitrite anion ($HONNO^-$; **Fig. 6e**), which loses a hydroxyl group to form N_2O and water at circumneutral pH (**Fig. 6f**). Considering that the HNO intermediate is completely removed by the end of the reaction (**Fig. 2**), it is possible to estimate the pseudo-second order rate constant of its removal by dimerization by representing the linear form of the integrated equation after the time of its maximum production (**Fig. 7**). The rate constant of HNO dimerization to N_2O, k_2, is found to be 239 ± 93 M^{-1} s^{-1}, significantly lower than that presented by Shafirovich and Lymar (2002) (8×10^6 M^{-1} s^{-1}), though their experiments were conducted at much higher pH than reported here. Adsorption of HNO on the excess MnO_2 used in these experiments may also be responsible for the decline in the rate of HNO dimerization. As NH_2OH consumption rates increased slightly at increasing MnO_2 concentration while no discernible change in N_2O production rates were observed, it is likely that the rate-limiting step occurs after the initial electron transfer. The good reproducibility of the dimerization kinetic data at varying MnO_2 concentrations (**Fig. 7**) suggest that the dimerization of HNO may be the rate-limiting step and controlled by the adsorption of HNO onto the MnO_2 surface.

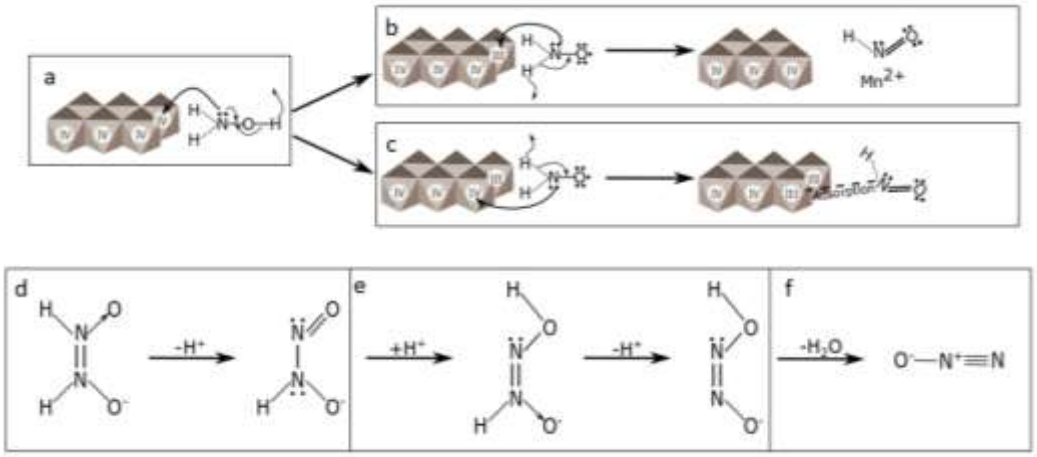

Figure 6. Proposed mechanism for NH_2OH oxidation by birnessite. (a) Electron transfer from NH_2OH to the Mn(IV) and deprotonation of the hydroxyl group allow formation the aminoxyl radical ($H_2NO\cdot$) and reduction of the Mn(IV) to Mn(III). The electron from the $H_2NO\cdot$ is transferred to either (b) the Mn(III) to produce nitroxyl (HNO) and Mn^{2+} or (c) to another Mn(IV) to produce another Mn(III) and HNO which then could adsorb onto the Mn(III) product. (d) Nitroxyl dimerizes to form *cis*-ON(H)N(H)O, which deprotonates to *cis*-$ON(H)NO^-$. (e) O-protonation occurs and forms *cis*-HONN(O)H, which deprotonates to the unstable *cis*-hyponitrite anion ($HONNO^-$). (f) The *cis*-hyponitrite anion loses its hydroxyl group to form N_2O.

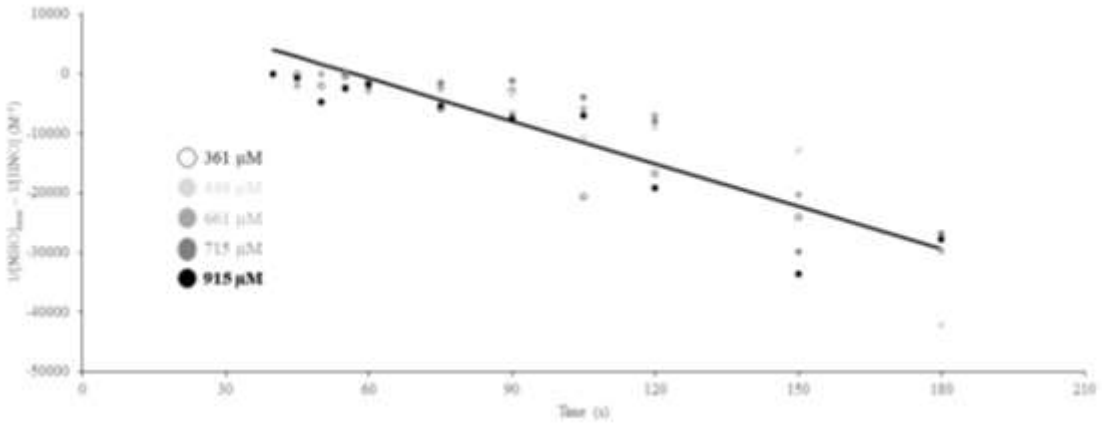

Figure 7. Nitroxyl dimerization exhibits pseudo-second order characteristics. Concentrations of HNO calculated from mass balance of varied MnO_2 experiments in Fig. 2b-f. The second-order rate constant of HNO dimerization, k_2, is found to be 239 ± 93 M-1 s-1 in the experiments. The line represents the best linear regression fit of all data sets.

1.11.4 *Environmental implications*

Based on our findings, rapid N_2O production from the coupled biotic-abiotic reaction of microbial NH_4^+ oxidation to NH_2OH, followed by abiotic NH_2OH oxidation by Mn(III, IV) oxides, could occur wherever active Mn^{2+}-oxidizing bacteria (Clement et al., 2009; Tebo, 1991) and nitrifying microbes coexist. Relevant environments include oxyclines above oxygen minimum zones (Beman et al., 2012; Bouskill et al., 2012; Bruland et al., 1994; Löscher et al., 2012; Neretin et al., 2003; Newell et al., 2011; Shiller and Gieskes, 1985; Trefry et al., 1984), sediment-water interfaces (Anschutz et al., 2005), and deep sea sediments that contain ferromanganese nodules (Blöthe et al., 2015; Shiraishi et al., 2016). In oceanic environments, particulate Mn tends to be low in concentration, decreasing the likelihood of aggregation and potentially leading to faster rates of N_2O production than observed in our experiments.

Hydroxylamine is likely the limiting substrate for Eq. 3 in nature because NH_2OH occurs at low concentrations and is an essential intermediate in nitrification. However, during periods of intense nitrification in coastal waters, NH_2OH can accumulate up to ~200 nM (Butler et al., 1987; Butler et al., 1988; Gebhardt et al., 2004; Schweiger et al., 2007). The presence of NH_2OH in natural waters indicates that it leaks out of cells and suggests that the fast N_2O production from abiotic NH_2OH oxidation with Mn(III/IV) oxides could be easily confused with N_2O from biological nitrification (Kozlowski et al., 2016b). Using representative conservative concentrations from the oxycline Baltic Sea (31 nM MnO_2 (Neretin et al., 2003) and 18 nM NH_2OH (Schweiger et al., 2007)) and Eq. 13, we calculated that rates of abiotic N_2O production from MnO_2 oxidation of NH_2OH would be ~500 nM N_2O d^{-1}, whereas measured rates were 135 nM N_2O d^{-1} from denitrifying bacterial cultures obtained from the Baltic Sea (Rönner and Sörensson, 1985). If concentrations of

NH_2OH (1.5-20.0 nmol L^{-1}; Korth et al., 2019) and MnO_x (0.067-0.45 µg L^{-1}; Lam et al., 2018) from the Eastern Tropical Pacific are used, abiotic rates range from 0.6 to 19.8 nM N_2O d^{-1}. These rates exceed those of N_2O production from both nitrification and denitrification in the Eastern Tropical South Pacific, which range from both nitrification (0-0.03 nM N_2O d^{-1}) and from denitrification (3.9-4.5 nM N_2O d^{-1}) in the Eastern Tropical South Pacific (Ji et al., 2015).

The finding that nitroxyl (HNO) and possibly the aminoxyl radical ($H_2NO\cdot$) are intermediates in the abiotic NH_2OH oxidation by Mn(III/IV) oxides suggests that alternative reactive N species may be involved in coupled biotic/abiotic interactions in the N cycle. Although HNO may also be produced as an enzymatic intermediate in the N cycle (Bykov et al., 2014; Hooper and Terry, 1979; Komarov et al., 2000; Xia et al., 2000), it is commonly assumed that it remains bound to the enzyme and is rapidly converted to NO_2^-, N_2O, or NH_4^+ during nitrification, denitrification, and dissimilatory nitrate reduction to ammonium, respectively. Free HNO, however, is essential in nitric oxide reduction by nitric oxide synthase (Turk and Hollocher, 1992), and Mn^{2+} inhibits the dehydrogenation of HNO by hydroxylamine dehydrogenase (formerly hydroxylamine oxidoreductase) to produce N_2O instead of NO_2^- (Hooper and Terry, 1979). Thus, biologically produced HNO could dimerize with HNO from abiotic NH_2OH oxidation to enhance N_2O production.

Although the detection limit of the N_2O microsensor (1 µM) used in this study required use of higher concentrations of NH_2OH than typically found in nature, the rate constants measured here should apply to lower substrate concentrations as well. The proposed rate law and the overall first order rate constant could be used in biogeochemical

models to account for the proportion of N_2O that is abiotically produced in a variety of environments.

1.12 Conclusions

To our knowledge, this is the first study that characterized the kinetics of NH_2OH oxidation by Mn(IV) oxides in seawater at circumneutral pH. We demonstrated that the reaction is overall first order with respect to NH_2OH concentrations. The reaction is rapid at circumneutral pH ($k = 0.01\ s^{-1}$), with complete oxidation occurring within minutes (half-life of ~23 seconds). Nitroxyl (HNO) was found to be an important intermediate in abiotic NH_2OH oxidation, as mass balance considerations indicate rapid formation and disappearance of an intermediate nitrogen species and N_2O production was reduced in the presence of a HNO scavenger. Our findings suggest the potential for a novel biotic-abiotic pathway by which any NH_2OH that leaks from nitrifying cells and comes in contact with reactive Mn(III/IV) oxide minerals will rapidly be oxidized to N_2O. The abiotic interactions between biotically produced nitrogenous intermediates and Mn oxide particles could have implications for Mn and N cycling. Future studies should focus on the distribution of ammonia-oxidizing organisms and suspended particulate Mn oxides in diverse ecosystems.

SIMUL-STAINING MANGANESE OXIDES AND MICROBIAL CELLS

This work was submitted to *Limnology and Oceanography: Methods* on February 7, 2020 after revisions, under the same title, by Amanda R. Cavazos and Jennifer Glass.

1.13 Abstract

Manganese oxide minerals ($Mn(III/IV)O_x$) are ubiquitous in natural environments and interactions between $Mn(III/IV)O_x$ and microbes play important roles in biogeochemical cycles. Current techniques for determining the spatial distribution of microbes with $Mn(III/IV)O_x$ include electron microscopy and synchrotron radiation analyses. However, these techniques may not be readily available in most laboratories or may be cost prohibitive. Here we present a rapid, cost-effective "simul-staining" method for imaging particulate $Mn(III/IV)O_x$ and cells on the same filter using epifluorescence microscopy with differential interference contrast (DIC) capability as a pre-screening tool before higher resolution and/or more time-intensive analyses. This method uses leucoberbelin blue (LBB) dye, which turns blue when oxidized by particulate $Mn(III/IV)O_x$ on filters, and the fluorescent nucleic acid stain, SYBR Green, which fluoresces when bound to nucleic acids. First, the DIC configuration is used to locate blue "haloes" of oxidized LBB around $Mn(III/IV)O_x$ particles. Second, the SYBR Green filter set (excitation: 395 nm/emission: 509 nm) is used to image nucleic acids in cells. Third, ImageJ is used for image analysis to associate $Mn(III/IV)O_x$ particles and microbes. We demonstrate that this simul-staining is

suitable for laboratory cultures of Mn^{2+}-oxidizing bacteria as well as environmental samples from a marine oxycline.

1.14 Introduction

Manganese oxides ($Mn(III/IV)O_x$) are ubiquitous in the environment and play key roles in biogeochemical cycles and environmental remediation (Feng et al., 2015; Hansel, 2017). $Mn(III/IV)O_x$ can serve as powerful sorbents or oxidants of a wide range of elements and organic and inorganic compounds because to their distinctive sheet-like structures that allow for rapid adsorption and high reactivity (Potter and Rossman, 1979; Remucal and Ginder-Vogel, 2014; Spiro et al., 2009). These characteristics also allow $Mn(III/IV)O_x$ to play a role in microbial interactions, either directly or indirectly through "cryptic" interactions (Hansel et al., 2015).

Manganese is cycled by microbial reduction or oxidation. Microbial Mn reduction is coupled to a wide range of substrates and performed by microbes that are capable of iron reduction (Lovley, 1991). Microbial Mn reduction is thermodynamically more advantageous than reduction of ferric iron or sulfate and is the prevalent means of carbon mineralization in surface shelf sediments of the Black Sea (Thamdrup et al., 2000). In other Mn-rich coastal sediments, 25-99% of carbon oxidation has been attributed to microbial Mn-reduction (Aller, 1990; Canfield et al., 1993a; Canfield et al., 1993b; Nickel et al., 2008; Thamdrup et al., 2000; Vandieken et al., 2014). Microbial Mn oxidation is performed by microbes and fungi, either enzymatically (Tebo et al., 2005), or via chemical reactions with enzymatically produced reactive oxygen species (Learman et al., 2013; Learman et al., 2011b).

To constrain and elucidate the role Mn(III/IV)O_x play in biogeochemical cycles, powerful methods are needed to co-localize Mn(III/IV)O_x particles and microbes (Templeton and Knowles, 2009). Electron microscopes capable of energy-dispersive X-ray spectroscopy provide high-resolution imaging of microbe-mineral associations. Synchrotron x-ray microprobes enables μm to nm elemental mapping of microbes and minerals and can also provide oxidation state. However, X-ray absorption spectroscopy facilities are often not readily available, making screening and analysis of large numbers of samples inconvenient. A rapid, cost-effective, and readily available method to "pre-screen" samples before more detailed analysis is needed.

Epifluorescent microscopes with differential interference contrast (DIC) capability are common in most laboratories. Epifluorescent microscopy is typically used for identifying microbes with nucleic acid stains such as SYBR Green or 4′,6-diamidino-2-phenylindole (DAPI). Both stains bind into the minor groove of DNA but SYBR Green then intercalates and extends its propyl groups along the groove of the DNA (Banerjee and Pal, 2008; Dragan et al., 2012). For staining cells from environments with higher mineral abundance, the more suitable nucleic acid stain is SYBR Green (Lunau et al., 2005), as it does not bind mineral surfaces as readily as DAPI. DIC microscopy is used for imaging samples with a low refractive index, which makes them nearly invisible or transparent using standard light microscopy methods. The high contrast of DIC microscopy also allows for the visualization of dyes that are difficult to detect with light or phase contrast microscopy. Thus, DIC and epifluorescent microscopy can be used in tandem with fluorescent and non-fluorescent dyes.

Here we describe a cost-effective and readily available method to rapidly visualize fluorescently-stained cells and Mn(III/IV)O_x particles in laboratory or environmental samples as a pre-screening technique. This method allows users to determine which samples to analyzed further by higher resolution and/or more time-intensive techniques without investing significant resources in less-than-ideal samples. This method utilizes a triphenylmethane compound, leucoberbelin blue (LBB), which selectively reacts with Mn(III), Mn(IV), Mn(V), Mn(VI), and Mn(VII) in successive one-electron transfer steps (Krumbein and Altmann, 1973). In the most common case of Mn(IV) reduction, the first electron transfer occurs when the C-H bond on LBB is broken and a hydrogen atom transfer forms Mn(III)OOH, which then reacts with the C· in the second hydrogen atom transfer to form Mn^{2+} and fully oxidized LBB (Krumbein and Altmann, 1973; Luther III et al., 2018). These hydrogen atom transfer reactions between LBB and Mn(III/IV)O_x are thermodynamically favorable at pH <7 (Luther III et al., 2018).

Oxidized LBB has a characteristic blue color, which can be measured by spectrophotometry as a proxy for Mn(III/IV)O_x concentration (Dick et al., 2006; Francis and Tebo, 2001). LBB is also used as visual evidence for spot testing of microbial Mn^{2+} oxidation in agar plates and microscope slide wells (Anandkumar et al., 2011; Geszvain et al., 2016; Lee and Tebo, 1994; Takeda et al., 2012). Most recently, LBB has been used to quantify reactive Mn(III) and particulate oxidized Mn at picomolar concentrations (Jones et al., 2019). Our new method enables LBB visualization at the micron-scale to visualize particulate Mn(III/IV)O_x in natural waters using DIC microscopy. LBB visualization can be coupled with common fluorescent stains like SYBR Green or DAPI to simultaneously stain Mn(III/IV)O_x and cells by epifluorescence microscopy.

1.15 Materials and procedures

1.15.1 *Methods*

Simul-staining of microbes and Mn(III/IV)O_x involves the following steps (**Fig. 8**). All materials are listed in **Table 4**.

1. *Sample preparation.* Aquatic samples are fixed with 4% paraformaldehyde (PFA) in phosphate buffered solution (PBS) for one hour at room temperature. The fixed samples are then filtered onto a white polycarbonate membrane filter (0.2 μm pore size, 25 mm diameter, Isopore GTTP02500) supported by a cellulose nitrate membrane (0.45 μm pore size, 25 mm diameter, Whatman) using a glass filter tower and ~20 mm Hg vacuum, followed by washing with 1× PBS (pH 7). Filters are stored at -20˚C until analysis. For a positive control, synthetic acid MnO_2 is prepared as described by Villalobos et al. (2003).
2. *Reagent preparation*. SYBR Green I is diluted to a 1:400 working solution in filter sterilized MilliQ 18.2 MΩ-cm water. LBB is diluted to 0.04% in 45 mM glacial acetic acid (Krumbein and Altmann, 1973) and filter-sterilized through a 0.2 μm syringe filter.
3. *LBB staining.* Filters are cut into sections using an ethanol-sterilized razor and placed onto a glass microscope slide. ~15 μL of 0.04% LBB solution is added to the center of the filter and allowed to react for 8 min in the dark. *The next two steps (4-5) must be performed ≤45 min after the 8 min LBB staining period.*

4. *SYBR Green staining.* Immediately after the 8 min LBB staining period, ~5 µL of SYBR Green I (1:400 dilution) is added to the center of the filter and allowed to react for 2 min in the dark. Next, a coverslip is placed on top of the filter.
5. *DIC-fluorescent imaging.* On an epifluorescent microscope, DIC imaging is performed at maximum brightness at 100x magnification to locate Mn(III/IV)O_x particles by their characteristic blue haloes. Once a Mn(III/IV)O_x particle is located, an image is captured. Without moving the stage, settings are changed to the SYBR Green (395/509) filter set and an image is captured. This process is repeated for numerous fields of view until a statistically significant number of Mn(III/IV)O_x particles and cells are imaged. *Because the color intensity of oxidized LBB fades over time, all image collection must be completed ≤45 min after completion of LBB staining (step 3).*
6. *ImageJ calibration.* Each laboratory should establish their own LBB color threshold values by calibrating HSB values for differences between microscopes. Control samples containing synthetic MnO_2 stained with LBB are used to determine the HSB (hue, saturation, brightness) colorspace thresholds for oxidized LBB using the free imaging software ImageJ. Hue values of 120-155 broadly select for oxidized LBB for smaller Mn(III/IV)O_x particles (e.g. <1 µm). Hue values of 140-155 should be used when imaging higher concentrations of Mn(III/IV)O_x or particles that are completely reduced. In both instances, saturation is set to exclude the peak at lower values to remove "background" color (**Fig. 9**, blue rectangle) during thresholding. Brightness is set to the middle of the histogram peak to eliminate inference from the background (**Fig. 9**, red rectangle).

Ideally, these values should remain constant during image analysis on the same filter, but they may change slightly due to small heterogeneities across the filter surface. Thus, adjusting to set values by histogram peaks will ensure consistent thresholding. These calibrated values are then used throughout all sample imaging analyses using the "HSB color threshold" tool.

7. *Image analysis with ImageJ*. To generate overlays of simul-stained images of Mn(III/IV)O_x and microbes, DIC images are opened in ImageJ and color thresholded as described in Step 6. The thresholded image is saved as its own file. Both the thresholded DIC and SYBR Green images are then opened in ImageJ. With the thresholded DIC image selected, an overlay is added under the "Image" menu, the SYBR Green image is selected, and the opacity is set to 70-80%. The overlay image is saved.

The area of Mn(III/IV)O_x particles can be measured in ImageJ after thresholding of DIC images. The thresholded DIC image is converted to greyscale (*Image* → *Type* → *8-bit*), a scale is set (draw a line over scale → *Analyze* → *Set Scale* → Enter known distance and units in window → check *Global* → click *OK*), and the image is made binary (*Process* → *Binary* → *Make Binary*). The area of interest is measured after selection using the rectangular selection tool and analyzed using the "Analyze Particles" tool under the "Analyze" menu. In the pop-up window, *Show Outlines* and *Display Results* are selected and a table with the area of the selected particle is displayed.

Table 4. List of required materials and instruments (n.d. = not determined).

Material	Company or Reference
Sample collection	
Sterile Falcon tubes, 50 mL	BD Falcon
20% paraformaldehyde (PFA)	Electron Microscopy Sciences
Reagents	
Phosphate-buffered solution (PBS)	n.d.
Ultra-pure water (18.2 M-Ω)	Millipore
Synthetic acid birnessite	n.d.
Leucoberbelin blue powder, dye content 65%	Sigma-Aldrich cat #432199
SYBR ® Green I Nucleic Acid Stain	Lonza cat # 50513
4',6-diamidino-2-phenylindole dihydrochloride (DAPI) powder	Sigma-Aldrich cat #10236276001
Glacial acetic acid	n.d.
Plastic sterile syringe	n.d.
Syringe filter	n.d.
Filtration	
Vacuum Pump: 1/8 hp Horsepower, Continuous, Single Phase, 120 V AC Volt, 24 in of Hg Max Vacuum, 2.1 A Current	Gamut #807U434 (or similar)
Microanalysis Filter Holder, 25 mm, fritted glass support, with clamp	Millipore XX1002500
White polycarbonate membrane filters, 0.2 µm pore size, 25 mm diameter	Isopore
Cellulose nitrate membrane, 0.45 µm pore size, 25 mm diameter	Isopore
Staining	
Glass microscope slides	VWR
Ethanol	n.d.
Stainless steel razor	n.d.
Forceps (plastic or stainless steel)	n.d.
Leucoberbelin blue solution (0.04%)	n.d.
Glass cover slips	VWR
Imaging	
Immersion oil	n.d.
Epifluorescent microscope with differential interference contrast	Zeiss (or similar)
Fluorescent light set (395/509)	Zeiss (or similar)
ImageJ software	NIH https://imagej.nih.gov/ij/
Computer	n.d.

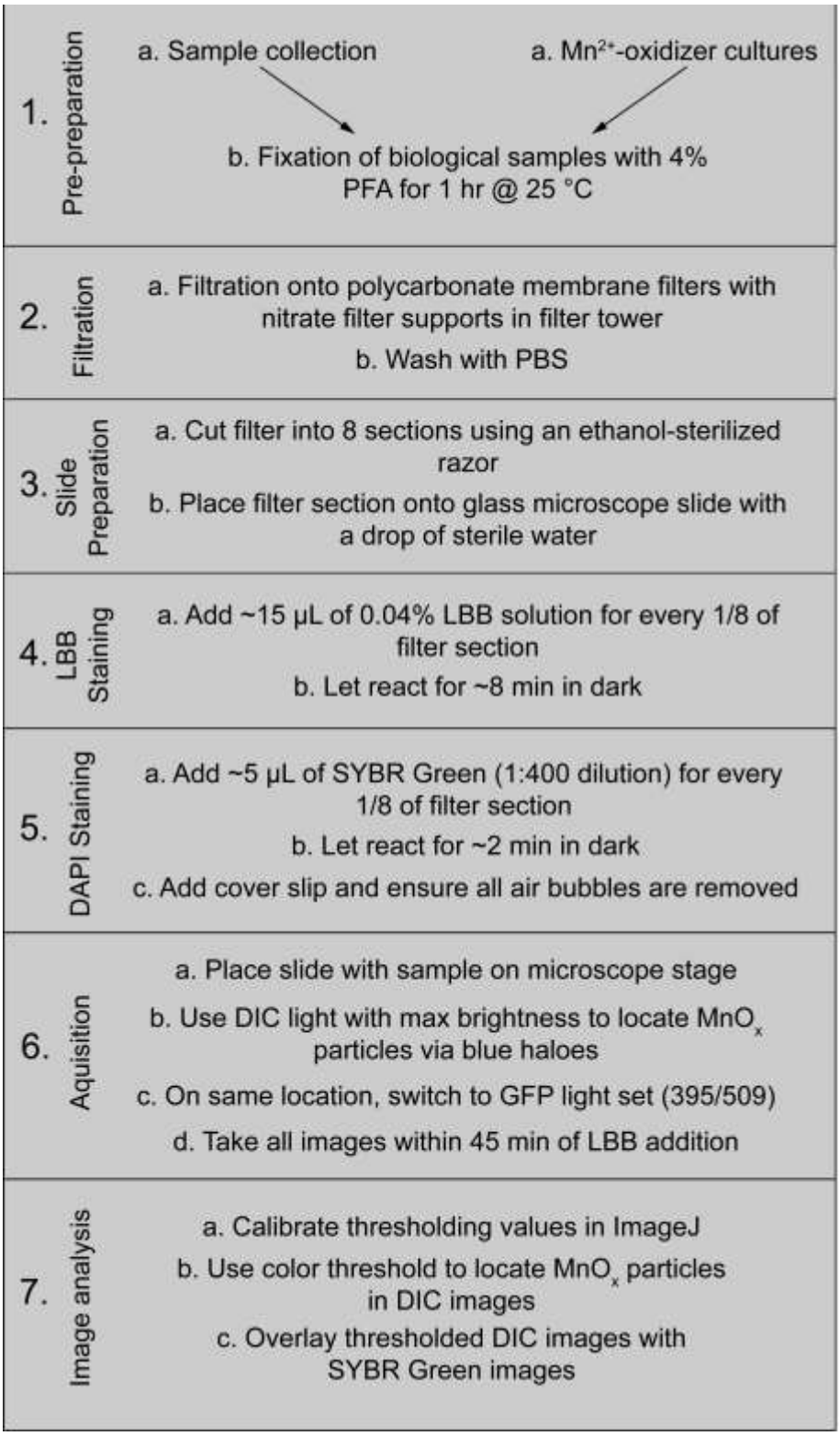

Figure 8. Schematic outline of the presented method.

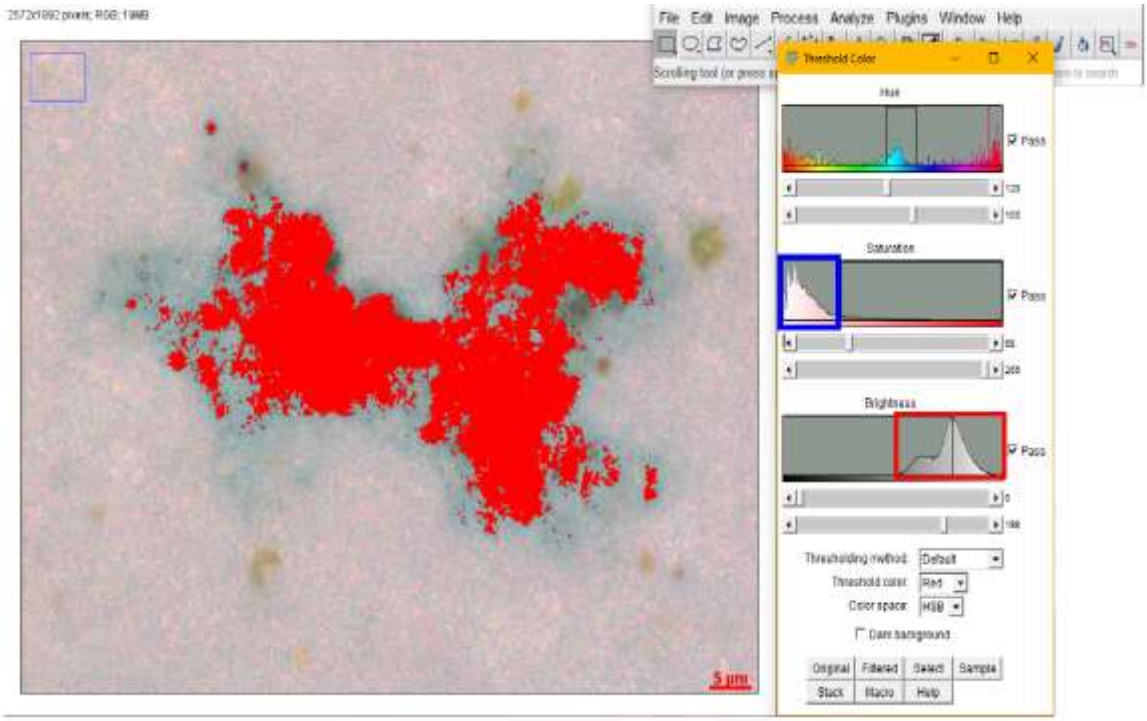

Figure 9. Setting the parameters for color threshold using the Color Threshold tool in ImageJ. Hue values have been set for "broad analysis." Saturation values should be set to exclude the histogram peak (blue rectangle), otherwise background color will threshold. Brightness maximum should be set to the center of the histogram peak (red rectangle) to prevent background color from thresholding. See Fig. 14 (bottom row) for original images.

1.16 Assessment

Current methods for inferring biogeochemistry of microbes and Mn(III/IV)O_x minerals tend to require significant time for sample preparation or require facilities with restricted access. Thus, element-specific dye(s) that can be coupled to cell-imaging via epifluorescent microscopy are needed for a rapid and cost-effective "pre-screen" to determine which samples would be worth the time investment of more powerful analytical techniques. We found that LBB specifically stains Mn(III/IV)O_x and remains oxidized and in position on the filter during staining with fluorescent dyes that strongly bind nucleic acids, such as DAPI and SYBR Green. DAPI fluoresces upon preferential binding to

adenine–thymine rich regions of DNA (Banerjee and Pal, 2008), and SYBR Green fluoresces when it binds to the minor groove of double-stranded DNA and extends the its propyl groups along the groove of DNA (Dragan et al., 2012). In the future, our method could be developed further for use with fluorescent probes that bind to specific nucleic acid sequences to identify the taxonomy of cells via fluorescent in situ hybridization (Section 5.2).

Like all other methods, LBB-nucleic acid simul-staining requires optimization and has limitations. In Sections 3.4.1-3.4.3, we describe how the method was optimized with synthetic samples. In Section 3.4.4, we show the applicability of the method to cultures of Mn^{2+}-oxidizing bacteria and environmental samples from the oxygen minimum zone (OMZ) of the Gulf of Mexico. In Section 3.4.5, we discuss the recommended uses and limitations of the method.

1.16.1 *Method optimization*

3.4.1.1 Time window for LBB imaging

We found that LBB requires a staining period of 8 min in the presence of Mn(III/IV)O_x for optimal development of blue haloes. The color intensity of LBB is prone to fading with time, usually within an hour when measured by spectrophotometry (Krumbein and Altmann, 1973). With simul-staining, the area of blue haloes decreased by 88-98% over 120 min, depending on the thresholding values **(Fig. 10).** If left to react for >120 min, the Mn(III/IV)O_x particles will completely dissolve and the blue haloes will disappear. We found that synthetic, biogenic, and natural Mn(III/IV)O_x particles could be imaged within 45 min after LBB addition. Thus, if determining the area of Mn(III/IV)O_x

particles is a priority, all images should be captured during the 45 min window to ensure accurate measurements.

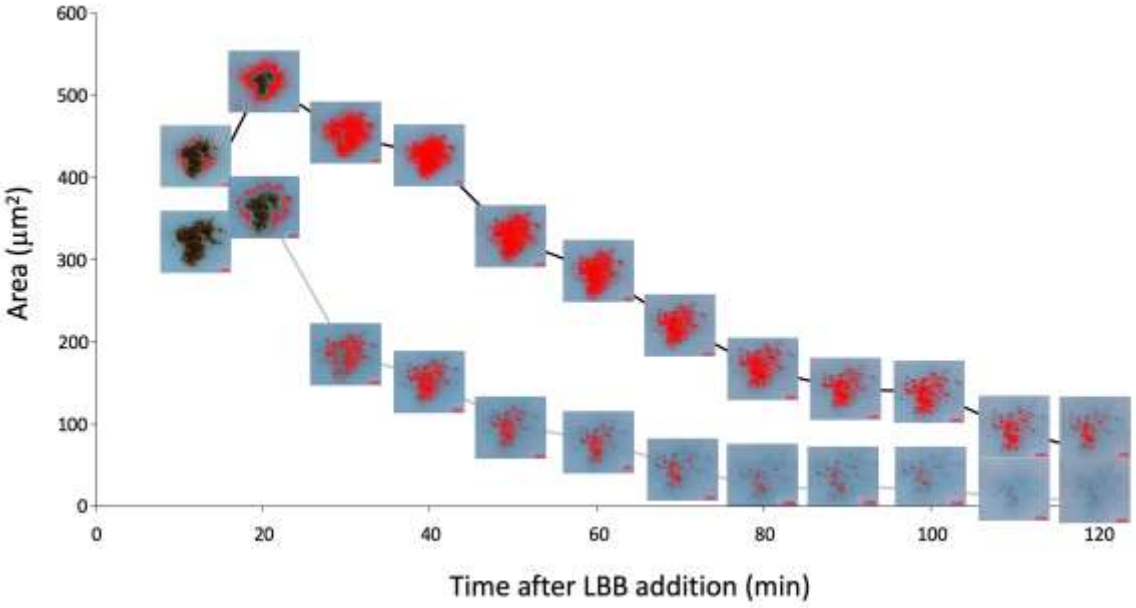

Figure 10. Staining with LBB is a time-sensitive method. Particle size and LBB color intensity decrease with time. False red color in all images is indicative of oxidized LBB, as determined through the threshold tool in ImageJ. Any blue color not covered by false red color did not meet threshold values indicative of oxidized LBB, as determined and "calibrated" in control experiments. Threshold values were defined as either broad (hue = 120-155, saturation = 103-255; black line) or specific (hue = 140-155, saturation = 123-255; gray line) color threshold parameters. Regardless of thresholding mode, particle size and LBB color intensity decrease with time.

3.4.1.2 Optimal LBB volume

The volume of LBB added to the filter was carefully optimized; too little LBB results in incomplete staining and the formation of air bubbles under the coverslip, excess LBB completely dissolves any particles or traces thereof. Differences in crystallinity of $Mn(III/IV)O_x$ particles could potentially affect the amount of LBB necessary for reduction.

We found that 10-15 µL of 0.04% LBB per eighth of a filter section was optimal for our various samples (biogenic, natural, and synthetic), but other users may adjust the volume as needed depending on the amount of $Mn(III/IV)O_x$ expected.

3.4.1.3 Filter contact with LBB staining solution

We recommend performing Step 3 with 0.04% LBB solution on a horizontal glass microscope slide to retain haloes. Any dilution of the 0.04% LBB stock solution resulted in minimal $Mn(III/IV)O_x$ reduction (e.g. no blue haloes or imprints). Other approaches that removed oxidized LBB solution from the filters failed: we tried soaking filters in LBB solution in the filter tower or in Eppendorf tubes, but both methods required removal of LBB solution, either by removal of the filter from solution or by filtration of LBB solution through the filter. Removal of the LBB resulted in complete erasure of any evidence of blue haloes or imprints.

3.4.1.4 Addition of LBB before nucleic acid stain

LBB should be added to filters in an acidic solution (Step 2) to ensure effective $Mn(III/IV)O_x$ reduction before addition of nucleic acid stains in circumneutral solutions. The order of Steps 2 and 3 is important as SYBR Green and DAPI dyes are stable at pH 4-10, whereas LBB reduction of $Mn(III/IV)O_x$ is optimal at pH 4-6 (Krumbein and Altmann, 1973). When a nucleic acid stain at circumneutral pH was added prior to LBB, MnO_2 reduction was slower and haloes were not as prominent (data not shown), likely because the pH of the LBB-nucleic acid stain solution was too high for LBB reduction.

1.16.2 *Possible interferences*

1.16.2.1 *Mn^{2+} does not photo-oxidize under DAPI, GFP, or Alexa568 filter sets*

Autofluorescence is a common interference in epifluorescence microscopy. Because dissolved Mn^{2+} can be photoreactive and some Mn(II) minerals are fluorescent, we investigated whether Mn^{2+} would interfere with either fluorescent or DIC microscopy. To test whether Mn^{2+} photo-oxidation occurs during simul-staining, we placed 20 µL of 100 µM $MnCl_2$ solution onto a fourth of a filter, followed by addition of 10 µL of LBB. The filter section was then exposed to DAPI (358/461), GFP (395/509), or Alexa568 (550-580/590-650), or all three, for 5 min each per filter set. Each filter was then examined under DIC and analyzed via ImageJ. No blue haloes or large areas of blue stain were observed, suggesting that Mn^{2+} does not photo-oxidize during fluorescent imaging.

1.16.2.2 *Mn^{2+} formed during LBB oxidation does not autofluoresce*

To test whether LBB or Mn^{2+} produced by Mn(III/IV) reduction by LBB interferes with fluorescent imaging, we imaged LBB-stained Mn(III/IV)O_x particles without DAPI. Blue haloes observed in DIC imaging did not fluoresce under the DAPI filter set (358/461), suggesting that Mn^{2+} does not autofluoresce.

1.16.2.3 *Glycerol-based anti-fade agents "bleed out" haloes*

When DAPI was prepared with Citifluor (Electron Microscopy Sciences), a glycerol-based anti-fade agent, the glycerol caused any blue haloes left behind by the LBB solution to "bleed out." While imaging cells with DAPI was possible without an anti-fade agent, it was noted that the fluorescent signal decreased more rapidly than with SYBR Green.

1.16.3 *Exclusive reactivity of LBB with Mn(III/IV)O_x*

We prepared mixtures of birnessite (hereafter MnO_2), ferrihydrite, and *Escherichia coli* to test whether LBB reacts with other components likely to be present in natural samples (e.g. Fe(III) minerals and microbial cells). We found that the exclusive reactivity of LBB to $Mn(III/IV)O_x$ allows for identification of $Mn(III/IV)O_x$ and can be used in tandem with fluorescent nucleic acid stains.

1.16.3.1 *Preparation of laboratory controls*

Ferrihydrite ($Fe(OH)_3$) was prepared by dissolving $FeCl_2$ in sterile H_2O to a concentration of 400 mM. The pH of this solution was slowly adjusted to 7 using NaOH. The precipitated $Fe(OH)_3$ was washed three times with sterile H_2O before use. Synthetic acid MnO_2 was prepared as described by Villalobos et al. (2003). *E. coli* cultures were prepared as follows: 500 µL of *E. coli* K12 culture grown overnight in Lysogeny Broth was added to 4% paraformaldehyde (PFA) and incubated overnight at 4°C. Fixed cells were washed 3 times in 1× PBS and resuspended in 1 mL of 1:1 PBS-ethanol solution. Samples were stored at -20°C until mixture preparation (50 µL PFA-fixed *E. coli*, 50 µL of MnO_2, and 900 µL 18.2 MΩ-cm MilliQ water). Samples were then filtered as described in Step 2.

1.16.3.2 *LBB reacts exclusively with MnO_2*

The solution containing MnO_2, $Fe(OH)_3$, and *E. coli* was prepared, filtered, stained, and analyzed (**Steps 3-7**). We confirmed that LBB reacted only with MnO_2 and not with $Fe(OH)_3$ or *E. coli* cells; blue haloes only appeared around MnO_2 particles and not $Fe(OH)_3$ particles (orange in DIC) or *E. coli* cells (blue in DAPI; **Fig. 11**).

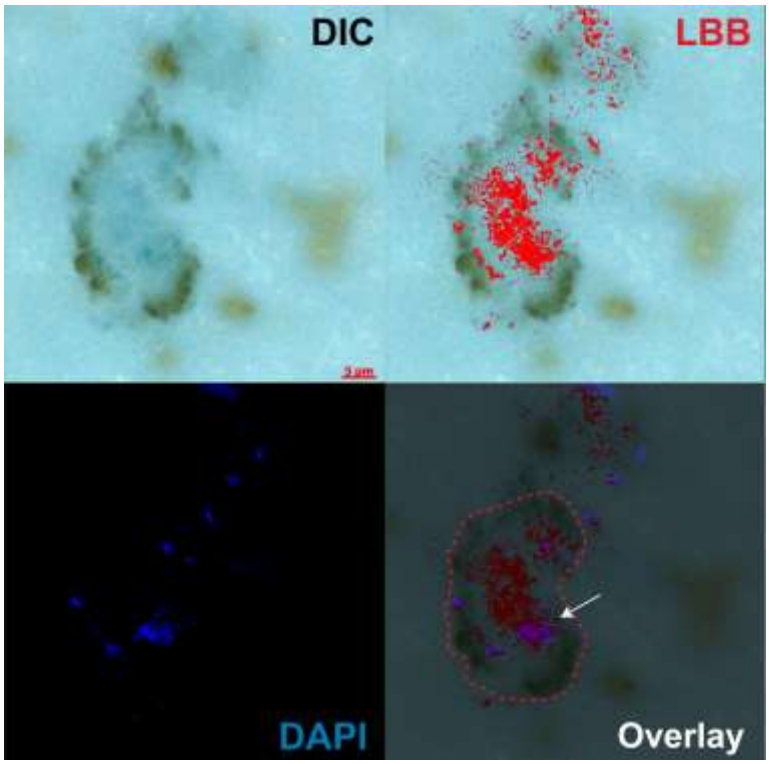

Figure 11. Simul-staining of microbes with MnO_2 in laboratory prepared samples. Filter with 50 µL PFA-fixed *E. coli*, 50 µL of synthetic MnO_2, and 900 µL 18.2 MΩ-cm MilliQ water. DIC: DIC image of MnO_2 (brown mineral with blue color in center) and $Fe(OH)_3$ particles (orange minerals). LBB: False red color indicates oxidized LBB after color threshold analysis of DIC image, indicating presence of MnO_2 particles. DAPI: Fluorescent image showing microbes stained with DAPI. Overlay: Image overlay of LBB and DAPI showing microbes associated with MnO_2 particle (white arrow). Dashed red line indicates traces of MnO_2 as inferred from *LBB* image. Scale bar is 5 µm.

1.16.4 *Application of method to laboratory cultures and environmental samples*

1.16.4.1 *Laboratory cultures of Mn^{2+}-oxidizing bacteria*

Two Mn^{2+}-oxidizing bacteria, the marine alphaproteobacterium *Roseobacter* AzwK-3b and the freshwater gammaproteobacterium *Pseudomonas putida* GB-1, were grown from glycerol stocks for two days on agar plates at 25°C in the light. AzwK-3b was grown on K-medium agar plates (Tebo et al., 2005) and GB-1 was grown on LEP agar plates (Boogerd and de Vrind, 1987). Single colonies were picked and grown in liquid K-medium

for two days. After liquid cultures reached lag phase, cultures were inoculated into fresh liquid K-medium containing 200 µM $MnCl_2$ at 0.05 and 0.005 OD_{600} cell density (Tebo et al., 2005). Cultures were sampled after 15 hours during exponential phase. Simul-staining was performed as described in Section 3.3.1.

Rod-shaped cells from both AzwK-3b (**Fig. 12**) and GB-1 (**Fig. 13**) successfully simul-stained with LBB. Mn(III/IV)O_x particles in GB-1 cultures were generally larger and more "clustered" than those in AzwK-3b cultures. The differences in microbial distributions and Mn(III/IV)O_x particle sizes could be contributed to the Mn^{2+} oxidation mechanisms. AzwK-3b oxidized Mn through biotic-abiotic coupling with superoxides, which produces smaller, less crystalline Mn(III/IV)O_x than those that are formed by GB-1 (Learman et al., 2013; Learman et al., 2011b). Cell counts tended to be greater around Mn(III/IV)O_x particles in GB-1 cultures, with half the particles imaged from the AzwK-3b cultures having less than 10 cells within 5 µm of the particle surface. Large areas of fluorescence with no defined cells in the GB-1 cultures suggest the formation of biofilms, which have been shown to play a role in Mn^{2+} oxidation by GB-1 (Toner et al., 2005).

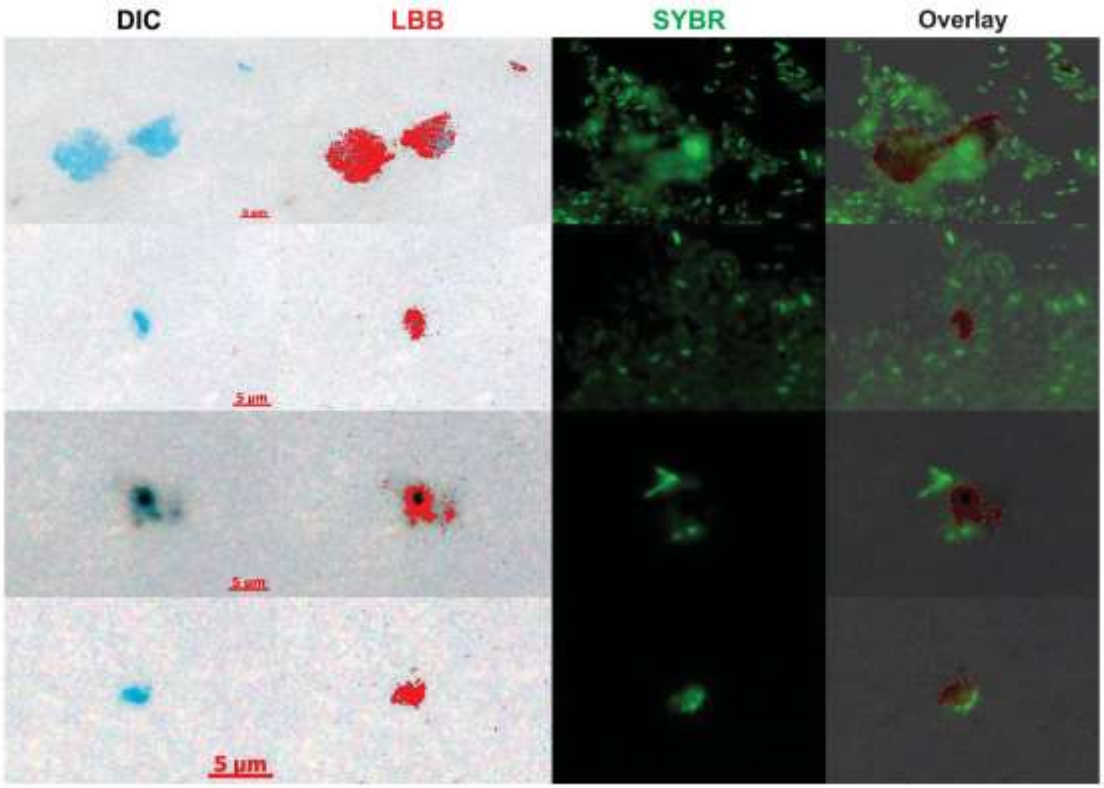

Figure 12. Simul-staining of the marine alphaproteobacterium *Roseobacter* AzwK-3b and biogenic Mn(III/IV)O_x. Cultures were grown with 200 µM Mn^{2+}. DIC: Mn(III/IV)O_x particles in DIC light with characteristic blue "haloes". LBB: False red color indicates oxidized LBB, as determined through color threshold analysis. "Haloes" or imprints that passed the color threshold indicate the presence of Mn(III/IV)O_x particles. SYBR: Fluorescent image of microbes stained with SYBR Green. Overlay: Image overlay of *LBB* and *SYBR* images showing microbes associated with Mn(III/IV)O_x particles. Dashed red line indicates traces of Mn(III/IV)O_x as inferred from *LBB* image. All scale bars are 5 µm.

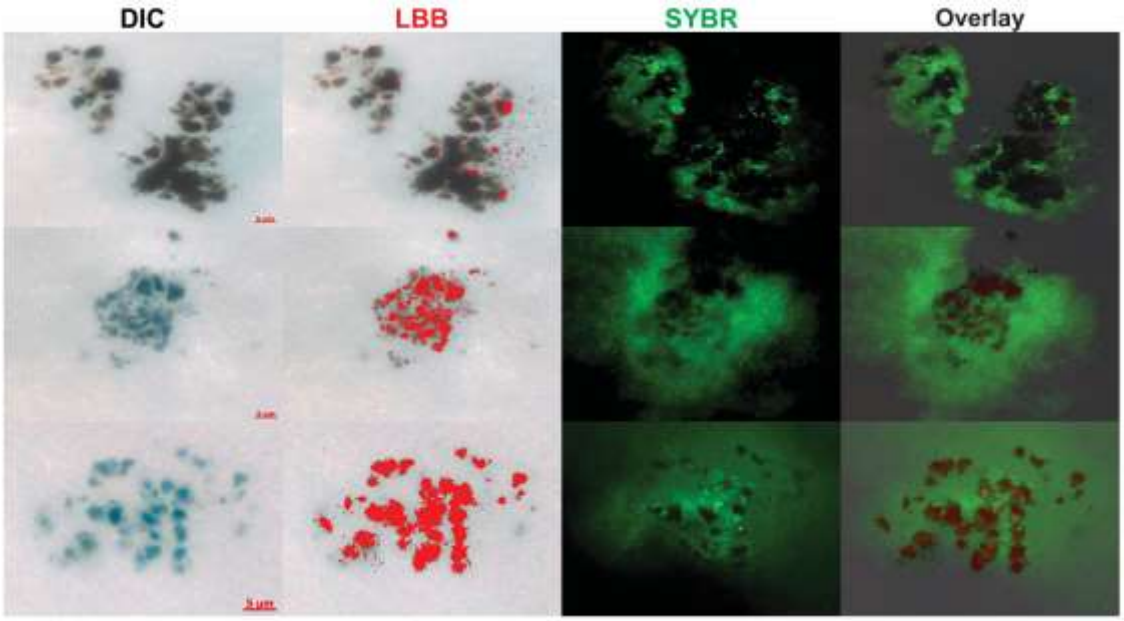

Figure 13. Simul-staining of the freshwater gammaproteobacterium *Pseudomonas putida* GB-1 and biogenic Mn(III/IV)O_x. Cultures were grown with 200 µM Mn^{2+}. DIC: Mn(III/IV)O_x particles in DIC light with characteristic blue "haloes". LBB: False red color indicates oxidized LBB, as determined through color threshold analysis. "Haloes" or imprints that passed the color threshold indicate the presence of Mn(III/IV)O_x particles. SYBR: Fluorescent image of microbes stained with SYBR Green. Overlay: Image overlay of *LBB* and *SYBR* images showing microbes associated with Mn(III/IV)O_x particles. All scale bars are 5 µm.

1.16.4.2 *Seawater from oxycline of Louisiana Shelf, Gulf of Mexico*

Simul-staining was applied to a water sample from the oxycline of the Louisiana Shelf, northern Gulf of Mexico, USA, where there are high fluxes of Mn^{2+} and Fe^{2+} from anoxic sediments to the water column (Devereux et al., 2015). During *R/V* Pelican cruise PE17-02 on 29 July 2016 at Station 6 (29.1°N, 92.2°W, maximum depth: ~16 m), a 40-mL water sample from 11.6 meter depth (27.7°C, 4-9 µM DO, 0.5 µM NH_4^+, 3.1 µM NO_2^-, 1.2 µM NO_3^-) was filtered and preserved as described in Kitzinger et al. (2019). The filter was stored at -20°C until prepared and analyzed as described in Steps 1-7.

Simul-staining revealed the presence of several cell morphologies (**Fig. 14**), including small cocci and larger, curved rods. The small cocci were inferred to be *Thaumarchaeota* and larger, curved rods were inferred to be *Nitrospina* based on CARD-FISH imaging of filter sections from the same water sample (Kitzinger et al., 2019). Black/brown particles were visible without microscopy on the filter. LBB staining confirmed that the particles were mostly $Mn(III/IV)O_x$. $Mn(III/IV)O_x$ tended to form in large clusters (>20 µm in length) with numerous cells. Overall, simul-staining revealed numerous cells with relatively large and abundant $Mn(III/IV)O_x$ particles, suggesting that samples from the oxycline of the Louisiana Shelf would be promising candidates for co-localization analyses with more powerful methods.

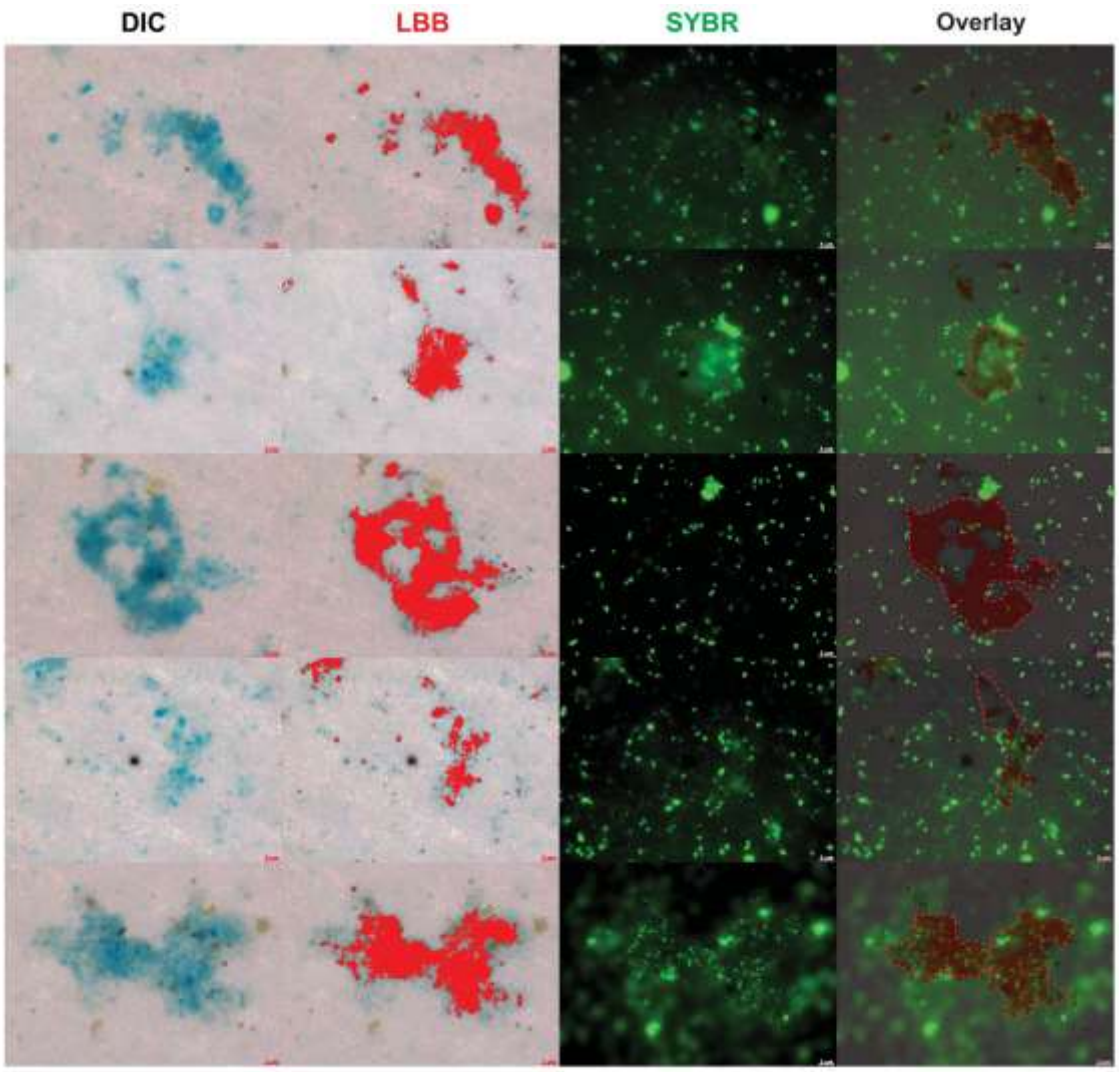

Figure 14. Simul-staining of water from the oxycline of the Louisiana Shelf, Gulf of Mexico, USA. DIC: Evidence of Mn(III/IV)O_x particles as viewed in DIC light. LBB: False red color indicates oxidized LBB, as determined through color threshold analysis. "Haloes" or imprints that passed the color threshold indicate the presence of Mn(III/IV)O_x particles. SYBR: Fluorescent image of microbes stained with SYBR Green. Overlay: Image overlay of *LBB* and *SYBR* images showing high concentrations of microbes and an abundance of large Mn(III/IV)O_x particles. Dashed red line indicates traces of Mn(III/IV)O_x as inferred from *LBB* image. All scale bars are 5 µm.

1.16.5 *Uses and limitations of simul-staining*

We envision the simul-staining method to be integrated into sample workflow as a tool for rapid, low-cost qualitative screening of microbes and Mn(III,IV)O_x-bearing phases

prior to time- and labor-intensive methods such as synchrotron or electron microscopy. Users should be aware of several limitations of the method. First, the method is only applicable to "simple" matrices such as aquatic samples; attempts to apply simul-staining to sediment samples were unsuccessful. Second, because our DIC imaging method uses transmitted light on white polycarbonate filters, image quality may be slightly compromised, especially when mineral matrices are imaged. Third, the method cannot be used to infer structural or compositional information about Mn oxides because LBB will indiscriminately reduce all high-oxidation state Mn-bearing compounds, including permanganate. Fourth, the method is time-sensitive and destructive with respect to Mn oxides: after LBB staining, Mn oxides will have dissolved and oxidized LBB will have faded. Fifth, sample filtration may induce false mineral-microbe associations via electrostatic interactions, so users should be cautious about extrapolations to *in situ* spatial relationships without additional analyses.

1.17 Discussion

Manganese oxides play an important role in global biogeochemical cycles due to their high oxidation state and reactive surface (Cavazos et al., 2018; Hansel, 2017; Hansel et al., 2015; Heil et al., 2015). Additionally, Mn(III/IV)O_x have important roles in remediation of heavy metals and organics (Remucal and Ginder-Vogel, 2014). In this study, we developed a method that couples DIC and epifluorescent microscopy to rapidly screen samples for the presence of microbes and Mn(III/IV)O_x minerals. We have shown that LBB can be used in tandem with nucleic acid dyes on filters, and that LBB's blue color can be detected with image analysis software.

We found preliminary evidence that planktonic microbes co-occur with Mn(III/IV)O_x particles in a marine oxycline. A previous study had reported abundant ammonia-oxidizing *Thaumarchaeota* in the same samples (Kitzinger et al., 2019). *Thaumarchaeota* use hydroxylamine (NH_2OH) as the intermediate during NH_3 oxidation (Vajrala et al., 2013) and NH_2OH has been detected in coastal waters during periods of high rates of nitrification (Butler et al., 1987; Butler et al., 1988; Gebhardt et al., 2004; Korth et al., 2019; Ma et al., 2018; Schweiger et al., 2007). Our previous research has shown that NH_2OH reacts rapidly in seawater with MnO_2, with near-complete conversion to the potent greenhouse gas nitrous oxide (Cavazos et al., 2018 and Ch. 2). We hypothesize that the high flux of nitrous oxide emissions from coastal waters, including the Louisiana Shelf (Kim, 2018; Walker et al., 2010), may be at least partially due to coupled biotic-abiotic reactions between Mn(III/IV)O_x particles and reactive intermediates in nitrogen cycle, such as hydroxylamine similar to reactions in soils (Rue et al., 2018). This hypothesis awaits further testing.

1.18 Comments and recommendations

In addition to the aquatic samples tested thus far with DAPI, the simul-staining method can potentially be applied to diverse environmental samples and used with more-specific fluorescent nucleic acid probes. Below we discuss the feasibility of such applications and potential challenges and solutions associated for each.

1.18.1 *Simul-staining in low-biomass samples*

For low biomass samples, the lack of an antifadent could pose challenges when imaging with DAPI. We found that glycerol-based antifadents “bled out” blue haloes, making

$Mn(III/IV)O_x$ identification difficult (Section 3.4.2.3). For low-biomass samples, users could experiment with glycerol-free antifadent solutions to assess compatibility with LBB. Use of glycerol-free antifadents should prevent "bleeding out" of haloes and allow imaging of low-biomass samples.

1.18.2 *Simul-staining with FISH*

Simul-staining method has the potential to be used with taxon-specific fluorescent *in situ* hybridization (FISH) in addition to non-specific nucleic acid staining. FISH requires that samples be fixed, dehydrated, mounted, and hybridized with oligonucleotide specific probes. Because FISH samples require multiple washings, we recommend that LBB be added after the final washing but before the addition of a glycerol-free antifadent. Simul-staining may also be feasible with gene-specific fluorescent dyes to locate abundant functional genes such as *amoA*, which encodes the ammonia monooxygenase enzyme that converts ammonia to hydroxylamine in the first step of nitrification. Use of simul-staining with catalyzed reported deposition (CARD)-FISH is not possible because CARD-FISH requires hydrogen peroxide for signal amplification, and hydrogen peroxide will reduce $Mn(III/IV)O_x$ (Archibald and Fridvich, 1982; Barnese et al., 2012; Sunda and Huntsman, 1994).

1.18.3 *Using simul-staining in tandem with other spectrophotometric methods*

LBB can be used as a colorimetric method to measure not only particulate-bound Mn(IV) but ligand-bound Mn(III) (Jones et al., 2019). If the filtrate is collected, users can use the method described in Jones et al. (2019) to measure soluble ligand-bound Mn(III) in tandem with microscopic imaging to get a quick, broad understanding of Mn biogeochemistry.

Additionally, the average oxidation state of the particulate Mn(III/IV)O_x can be determined from remaining filter sections as described by Zhu et al. (2017).

A PROPOSED IMPROVEMENT FOR MEASURING HYDROXYLAMINE IN SEAWATER

This work was presented as Lily Sandler's undergraduate thesis which was submitted in Fall 2019. I supervised the work performed by Sandler.

1.19 Abstract

Hydroxylamine (NH_2OH) is a chemical intermediate in the N cycle that can quickly react via biotic and abiotic processes to yield N_2O, a potent greenhouse gas. Because of its high reactivity, NH_2OH tends to be present at low concentrations in aquatic ecosystems. High reactivity and low concentrations also make NH_2OH difficult to measure. Our goal was to improve the method for measuring environmental concentrations of NH_2OH. The current method involves converting NH_2OH to N_2O with ferric ammonium sulfate at low pH and analyzing the N_2O produced by gas chromatography. This method requires a recovery curve because the conversion of NH_2OH to N_2O does not always go to completion. Here, we propose a new method using a Mn oxide mineral pyrolusite, which rapidly oxidizes NH_2OH and completely converts it to N_2O, thus eliminating the need for a recovery curve and sample acidification. The method involves (1) crushing and sieving commercial pyrolusite to increase reactive surface area; (2) adding crushed pyrolusite to airtight bottles containing NH_2OH in artificial seawater at neutral pH; (3) incubating for two hours; and (4) analyzing the oxidized product, N_2O, by gas chromatography. Hydroxylamine concentrations are calculated from the concentration of N_2O in headspace before and after pyrolusite addition. Addition of crushed pyrolusite resulted in complete conversion of

NH_2OH to N_2O within two hours, whereas minimal conversion occurred without pyrolusite. This method has a shorter reaction time and goes to completion, allowing for more rapid and accurate measurements of NH_2OH in aquatic environments.

1.20 Introduction

Nitrous oxide is a greenhouse gas with 250 times the warming potential of carbon dioxide over a 100-year period (IPCC, 2007). Approximately one-quarter of global atmospheric N_2O is emitted from the oceans (Davidson and Kanter, 2014). Nitrification, the microbial oxidation of NH_3 to NO_2^- and NO_3^-, produces N_2O as a by-product. A key intermediate in the first step of nitrification is NH_2OH (Zhu-Barker et al., 2015). Because NH_2OH is highly reactive, it is typically undetectable in natural waters, though it has been detected in coastal seawater during periods of intense nitrification (Butler et al., 1987; Butler et al., 1988; Gebhardt et al., 2004; Liu et al., 2017b). In natural waters, NH_2OH is typically present in the range of 1 to 250 nM and is thought to play a role in N_2O production via biotic and/or abiotic processes (Zhu-Barker et al., 2015). The production of N_2O could occur as a side reaction of nitrification if NH_2OH leaks out of cells and reacts with other species before further oxidation during nitrification. This pathway could potentially serve as a significant source of N_2O production from oceans (Kozlowski et al., 2016a).

Abiotic transformation of NH_2OH to N_2O occurs in soils (Heil et al., 2015; Liu et al., 2017a; Rue et al., 2018) and seawater (Zhu-Barker et al., 2015). Additionally, NH_2OH, a strong reductant, can react quickly and to completion with manganese oxides, a group of strong oxidants, to produce N_2O (Cavazos et al., 2018; Rue et al., 2018).

Manganese oxides are ubiquitous in nature and tend to accumulate at oxic-anoxic interfaces where soluble dissolved Mn^{2+} meets oxygen-rich waters (Lam et al., 2018). Nitrification also peaks at oxic-anoxic boundaries, where NH_2OH can reach concentrations upwards of 200 nM (Butler et al., 1987; Gebhardt et al., 2004). Even in low quantities, NH_2OH and Mn oxides can react rapidly to produce N_2O to near completion at circumneutral pH (Cavazos et al., 2018; Rue et al., 2018) according to Eq. 3. Hydroxylamine chemo-oxidation has been identified in soil, but not in the ocean due to the difficulties involved with measuring low NH_2OH concentrations in seawater.

Hydroxylamine is a chemical relevant to many fields of science, including, but not limited to, geochemistry, soil chemistry, and pharmaceuticals. Thus, many methods have been developed to quantify NH_2OH (**Table 5**). These methods use gas chromatographic and spectrophotometric techniques. Methods developed for natural samples (e.g. soil and natural waters) are optimized for nanomolar concentrations typical for natural environments. The most commonly used method for measuring NH_2OH in natural waters at nanomolar concentrations involves collecting samples in airtight bottles, injecting glacial acetic acid and then ferric ammonium sulfate solution to convert NH_2OH to N_2O, and analyzing the sample headspace by gas chromatography with Electron Capture Detector (GC-ECD). Because the reaction of acidic ferric ammonium sulfate and NH_2OH does not always go to completion, with yields ranging from 20 to 80% (Butler and Gordon, 1986), a recovery curve must be created to infer the actual NH_2OH concentration in the samples (Butler and Gordon, 1986). The recovery curve requires additional sample volume and introduces extra steps, creating more room for error. These issues have made

widespread NH_2OH measurements elusive and hindered a deeper understanding of the biogeochemical role of NH_2OH.

A more effective and streamlined method for NH_2OH quantification could expand our understanding of the role of NH_2OH in ocean biogeochemistry by enabling NH_2OH to be more commonly measured in addition to standard N species (NO_3^-, NO_2^-, NH_3, etc.). The current method for NH_2OH quantification has been the standard since its development by von Breymann et al. (1982) and has been optimized for various environments, including sediments and seawater, but remains relatively unchanged. Because NH_2OH is rapidly oxidized to completion by Mn oxides at neutral pH (Cavazos et al., 2018; Rue et al., 2018), we propose to improve the current method by using Mn oxides in place of Fe(III). This change would eliminate the need for a recovery curve, prevent the need to acidify the sample, and reduce the amount of inherent error in the method by reducing the number of steps. Here, we provide an improvement to the GC method by replacing iron with a commercially available Mn oxide. Complete conversion of NH_2OH to N_2O occurs within two hours without the need for sample acidification.

Table 5. Established methods for quantifying NH_2OH. These methods use gas chromatography or spectrophotometry. Only the ferric ammonium sulfate method can detect low nanomolar concentrations.

Instrument	Oxidant	Chemical Measured	Absorption Peak (nm)	Sample Stability (hrs)	Sample Type	Quantification Range (µM)	Reference
Spectrophotometer	8-Quinolinol	5.8-quinolinequinone-5-(8-hydroxy-5-quinolylimide)	705	0.5	Varied	50,000	Frear and Burrell (1955)
	Sodium Arsenate	Nitrite	545	3	Pharmaceutical	N/A	Deepa et al. (2004)
	Iodate		530	N/A	Soil	3-27	Danilina and Buskina (2017)
	Iodine		543	2-3	Seawater	0.5-91	Fiadeiro et al. (1967); Strickland and Parsons (1972)
	Bromide	Bromine	520	N/A	Pharmaceutical	6	George et al. (2007)
Gas chromatograph with ECD detector	Ferric ammonium sulfate	Nitrous oxide	N/A	384	Aqueous	0.0012-0.560	Koch and Bange (2013); von Breymann et al. (1982)
	Iron(III) chloride hexahydrate			N/A	Soil	> 0.3 µg N kg^{-1} dry soil	Liu et al. (2014)

1.21 Methods

1.21.1 *Preparation of synthetic ocean water*

All serum bottles, stoppers, and Falcon tubes were cleaned with dilute oxalic acid and rinsed thoroughly with MilliQ 18.2 MΩ-cm water. Synthetic Ocean Water (SOW, pH 7.8) was prepared according to the protocol of Morel et al. (1979) using MilliQ 18.2 M Ω-cm water. No trace metals were added to SOW. The pH of the SOW was adjusted to 7.8 using KOH.

1.21.2 *Preparation of pyrolusite solution*

Pyrolusite (Millipore Sigma, catalog # 805958) was crushed to a fine powder using a mortar and pestle that were cleaned with dilute oxalic acid, rinsed thoroughly with 18.2 MΩ-cm water, and dried prior to use. After thorough crushing, the pyrolusite was sieved (106 μm; Fischer Scientific USA Standard Testing Sieve) to increase the reactive surface area. The <106 μm pyrolusite fraction was stored in a 10-mL Falcon tube prior to use. On the day before the experiment, a pyrolusite suspension (200 mM) was prepared in a serum bottle containing 25 mL SOW for later injection into experimental bottles. The pyrolusite suspension was placed in the shaker at 115 rpm to allow the surface of pyrolusite to equilibrate with the ions in SOW.

1.21.3 *Experimental design and procedure*

On the day of the experiment, a 1 M solution of $NH_2OH{\cdot}HCl$ (Acros Organics) was prepared in SOW and diluted to 10 or 100 μM working stocks. In 37 mL serum bottles, final concentrations of 50, 100, 500, or 1000 nM NH_2OH were prepared from the working

stocks. The final volume in each bottle was 25 mL with 12 mL headspace. Bottles were immediately sealed with thick butyl rubber stoppers and aluminum crimps.

To initiate the incubation, 0.25 mL of 200 mM pyrolusite solution was injected via a plastic syringe into select incubation bottles for a final concentration of 20 mM pyrolusite. The pyrolusite solution was shaken immediately prior to each extraction to obtain a consistent concentration of pyrolusite with each injection. Larger gauge needles (≤20 gauge) are necessary for pyrolusite extraction; >23-gauge needles caused larger particles to get lodged in the needle. All samples were stored upside down in the dark in a shaker (New Brunswick Scientific, Excella E24 Incubator Shaker) at 30°C at 115 rotations per minute for two hours.

1.21.4 *Gas chromatography*

The samples were analyzed for headspace N_2O with a GC-ECD (SRI 8610C). Glass airtight syringes were used for all injections. A calibration curve was created with 6 to 7 points using ultra-high purity (UHP) N_2O calibration gas (Scotty Brand Transportable 17L). For each sample, the volume of air to be analyzed was injected into the bottle and then extracted from the bottle to conserve atmospheric pressure in the bottle. All injections and extractions were performed using airtight syringes. The N_2O peak areas of each of these samples were recorded at 2.6 min of a 3.5 min total run-time.

1.21.5 *Calibration and calculations*

For the calibration curve, moles of gas (based on volume injected) and peak area were plotted against each other, and the slope of the line was obtained to calculate the nanomoles

of N_2O per 1 mL gas injected. Then, Eq. 22 was used to calculate the concentration of N_2O per 12 mL of headspace:

$$(nmols/12\ mL\ HS) = (nmols/1\ mL\ gas\ injected) \times \frac{(12\ mL\ HS)}{(x\ mL\ gas\ injected)} \quad (22)$$

where *HS* is the headspace of the bottle. The Bunsen coefficient, β, of 0.01818 ml L^{-1} atm^{-1} was used based on a salinity of 35 ppt and a temperature of 30˚C from Weiss and Price (1980).

The total number of moles of N_2O in the bottle, n_{N_2O}, is equal to the number of moles of N_2O in the water ($n_{N_2O_W}$) plus the number of moles of N_2O in the headspace ($n_{N_2O_{HS}}$) (Eq. 23).

$$n_{N_2O} = n_{N_2O_W} + n_{N_2O_{HS}} \quad (23)$$

The concentration of N_2O in the bottle (mol L^{-1}) was obtained by dividing n_{N_2O} by the volume of water in the bottle (V_w) (Eq. 24).

$$[N_2O] = \frac{n_{N_2O}}{V_w} \quad (24)$$

The number of moles of N_2O in the headspace was obtained by multiplying the partial pressure of N_2O in the headspace ($P_{N_2O_{headspace}}$) by the volume of the headspace (V_{HS}) in liters (L), and dividing by the ideal gas constant (0.08206 L atm mol^{-1} K^{-1}) and the temperature of the solution in Kelvin (Eq. 25).

$$n_{N_2O_{HS}} = \frac{P_{N_2O_{HS}} V_{HS}}{R(298.15\ K)} \quad (25)$$

The number of moles of N_2O in the water was obtained by multiplying the partial pressure of N_2O in the headspace ($P_{N_2O_{HS}}$) by the ratio of the water to headspace volumes ($\frac{V_W}{V_{HS}}$) and the Bunsen coefficient for N_2O, and dividing by the ideal gas constant (0.08206 L atm mol^{-1} K^{-1}) and the temperature of the solution in Kelvin (Eq. 26).

$$n_{N_2O_W} = \beta \frac{P_{N_2O_{HS}} \times \frac{V_W}{V_{HS}}}{R \times (298.15\ K)} \quad (26)$$

1.21.6 *Determination of hydroxylamine recovery*

Bottles with solely SOW were analyzed from GC-ECD to quantify the amount of background N_2O in the bottles ($n_{background}$). A background concentration of 80 nM was obtained. Conversion of NH_2OH to N_2O for each bottle ($n_{conversion}$) was calculated by subtracting the background N_2O from the total N_2O (n_{N_2O}) obtained from each sample.

1.22 Results

Complete conversion of NH_2OH to N_2O occurred within two hours in all bottles with pyrolusite. Bottles without pyrolusite had little to no conversion to N_2O (<1%). Bottles with pyrolusite had significant conversion (161 ± 76%). Complete conversion occurred in all trials, from 50 nM to 1 μM NH_2OH (**Fig. 15**), suggesting that this method is as sensitive as the von Breymann method (**Table 5**). Percent recovery varied based on whether the bottles without pyrolusite added or average background N_2O was used. The average

concentration of N_2O in the laboratory was 80 nM, but values varied from 50 to 114 nM N_2O. Percent error of NH_2OH recovery using the lab average background N_2O ranged from 2-420%, while percent error using values from bottes with no pyrolusite ranged from 1-600%. Highest percent error occurred in 10 nM NH_2OH bottles, with 1000 nM NH_2OH bottles had lowest percent error in recovery. Any conversion in bottles without pyrolusite was attributed to autooxidation of NH_2OH or varying background levels of atmospheric N_2O in the laboratory.

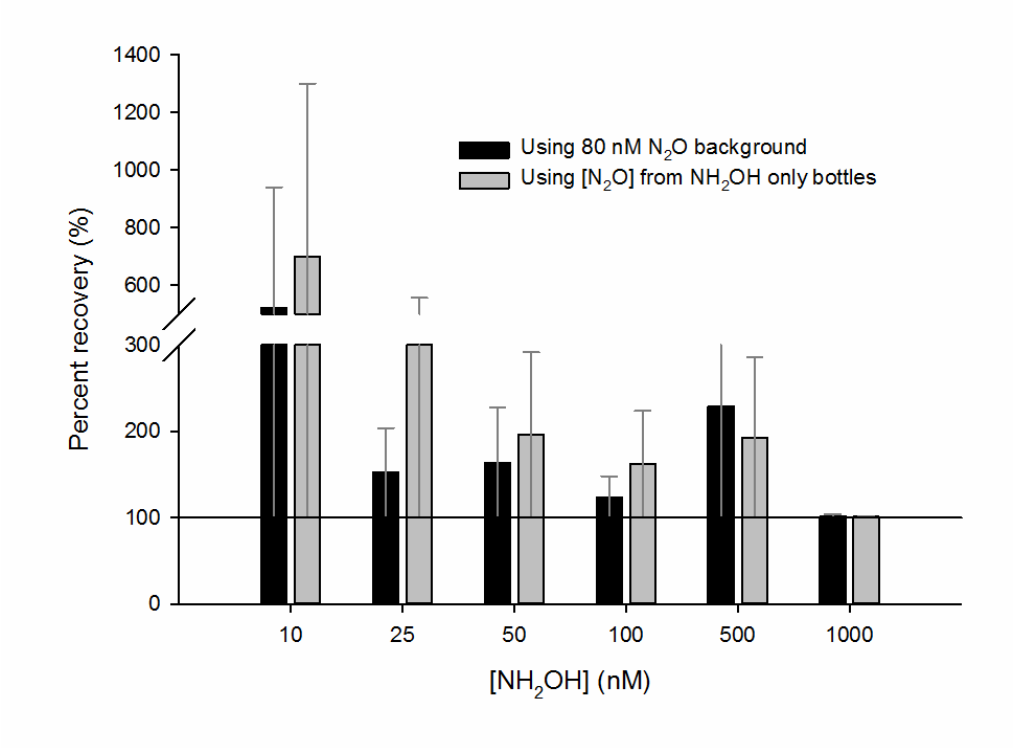

Figure 15. Percent NH_2OH recovery using different background values of N_2O. Error bars represent percent error (n = 3 or 4).

1.23 Discussion

Any N_2O conversion in the negative controls beyond the calculated background N_2O is the result of autooxidation of NH_2OH, as NH_2OH is known to autooxidize to form

N_2O over time (Cooper et al., 1970). Up to 35% of NH_2OH has been found to autooxidize in oxic environments (Moews and Audrieth, 1959). Another possible source of error is in the varying levels of N_2O in the laboratory. Any conversion in the bottles with pyrolusite added that had N_2O headspace concentrations exceeding the autooxidation values detected in the bottles with no pyrolusite added could be due to conversion by pyrolusite.

The sensitive detection limit of this method is essential to understanding NH_2OH in marine environments, as it is typically present in nanomolar concentrations. The proposed method may be prone to wide error margins in low concentrations of NH_2OH, as was observed with the wide range of percent conversion in 10 and 25 nM NH_2OH. The detection limit of this method still allows for the measurement of nanomolar levels of NH_2OH, but may not be as sensitive as the original method developed and improved by von Breymann et al. (1982) and Butler and Gordon (1986), respectively.

This simplified method for quantifying NH_2OH will allow for more detailed investigation into global aqueous concentrations of NH_2OH and its potential contribution to abiotic production of N_2O. While the role of NH_2OH in N_2O production has been shown in terrestrial environments (Heil et al., 2015; Liu et al., 2017b), NH_2OH in oceanic environments is scarcely studied (Zhu-Barker et al., 2015). A simplified, more time-efficient method should allow for more widespread measurements of NH_2OH in marine systems and allow elucidation of the role NH_2OH plays in oceanic N_2O emissions. A better understanding of this pathway could help scientists to develop improved models for both marine and global N_2O production.

This method is a significant improvement when compared to other methods. Unlike the current von Breymann method for NH_2OH conversion via ferric ammonium sulfate, this Mn oxide-based method requires no recovery curve, does not require sample acidification, and greatly reduces reaction time for conversion to N_2O. These factors should allow for greater ease in analysis and application to natural samples.

Our method used pyrolusite because it is shelf-stable, and preparation of the crushed and sieved powder only takes a matter of minutes. Other forms of Mn oxides might be suitable as oxidants, if they are stable and equilibrated with the solution. It should be noted that different Mn oxide minerals are known to change structure over time. For example, birnessite would be an ideal candidate to use for this method if not for its limitations of stability and preparation. It is known to react rapidly and to completion with NH_2OH within minutes (Cavazos et al., 2018). However, birnessite must be synthesized and is only reactive for a matter of days, making it inconvenient for everyday laboratory use or prolonged sampling trips. Because of the variability in reactivity and storage life of different Mn minerals, any Mn mineral of interest should be tested using the proposed method with known concentrations of NH_2OH before application to environmental samples.

1.24 Conclusions

We present an improved method to measure NH_2OH in aqueous samples using GC-ECD that replaces ferric ammonium sulfate with pyrolusite. Using pyrolusite reduces reaction time, results in complete conversion of NH_2OH to N_2O, and removes the need for sample acidification and the construction of a recovery curve. These improvements reduce

the overall time of analysis and reduce the amount of sample volume required. The most challenging aspect of this proposed improvement is ensuring that the injected pyrolusite remains suspended in solution so that concentrations remain consistent in each bottle.

Our method makes NH_2OH analysis easier and more efficient, which should allow for more widespread measurements of oceanic NH_2OH. As the role of NH_2OH in N_2O production is being studied in terrestrial environments (Heil et al., 2015; Liu et al., 2017b), studies in marine systems are limited (Zhu-Barker et al., 2015). It has been suggested that NH_2OH reacting rapidly with Mn oxides could be a significant source of oceanic N_2O (Cavazos et al., 2018). More thorough measurements of marine NH_2OH are needed to better estimate the contribution of oceanic N_2O from NH_2OH interactions.

While this method has proven successful in laboratory conditions and solutions, future work is needed to test this method's applicability to environmental samples. The true value of this method is in its ability to facilitate a deeper understanding of where NH_2OH exists in aqueous bodies and in what concentrations. Environmental samples would need to be injected with mercury or zinc chloride to ensure complete eradication of biotic activity within the bottles. Complications could arise from possible adsorption of the mercury or zinc chloride to the pyrolusite surface (Thanabalasingam and Pickering, 1985), which could lead to error in N_2O measurements if microbes capable of producing N_2O are not killed due to the adsorption of mercury or zinc chloride onto the pyrolusite.

CONCLUSIONS

This dissertation investigated the potential role that coupled biotic/abiotic N-Mn interactions play in marine N_2O emissions. A rate law and constant for N_2O production from NH_2OH chemo-oxidation in modern marine conditions were obtained by microsensors and colorimetry. Using LBB in tandem with SYBR Green on white filters allows for rapid visualisation of $Mn(III/IV)O_x$ particles and microbes, thus providing a useful "pre-screen" to determine which samples would be worth more extensive, time-consuming analysis. Because NH_2OH chemo-oxidation is so rapid, substituting iron for $Mn(III/IV)O_x$ greatly reduces time of analysis, negates the need for a recovery curve, and provides greater accuracy for NH_2OH measurements in marine waters. Additionally, it was shown that abiotic N_2O production from NH_2OH chemo-oxidation is more rapid than from microbial denitrification, except at extremely low $Mn(III/IV)O_x$ concentrations. The work presented in this dissertation shows that reactive nitrogenous intermediates such as NH_2OH could play a role in marine N_2O production (**Fig. 16**) and lays the groundwork for assessing the importance of marine N_2O emissions from the coupling of biotic and abiotic processes in the N and Mn cycles.

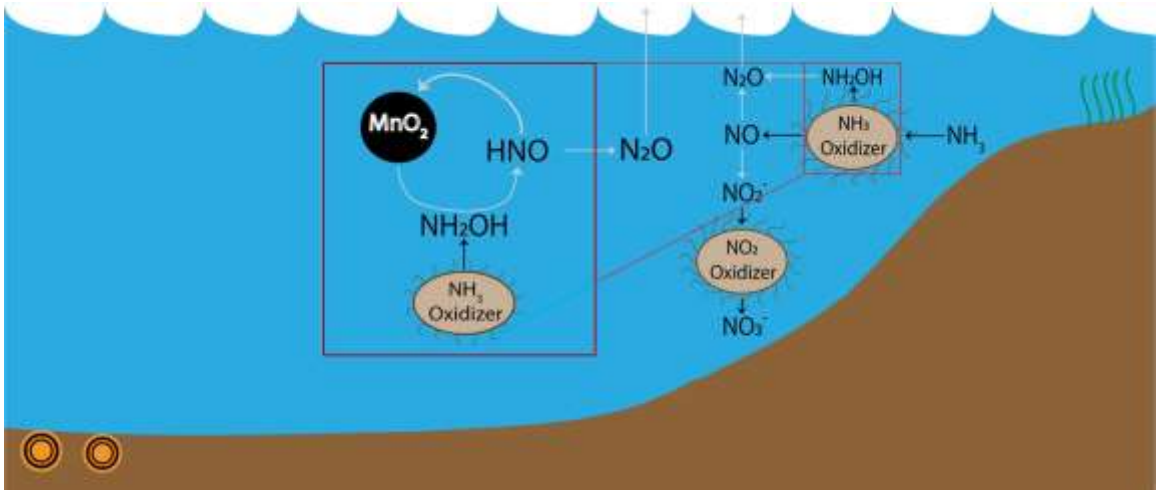

Figure 16. The abiotic oxidation of the nitrogenous intermediate, NH_2OH, by $Mn(III/IV)O_x$ in marine water column. Hydroxylamine leaks out of NH_3-oxidizing microbes to rapidly react with $Mn(III/IV)O_x$ to produce N_2O. Association of microbial cells and $Mn(III/IV)O_x$ particles in the OMZ of the Gulf of Mexico provide evidence for this process in marine environments.

5.1 Assessing the importance of N-Mn interactions in marine N_2O production

Coupled biotic/abiotic interactions between the N and Mn cycles are important for terrestrial N_2O emissions (Heil et al., 2015). In marine environments, the relatively lower concentrations and densities of NH_3-oxidizing microbes and $Mn(III/IV)O_x$ would suggest that these interactions are less relevant than in soils. This dissertation showed (1) that the reaction between the nitrogenous intermediate NH_2OH and $Mn(III/IV)O_x$ is extremely rapid in seawater and (2) that microbial cells and $Mn(III/IV)O_x$ particles accumulate at the interface between oxic and anoxic seawater. The rate of production of N_2O from abiotic NH_2OH chemo-oxidation compared to that of nitrification or denitrification suggests possible cryptic cycling even with low concentrations of $Mn(III/IV)O_x$ and NH_2OH.

5.2 Reactivity vs. abundance: Mn and Fe in N_2O production in marine environments

Particulate Fe and Mn concentrations tend to be low in marine waters because they sink as part of marine snow. In a transect of the North Atlantic Ocean at similar depths, maximum particulate Fe concentrations were similar at 47.1 nM, but particulate Mn was significantly lower at 0.05 nM (Lam et al., 2015). Concentrations of Fe and Mn oxides peaked near the East Pacific Rise hydrothermal plume (44.1 nM and 5.2 nM, respectively; Lam et al., 2018). In the upper 150 m of the North Atlantic water column, particulate Fe reaches 9 nM and particulate Mn peaks at 1.25 nM (Twining et al., 2015). Typically, particulate Fe concentrations are higher than particulate Mn, but how rapidly they are cycled throughout the water column affects their availability for abiotic interactions.

It is generally assumed that the higher concentration of particulate Fe makes it more available for coupled interactions with the N cycle. However, in the Eastern Pacific, dissolved Mn from hydrothermal vents has a residence time ranging from one month to a year (Mandernack and Tebo, 1993), compared to 100-200 years for Fe (Johnson et al., 1997). After the dissolved Mn^{2+} oxidized, the particulate $Mn(III/IV)O_x$ sinks and is rapidly reduced in sediments. The dissolved Mn^{2+} again becomes mobile and fluxes back into the water column, creating a "Mn conveyer belt" along the continental shelf (Brumsack, 2006; Klinkhammer and Bender, 1980). Oxidized Mn particles can then accumulate just below the oxycline (Brumsack, 2006), allowing for the possibility of reduction by NH_2OH from ammonia-oxidizers (Ch. 3).

Iron has long been known to be coupled to the N cycle. In anoxic marine waters and sediments, Fe^{2+} can reduce NO_2^- to N_2O through chemodenitrification (Picardal, 2012). Particulate Fe(III) can oxidize NH_2OH to N_2O in oxic waters and sediments (Butler et al., 1987; Butler et al., 1988; Gebhardt et al., 2004; Law, 2008; Schweiger et al., 2007; Zhu-

Barker et al., 2015). Coupled N-Fe interactions tend to be kinetically slow in most marine environments, with reaction times ranging from hours (Buchwald et al., 2016; Kampschreur et al., 2011; Moraghan and Buresh, 1977) to days (Buchwald et al., 2016; Grabb et al., 2016; Rue et al., 2018). NH_2OH chemo-oxidation by $Mn(III/IV)O_x$ occurs within minutes (Ch. 2) to hours (Rue et al., 2018) in circumneutral marine conditions, suggesting an important role in biogeochemical cycling with the N cycle.

5.3 Future Directions

The coupling of Fe and N in N_2O production has long been considered in biogeochemical studies due to the relative abundance of Fe on the Earth surface. But given the difference in kinetic reaction rates of NH_2OH chemo-oxidation by Fe(III) and $Mn(III/IV)O_x$, future studies and models should investigate how reactivity and abundance affect microbe-mineral interactions and subsequent N_2O emissions.

The high reactivity of $Mn(III/IV)O_x$ particles has long been a subject of interest in geochemistry and its relevance has long been known. Other interactions between the N and Mn cycles could include the possibility of AOA or AOB using $Mn(III/IV)O_x$ for extra-cellular detoxification. One such example could be in ferromanganese nodules where AOA serve as a source of fixed carbon and co-localize with Mn^{2+}-oxidizers in what could be a symbiotic relationship.

The importance of reactive intermediates in biogeochemical cycles has long been recognized, but measurements of these intermediates are generally few and scattered. Hydroxylamine has only been measured in a few oceanic locations (Zhu-Barker et al., 2015 and Table 6), and particulate $Mn(III/IV)O_x$ is generally assumed to not remain suspended

in the water column. Future work should focus on measuring NH_2OH and $Mn(III/IV)O_x$ in areas where NH_2OH chemo-oxidation by $MnO(III/IV)O_x$ is likely to occur, such as oxyclines or estuaries with high N input. These measurements can then be used in N_2O oceanic emission models.

Table 6. Hydroxylamine concentrations in various environments.

Location	NH_2OH concentration	Reference
Oregon coast	<1-8 nM	von Breymann et al. (1982)
Yaquina Bay, Oregon	<1-250 nM	Butler et al. (1987)
Big Lagoon, California	<1-175 nM	Butler et al. (1988)
Baltic Sea	2-179 nM	Gebhardt et al. (2004)
Southwestern Baltic Ocean	<19 nM	Schweiger et al. (2007)
Southwest Indian Ocean	<6.76 nM	Ma et al. (2018)
Equatorial Atlantic	2-9.5 nM	Korth et al. (2019)
Open ocean ETSP	0.6-23.8 nM	Korth et al. (2019)
Norway spruce forest	0.3-35 µg N kg^{-1} dry soil	Liu et al. (2014)
Norway spruce forest	1.72-11.1 µg N kg^{-1} dry soil	Liu et al. (2016)

Current models of marine N_2O emissions assume solely biotic sources of N_2O. Therefore, kinetic rate laws of abiotic reactions that produce N_2O cannot currently be applied to marine systems. The work in this dissertation suggests that abiotic sources of N_2O contributes to marine N_2O emissions. Future models of marine N_2O emissions could incorporate the rate law and constant derived from this dissertation. These models could be better constrained once additional measurements of NH_2OH and $Mn(III/IV)O_x$ are made in various marine water columns. Marine N_2O production is complex and can originate from various sources and future models should consider incorporating coupled biotic-abiotic interactions.

APPENDIX A. NITROUS OXIDE PROFILES FROM SHELF SEDIMENTS IN CAPE HATTERAS, NC

This work was done to find evidence of chemodenitrification in natural marine sediments. High-resolution N_2O profiles were correlated with other nutrients/parameters to access the possibility of chemodenitrification.

A.1 Sample site

Sediment cores were collected aboard the *R/V Savannah* in July 2015 from the continental slope near Cape Lookout, North Carolina. Sampled cores were from collected the mid-slope (500-700 m depth). A more detailed site description is provided in Eitel et al. (2020). Cores were named after site names, which were HAT5, HAT11, and HAT12.

A.2 Materials and methods

Sediment cores were collected using a single corer (Eitel et al., 2020) or MC-800 multicorer (Ocean Instruments, Inc.). Nitrous oxide was measured in overlaying water 1 mm above the water-sediment interface to 0-40 mm below the surface every millimeter using a 500 µm diameter N_2O microsensor electrode and multimeter (Unisense, Aarhus, Denmark) mounted on a micromanipulator. Core The microsensor was calibrated according to manufacturer's protocol using N_2O-saturated MilliQ 18.2 MΩ water. All other parameters were measured as described in Eitel et al. (2020).

A.3 Results

High-resolution depth profiles of N_2O concentrations were measured for three cores. Generally, N_2O was undetectable in the upper oxic zone (~0-10 mm) and increased below 10 mm, where O_2 was undetectable. The highest N_2O concentration was approximately 0.5 µM at 18 mm sediment depth at HAT11. At HAT11 and HAT12, two N_2O peaks are observed, with highest concentrations occurring at 19 and 38 mm, respectively. In the overlying water, low levels of N_2O ($\leq$ 0.1 µM) were measured at HAT5 and HAT12.

Substrates that could contribute to chemodenitrification were checked for correlation to measured N_2O. Nitrate concentrations typically ranged from 10 to 32 µM, with no discernable correlation to N_2O concentrations. Core 5 was the only core that had NO_2^- measured, and none was detected. In cores 11 and 12, Fe(II) concentrations appeared to peak just before N_2O peaked. When N_2O concentrations start decreasing, Fe(III) appeared to increase.

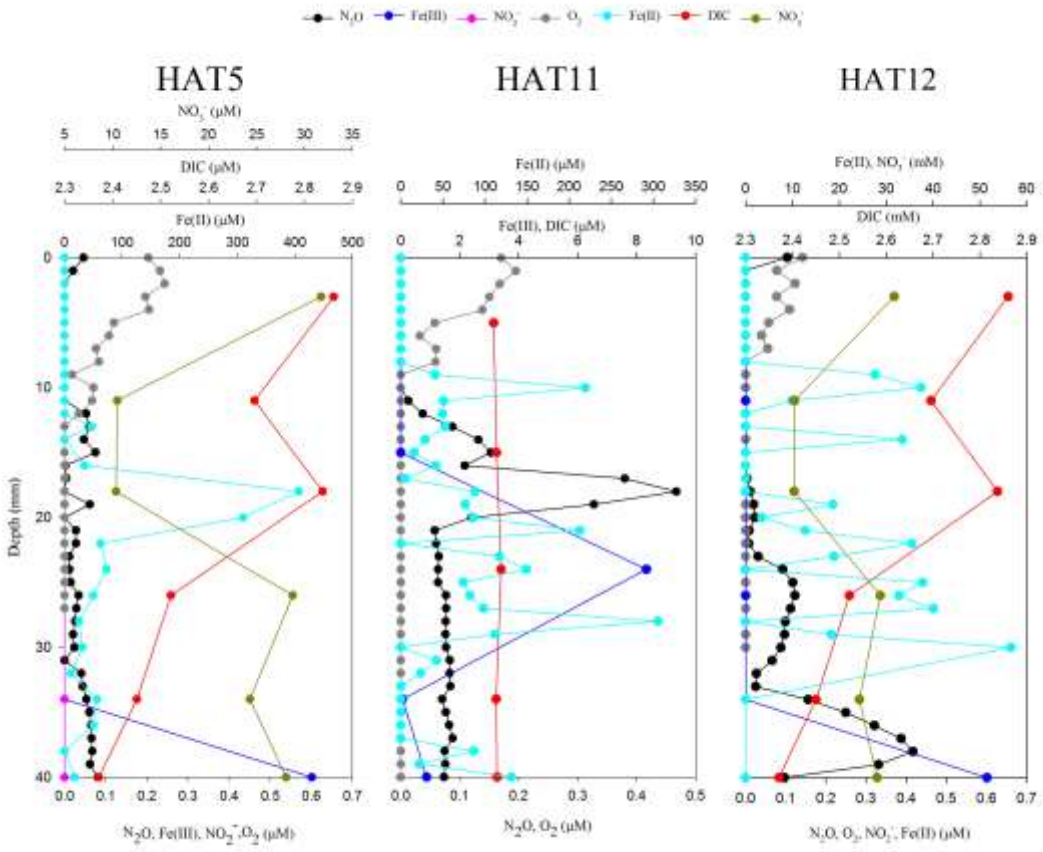

Figure A1. Profiles of N_2O, Fe(II), Fe(III), DIC, NO_2^-, NO_3^-, and O_2 from three sediment cores collected from Cape Hatteras, NC (HAT5, HAT11, and HAT12).

APPENDIX B. INTERACTIONS OF MANGANESE (III) WITH AMMONIA

This work was part of another study, "Novel insights into the taxonomic diversity and molecular mechanisms of bacterial Mn(III) reduction", currently in revision for Environmental Microbiology Reports, by Nadia Szeinbaum, Brook L. Nunn, Amanda R. Cavazos, Sean A. Crowe, Frank J. Stewart, Thomas J. DiChristina, Christopher T. Reinhard, and Jennifer B. Glass. These experiments were done as abiotic controls to confirm the biotic source of N_2O from microbial incubations.

B.1 Materials and methods

All glassware was washed with 1.2 N HCl to minimize metal contamination. Incubations were done in 160 mL glass serum bottles. All bottles were filled with 80 mL of 200 µM NH_4^+ (ammonium chloride, Sigma Aldrich, USA). Half of the bottles were amended with 1 mM acetate-free Mn(III)-pyrophosphate (Kostka et al., 1995). After all solutions were added to the bottles, they were immediately stoppered with blue butyl stoppers (Geo-Microbial Technologies, Ochelata, OK, USA) and crimped with aluminium crimps. Bottles were stored upside down at room temperature in the dark to minimize loss of N_2O and photochemical reactions. Another set of bottles had 2 mL of solution withdrawn for colorimetric analysis of NH_4^+. The incubation lasted for 22 days with measurements occurring every 2-4 days.

Nitrous oxide was measured using a gas chromatograph with electron capture detection (GC-ECD, SRI) with a HayeSep N column. Headspace was sampled via air-tight

glass syringes with 27-gauge needles and injected immediately into the sample port of the GC-ECD. During sampling, atmospheric pressure was maintained by injecting the same volume of air into the bottle that was removed. Calculations were done as described in Section 4.3.5. Ammonia was measured via the method described in Riley (1953).

B.2 Results

For the first half of the incubations, there was, on average, more N_2O in the control bottles (only NH_4^+) than in those amended with Mn(III). During the second half of the incubation, N_2O concentrations appeared to increase in Mn(III)-amended bottles, but that was due to one bottle that had unusually high concentration of N_2O. The error was too high to be significant (Fig. B1). There was little variability in N_2O concentrations during the incubation period within the control bottles. If the bottle with unusually high N_2O concentration was removed from the data, N_2O concentrations appeared to remain the same in the Mn(III) amended bottles. The difference between the controls and Mn(III)-amended bottles was insignificant, and thus not inferred to contribute to N_2O production from NH_4^+ oxidation by Mn(III).

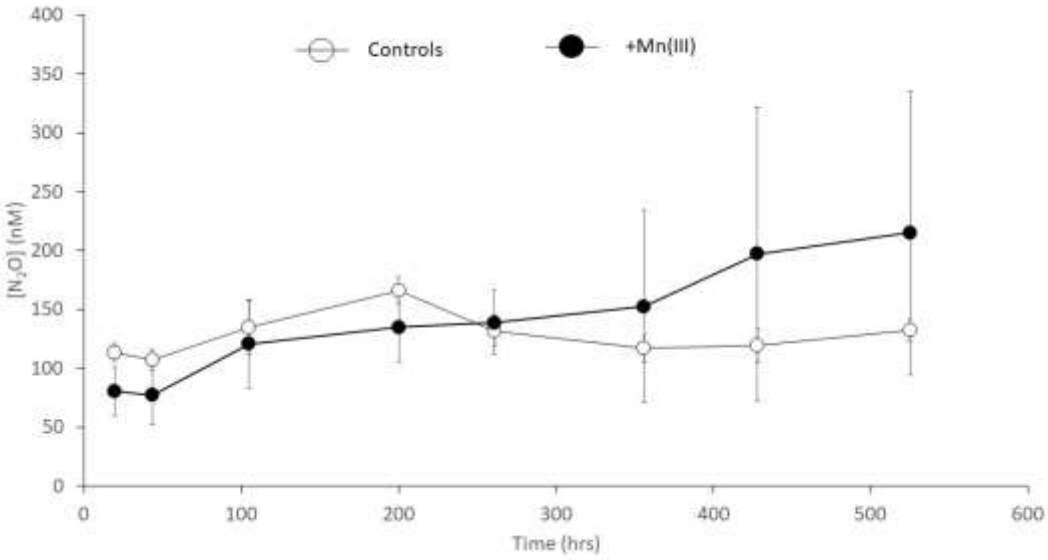

Figure B1. Time series of N_2O in bottle incubations. Control bottles had only 200 µM NH_4^+ and amended bottles (+Mn(III)) had 200 µM NH_4^+ and 1 mM Mn(III). Incubations were done in triplicates.

Ammonium concentrations were generally lower in Mn(III)-amended bottles than those without Mn(III). However, NH_4^+ concentrations tended to remain constant throughout the experiment (Fig. B2).

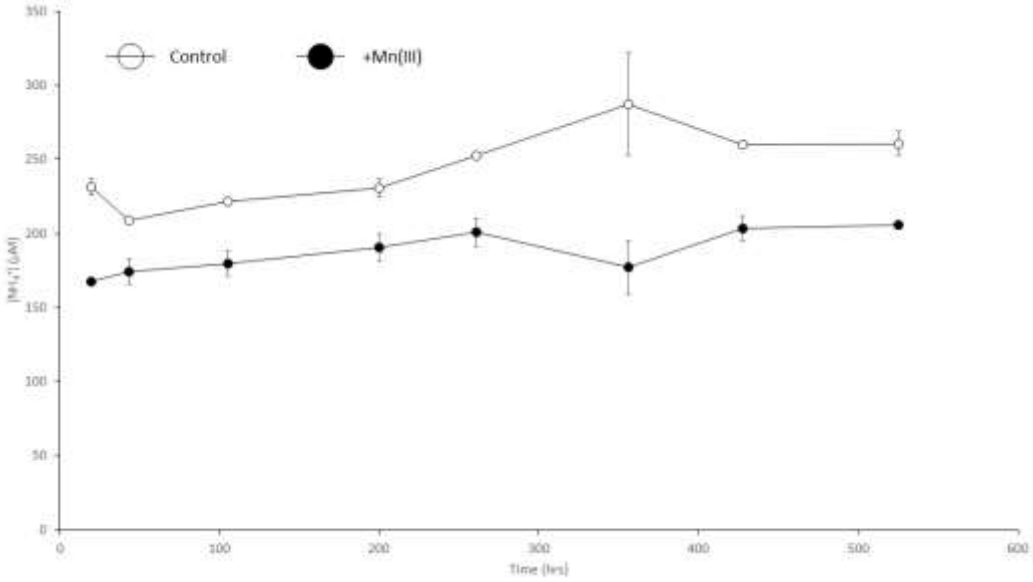

Figure B2. Concentration of NH_4^+ in bottles with no Mn(III) added (open circles) and with Mn(III) added (filled circles). Data from bottles with 200 uM NH_4^+ and 1 mM Mn(III). Bottles were done in duplicates.

B.3 Discussion and Conclusions

These incubations were done to determine the feasibility of abiotic N_2O production from NH_4^+ oxidation by Mn(III). The lack of measurable N_2O production and NH_4^+ depletion suggests that NH_4^+ oxidation by Mn(III) is minimal. Ammonia (NH_3), but not NH_4^+, can adsorb to and react with Mn(III/IV)O_x surfaces to produce hydrazine, which can react with Mn(III/IV)O_x to produce N_2 (Luther III et al., 2018). However, a ligand-bound Mn(III) was used in these experiments, possibly not providing a surface for NH_4^+ to bind to and react. Additionally, the experiments were conducted below the p*K*a of NH_4^+, further reducing reactivity.

APPENDIX C. HYDROXYLAMINE OXIDATION VIA IRON(III)

This was the preliminary work for Ch. 2. The oxidation of NH_2OH by various species Fe(III) was found to be kinetically slow and difficult to elucidate.

C.1 Materials and methods

All solutions were prepared in SOW and acid-cleaned glassware. Nitrous oxide production from NH_2OH oxidation by ferric ammonium ($FeNH_4(SO_4)_2 \cdot 12H_2O$; Sigma-Aldrich, USA), ferrihydrite (Section 3.4.3.1), and ligand bound Fe was measured via microsensor electrode (as described in Section 2.2.2). All experiments were done with excess concentration of all Fe species (at least 2× greater than NH_2OH concentration). All calculations described in Sections 2.3.2 and 2.3.3 were used to determine the orders of reaction with respect to each reactant and rate law, respectively, but replacing MnO_x with a Fe species.

C.2 Results

Maximum percent yield for every Fe species was generally < 1%. The highest percent yield and production rate was from 50 µM NH_2OH with 851 µM ligand-bound Fe (1.6% and 8.4×10^{-9} M N_2O s^{-1}, **Fig. C1**). While most experiments were allowed reaction times of 5-10 min, even when allowed to react for nearly 1 hr N_2O yield was minimal (**Fig. C2**). Maximum N_2O yield and production rate increased when pH was = 4.6 (**Fig. C3a**), conditions not representative of modern oceanic conditions. When ferrihydrite was the used oxidant, N_2O production rates tended to increase with initial NH_2OH concentrations (**Fig. C2**).

In $FeNH_4$ experiments, increasing $FeNH_4$ or NH_2OH concentrations did not significantly increase N_2O production rates or yields. The average production rate from the varied NH_2OH experiments was 2×10^{-10} M N_2O s^{-1} (**Fig. C3a**). When $FeNH_4$ was varied, rates ranged from $1\text{-}3\times10^{-10}$ M N_2O s^{-1} with no general increase with $FeNH_4$ concentrations (**Fig. C3b**) The only increase in N_2O production rate and yield were when pH < 5 (5×10^{-10} M N_2O s^{-1}; **Fig. C3c**). The overall order of reaction within the duration of the experiments (~ 6 min) was zero.

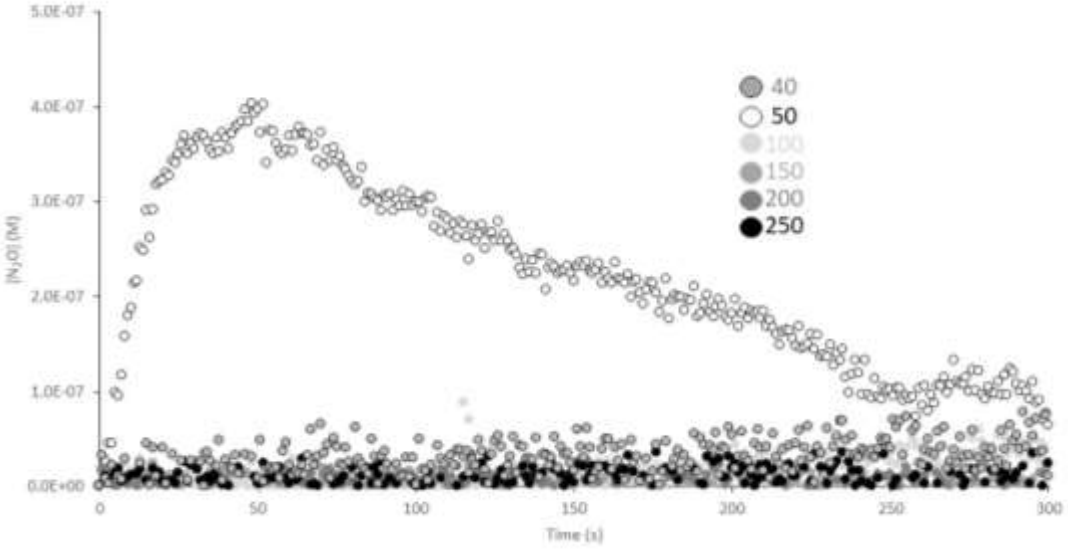

Figure C1. Production rates of N_2O in ligand-bound $FeNH_4$ do not significantly increase with NH_2OH concentrations. All experiments were done in 851 µM ligand-bound $FeNH_4$, pH 7.8, and production measured for 6 min. Legend shows the varied concentrations of NH_2OH in µM.

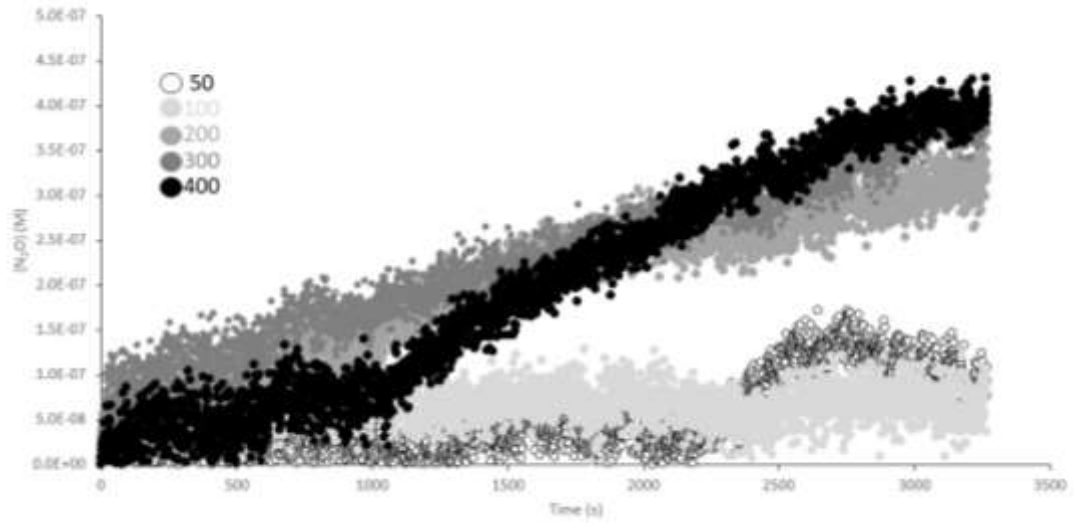

Figure C2. Production of N_2O from ferrihydrite increase with NH_2OH concentration if allowed to react for at least an hour. Experiments were done in 800 µM ferrihydrite at pH 7.9. Legend shows the varied concentrations of NH_2OH in µM.

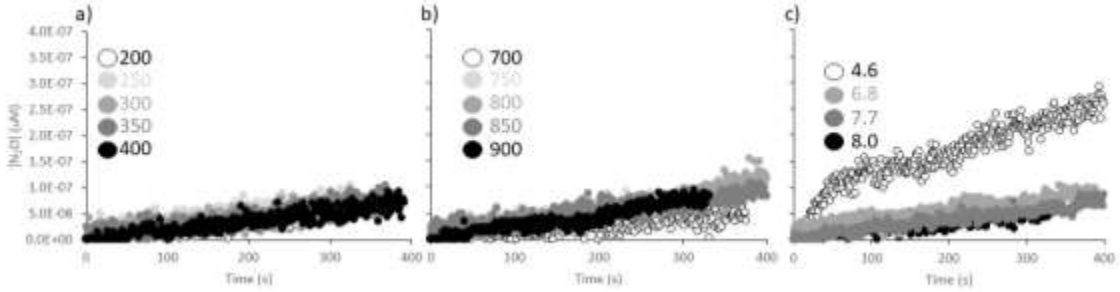

Figure C3. Production of N_2O does not greatly increase with NH_2OH, $FeNH_4$, or H^+ concentrations. (a) N_2O production from varied NH_2OH into 900 µM $FeNH_4$ at pH 7.9. Legend shows the varied concentrations of NH_2OH in µM. (b) N_2O production from varied $FeNH_4$ concentrations with 300 µM NH_2OH. Legend shows the varied concentrations of $FeNH_4$ in µM. (c) N_2O production from 200 µM NH_2OH into 600 µM $FeNH_4$ at varied pH. Legend shows the varied pH levels.

C.3 Discussion

At circumneutral pH, NH_2OH chemo-oxidation by Fe(III) is kinetically slow. Soluble and low-crystallinity Fe(III) did not oxidize NH_2OH to N_2O within the duration of

the experiments. Ferrihydrite was the only form of Fe that had an increase in N_2O production with increasing NH_2OH concentrations. However, N_2O production from ferrihydrite experiments were still significantly slower than birnessite experiments.

REFERENCES

Aller, R. (1990) Bioturbation and manganese cycling in hemipelagic sediments. Philos T R Soc A 331, 51-68.

Anandkumar, B., George, R., Tamilvani, S., Padhy, N. and Mudali, U. (2011) Studies on microbiologically influenced corrosion of SS304 by a novel manganese oxidizer, *Bacillus flexus*. Biofouling 27, 675-683.

Andeer, P., Learman, D., McIlvin, M., Dunn, J. and Hansel, C. (2015) Extra-cellular heme peroxidases mediate Mn(II) oxidation in a marine *Roseobacter* bacterium via superoxide production. Environ Microbiol 17, 3925-3936.

Anderson, C., Johnson, H., Caputo, N., Davis, R., Torpey, J. and Tebo, B. (2009) Mn(II) oxidation is catalized by heme peroxidase in "*Aurantimonas manganoxydans*" strain SI85-9A1 and *Erythrobacter* sp. strain SD-21. Appl Environ Microbiol 75, 4130-4138.

Anderson, J. (1964) The copper-catalysed oxidation of hydroxylamine. Analyst 89, 357-362.

Anschutz, P., Dedieu, K., Desmazes, F. and Chaillou, G. (2005) Speciation, oxidation state, and reactivity of particulate manganese in marine sediments. Chem Geol 218, 265-279.

Archibald, F. and Fridvich, I. (1982) The scavenging of superoxide radical by manganous complexes: *In vitro*. Arch Biochem Biophys 214, 452-463.

Arévalo-Martínez, D., Kock, A., Löscher, C., Schmitz, R. and Bange, H. (2015) Massive nitrous oxide emissions from the tropical South Pacific Ocean. Nat Geosci 8, 530-535.

Babbin, A., Bianchi, D., Jayakumar, A. and Ward, B. (2015) Rapid nitrous oxide cycling in the suboxic ocean. Science 348, 1127-1129.

Balistrieri, L. and Murray, J. (1982) The surface chemistry of δMnO_2 in major ion seawater. Geochim Cosmochim Ac 46, 1041-1052.

Banerjee, D. and Pal, S. (2008) Dynamics in the DNA recognition by DAPI: Exploration of the various binding modes. J Phys Chem B 112, 1016-1021.

Banerjee, S., Choudhury, U., Banerjee, R. and Mukhopadhyay, S. (2002) Kinetic and mechanistic studies on the oxidation of hydroxylamine by a tri-bridged manganese(IV,IV) dimer in weakly acidic media. J Chem Soc, Dalton Trans, 2047-2052.

Bargar, J., Webb, S. and Tebo, B. (2005) EXAFS, XANES and *in-situ* SR-XRD characterization of biogenic manganese oxides produced in seawater. Physica Scripta T115, 888-890.

Bari, S., Amorebieta, V., Gutiérrez, M., Olabe, J. and Doctorovich, F. (2010) Disproportionation of hydroxylamine by water-soluble iron(III) porphyrinate compounds. J Inorg Biochem 104, 30-36.

Barnese, K., Gralla, E., Valentine, J. and Cabelli, D. (2012) Biologically relevant mechanism for catalytic superoxide removal by simple manganese compounds. PNAS 109, 6892-6897.

Beman, J., Popp, B. and Alford, S. (2012) Quantification of ammonia oxidation rates and ammonia-oxidizing archaea and bacteria at high resolution in the Gulf of California and the eastern tropical North Pacific Ocean. Limnol Oceanogr 57, 711-726.

Bengtsson, G. (1973) A kinetic study of the reaction between iron(III) and hydroxylamine in strongly acid perchlorate solutions. Acta Chemica Scandinavica 27, 1717-1724.

Bengtsson, G., Fronaeus, S. and Bengtsson-Kloo, L. (2002) The kinetics and mechanism of oxidation of hydroxylamine by iron(III). J Chem Soc, Dalton Trans, 2548-2552.

Bernhard, A., Landry, Z., Blevins, A., de la Torre, J., Giblin, A. and Stahl, D. (2010) Abundance of ammonia-oxidizing archaea and bacteria along an estuarine salinity gradient in relation to potential nitrification rates. Appl Environ Microbiol 76, 1285-1289.

Blöthe, M., Wegorzewski, A., Müller, C., Simon, F., Kuhn, T. and Schippers, A. (2015) Manganese-cycling microbial communities inside deep-sea manganese nodules. Environ Sci Technol 49, 7692-7700.

Bonner, F., Dzelzkalns, L. and Bonucci, J. (1978) Properties of nitroxyl as intermediate in the nitric oxide-hydroxylamine reaction and in trioxodinitrate decomposition. Inorg Chem 17, 2487-2494.

Boogerd, F. and de Vrind, J. (1987) Manganese oxidation by *Leptothrix discophora*. J. Bacteriol. 169, 489-494.

Boone, D., Liu, Y., Zhao, Z.-J., Balkwill, D., Drake, G., Stevens, T. and Aldrich, H. (1995) *Bacillus infernus* sp. nov., an Fe(III)- and Mn(IV)-reducing anaerobe from the deep terrestrial subsurface. Intern J Sys Bacteriol 45, 441-448.

Boumaiza, H., Coustel, R., Despas, C., Ruby, C. and Bergaoui, L. (2018) Interaction of ammonium with birnessite: Evidence of a chemical and structural transformation in alkline aqueous medium. J Solid State Chem 258, 543-550.

Bouskill, N., Eveillard, D., Chien, D., Jayakumar, A. and Ward, B. (2012) Environmental factors determining ammonia-oxidizing organism distribution and diversity in marine environments. Environ Microbiol 14, 714-729.

Bräuer, S., Adams, C., Kranzler, K., Murphy, D., Xu, M., Zuber, P., Simon, H., Baptista, A. and Tebo, B. (2011) Culturable *Rhodobacter* and *Shewanella* species are abundant in estuarine turbidity maxima on the Columbia River. Environ Microbiol 13, 589-603.

Bremmer, J. (1997) Sources of nitrous oxide in soils. Nutrient Cycling in Agroecosystems 49, 7-16.

Bremmer, J., Blackmer, A. and Waring, S. (1980) Formation of nitrous oxide and dinitrogen by chemical decomposition of hydroxylamine in soils. Soil Biol Biochem 12, 263-269.

Brouwers, G., Corstjens, P., de Vrind, J., Verkammen, A., De Kuyper, M. and de Vrind-de Jong, E. (2000a) Stimulation of Mn^{2+} oxidation in *Leptothrix discophora* SS-1 by Cu^{2+} and sequence analysis of the region flanking the gene encoding putative multicopper oxidase MofA. Geomicrobio J 17, 25-33.

Brouwers, G., de Vrind, J., Corstjens, P., Cornelis, P., Baysse, C. and de Vrind-de Jong, E. (1999) *cumA*, a gene encoding a multicopper oxidase, is involved in Mn^{2+} oxidation in *Pseudomonas putida* GB-1. Appl Environ Microbiol 65, 1762-1768.

Brouwers, G., Vijgenboom, E., Corstjens, P., de Vrind, J. and de Vrind-de Jong, E. (2000b) Bacterial Mn^{2+} oxidizing systems and multicopper oxidases: An overview of mechanisms and functions. Geomicrobio J 17, 1-24.

Bruland, K., Orians, K. and Cowen, J. (1994) Reactive trace metals in the stratified central North Pacific. Geochem Cosmochim Ac 58, 3171-3182.

Brumsack, H.-J. (2006) The trace metal content of recent organic carbon-rich sediments: Implications for Cretaceous black shale formation. Palaeogeogr Palaeoclimatol Palaeoecol 232, 344-361.

Buchwald, C., Grabb, K., Hansel, C. and Wankel, S. (2016) Constraining the role of iron in environmental nitrogen transformations: Dual stable isotope systematics of abiotic NO_2^- reduction by Fe(II) and its production of N_2O. Geochem Cosmochim Ac 186, 1-12.

Burdige, D. and Nealson, K. (1986) Microbiological manganese reduction by enrichment cultures from coastal marine sediments. Appl Environ Microbiol 50, 491-497.

Butler, J. and Gordon, L. (1986) An improved gas chromatographic method for the measurement of hydroxylamine in marine and fresh waters. Marine Chemistry 19, 229-243.

Butler, J., Jones, R., Garber, J. and Gordon, L. (1987) Seasonal distribution and turnover of reduced trace gases and hydroxylamine in Yaquina Bay, Oregon. Geochem Cosmochim Ac 31, 697-706.

Butler, J., Pequegnat, J., Gordon, L. and Jones, R. (1988) Cycling of methane, carbon monoxide, nitrous oxide, and hydroxylamine in a meromictic, coastal lagoon. Estuarine, Coastal and Shelf Science 27, 181-203.

Bykov, D., Plog, M. and Neese, F. (2014) Heme-bound nitroxyl, hydroxylamine, and ammonia ligands as intermediates in the reaction cycle of cytochrome *c* nitrite reductase: a theoretical study. J Biol Inorg Chem 19, 97-112.

Canfield, D., Jørgensen, B., Fossing, G., Glud, R., Gundersen, J., Ramsing, N., Thamdrup, B., Hansen, J., Nielsen, L. and Hall, P. (1993a) Pathways of organic carbon oxidation in three continental margin sediments. Mar Geol 113, 27-40.

Canfield, D., Thamdrup, B. and Hansen, J. (1993b) The anaerobic degradation of organic matter in Danish Coastal sediments: Iron reduction, manganese reduction, and sulfate reduction. Geochim Coscmochim Acta 57, 3867-3885.

Caranto, J. and Lancaster, K. (2017) Nitric oxide is an obligate bacterial nitrification intermediate produced by hydroxylamine oxidoreductase. PNAS 114, 8217-8222.

Caranto, J., Vilbert, A. and Lancaster, K. (2016) *Nitrosomonas europaea* cytochrome P460 is a direct link between nitrification and nitrous oxide emission. PNAS 113, 14704-14709.

Cavazos, A., Taillefert, M., Yuanzhi, T. and Glass, J. (2018) Kinetics of nitrous oxide production via hydroxylamine decomposition by birnessite in seawater. Marine Chemistry 202, 49-57.

Clement, B., Luther, G. and Tebo, B. (2009) Rapid, oxygen-dependent microbial Mn(II) oxidation kinetics at sub-micromolar oxygen concentrations in the Black Sea suboxic zone. Geochem Cosmochim Ac 73, 1878-1889.

Cooper, J.N., Chilton, J.E. and Powell, R.E. (1970) Reaction of nitric oxide with alkaline hydroxylamine. Inorganic Chemistry 9, 2303-2304.

Corstjens, P., de Vrind, J., Goosen, T. and de Vrind-de Jong, E. (1997) Identification and molecular analysis of the *Leptothrix discophora* SS-1 *mofA* gene, a gene putatively encoding a manganese oxidizing protein with copper domains. Geomicrobio J 14, 91-108.

Cowen, J. and Silver, M. (1984) The association of iron and manganese with bacteria on marine microparticulate material. Science 224, 1340-1342.

Dalsgaard, T., Stewart, F., Thamdrup, B., De Brabandere, L., Revsbech, N., Ulloa, O., Canfield, D. and DeLong, E. (2014) Oxygen at nanomolar levels reversibly

suppresses process rates and gene expression in anammox and denitrification in the oxygen minimum zone off Northern Chile. American Society of Microbiology 5, e01966-01914.

Danilina, E. and Buskina, K. (2017) Kinetic spectrophotometric determination of hydroxylamine and nitrite ion in a mixture by their reactions with neutral red. Bull South Ural State Univ Chem Series 9, 5-13.

Davidson, E. and Kanter, D. (2014) Inventories and scenarios of nitrous oxide emissions. Environ Res Lett 9, 105012.

Davidson, E., Kanter, D., Suddick, E. and Suntharalingam, P. (2013) N_2O: Sources, inventories, projections, Drawing down N_2O to protect climate and the ozone layer: A UNEP Synthesis Report. United Nations Environment Programme, Nairobi, Kenya, pp. 9-15.

Davies, G. and Kustin, K. (1969) The stoichiometry and kinetics of manganese(III) reactions with hydroxylamine, O-methylhydroxylamine, and nitrous acid in acid perchlorate solution. Inorg Chem 8, 484-490.

de Vries, W., Du, E., Butterbach-Bahl, K., Schulte-Uebbing, L. and Dentener, F. (2016) Human nitrogen fixation and greenhouse gas emissions: a global assessment, 7th International Nitrogen Initiative 2016.

de Vrind, J., Brouwers, G., Corstjens, P., den Dulk, J. and de Vrind-de Jong, E. (1998) The cytochrome c mutation operon is involved in manganese oxidation in *Pseudomonas putida* GB-1. Appl Environ Microbiol 64, 3556-3562.

de Vrind, J., De Groot, A., Brouwers, G., Tommassen, J. and De Vrind-de Jong, E. (2003) Identification of a novel Gsp-related pathway required for secretion of the manganese-oxidizing facor of *Pseudomonas putida* strain GB-1. Molec Microbiol 47, 993-1006.

Deepa, B., Balasubramanian, N. and Nagaraja, K. (2004) Spectrophotometric determinaion of hydroxylamine and its derivatives in pharmaceuticals. Chem Pharm Bull 52, 1473-1475.

Devereux, R., Lehrter, J.C., Beddick Jr, D.L., Yates, D.F. and Jarvis, B.M. (2015) Manganese, iron, and sulfur cycling in Louisiana continental shelf sediments. Cont. Shelf Res. 99, 46-56.

DiChristina, T. (1992) Effects of nitrate and nitrite on dissimilatory iron reduction by *Shewanella putrefaciens* 200. J Bacteriol 174, 1891-1896.

Dick, G.J., Lee, Y.E. and Tebo, B.M. (2006) Manganese(II)-oxidizing *Bacillus* spores in Guaymas Basin hydrothermal sediments and plumes. Appl. Environ. Microbiol. 72, 3184-3190.

Dragan, A., Pavlovic, R., McGivney, J., Casas-Finet, J., Bishop, E., Strouse, R., Schenerman, M. and Geddes, C. (2012) SYBR Green I: Fluorescence properties and interaction with DNA. J. Fluoresc. 22, 1189-1199.

Ehrlich, H. (1976) Manganese as an energy source for bacteria, in: Nriagu, J. (Ed.), Environmental biogeochemistry. Ann Arbor Science Publication, Ann Arbor, MI, pp. 633-644.

Ehrlich, H. (1983) Manganese oxidizing bacteria from a hydrothermally active area on the Galapagos Rift. Bull Ecolog Soc Amer 35, 357-366.

Ehrlich, H. and Newman, D. (2008) Geomicrobiology, 5th ed. ed, New York, NY.

Ehrlich, H. and Salerno, J. (1990) Energy coupling in Mn^{2+} oxidation by a marine bacterium. Arch Microbiol 154, 12-17.

Eitel, E., Owings, S., Belli, K., Beckler, J., Williams, A., Fields, B., Brown, M., Craig, J., Studebaker, O., Nuzzio, D. and Taillefert, M. (2020) Variaitions in sediement production of dissolved iron across a continental margin not dominated by major upwelling or riverine inputs. Mar Chem.

Fehling, C. and Friedrichs, G. (2011) Dimerization of HNO in aqueous solution: An interplay of solvation effects, fast acid-base equilibria, and intramolecular hydrogen bonding? J Am Chem Soc 133, 17912-17922.

Feng, X., Li, W., Zhu, M. and Sparks, D. (2015) Advances in the Environmental Biogeochemistry of Manganese Oxides. American Chemical Society.

Fernandes, S., Javanaud, C., Aigle, A., Michotey, V., Guasco, S., Deborde, J., Deflandre, B., Anschutz, P. and Bonin, P. (2015) Anaerobic nitrification-denitrification mediated by Mn-oxides in meso-tidal sediments: Implications for N_2 and N_2O production. J Mar Syst 144, 1-8.

Fiadeiro, M., Solórzano, L. and Strickland, J. (1967) Hydroxylamine in seawater. Limnol Oceanogr 12, 555-556.

Ford, P., Wink, D. and Stanbury, D. (1993) Autoxidation kinetics of aqueous nitric oxide. Federation of European Biochemical Societies 326, 1-3.

Frame, C. and Casciotti, K. (2010) Biogeochemical controls and isotopic signatures of nitrous oxide production by a marine ammonia-oxidizing bacterium. Biogeosciences 7, 2695-2709.

Francis, C., Roberts, K., Beman, J., Santoro, A. and Oakley, B. (2005) Ubiquity and diversity of ammonia-oxidizing archaea in water columns and sediments of the ocean. PNAS 102, 14683–14688.

Francis, C.A. and Tebo, B.M. (2001) Enzymatic manganese (II) oxidation by a marine α-proteobacterium. Appl. Environ. Microbiol. 67, 4024-4029.

Frear, D. and Burrell, R. (1955) Spectrophotometric method for determining hydroxylamine reductase activity in higher plants. Analytical Chem 27, 1664-1665.

García-Rodledo, E., Corzo, A. and Papaspyrou, S. (2014) A fast and direct spectrophotometric method for the sequential determination of nitrate and nitrite at low concentrations in small volumes. Marine Chemistry 162, 30-36.

Gebhardt, S., Walter, S., Nausch, G. and Bange, H. (2004) Hydroxylamine (NH_2OH) in the Baltic Sea. Biogeosciences Discuss, EGU 1, 709-724.

George, M., Balasubramanian, N. and Nagaraja, K. (2007) Spectrophotometric determination of hydroxylamine and its derivatives in drug formulation using methyl red. Ind Jour Chem Tech 14, 412-416.

Geszvain, K., Smesrud, L. and Tebo, B. (2016) Identification of a third Mn(II) oxidase enzyme in *Pseudomonas putida* GB-1. Appl Environ Microbiol 82, 3774-3782.

Goreau, T., Kaplan, W., Wofsy, S., McElroy, M., Valois, F. and Watson, S. (1980) Production of NO_2^- and N_2O by nitrifying bacteria at reduced concentrations of oxygen. Appl Environ Microbiol 40, 525-532.

Grabb, K., Buchwald, C., Hansel, C. and Wankel, S. (2016) A dual nitrite isotopic investigation of chemodenitrification by mineral-associated Fe(II) and its production of nitrous oxide. Geochem Cosmochim Ac, http://dx.doi.org/10.1016/j.gca.2016.1010.1026.

Hansard, S., Easter, H. and Voelker, B. (2011) Rapid reaction of nanomolar Mn(II) with superoxide radical in seawater and simulated freshwater. Environ Sci Technol 45, 2811-2817.

Hansel, C. (2017) Manganese in marine microbiology, in: Poole, R. (Ed.), Advances in Microbial Physiology. Academic Press, pp. 37-83.

Hansel, C., Ferdelman, T. and Tebo, B. (2015) Cryptic cross-linkages among biogeochemical cycles: Novel insights from reactive intermediates. Elements 11, 409-414.

Hansel, C. and Francis, C. (2006) Coupled photochemical and enzymatic Mn(II) oxidation pathways of a planktonic *Roseobacter*-like bacterium. Appl Environ Microbiol 72, 3543-3549.

Hansel, C. and Learman, D. (2015) Geomicrobiology of manganese, in: Ehrlich, H., Newman, D., Kappler, A. (Eds.), Ehrlich's geomicrobiology. CRC Press, New York, NY, pp. 401-452.

Heil, J., Liu, S., Vereecken, H. and Brüggemann, N. (2015) Abiotic nitrous oxide production from hydroxylamine in soils and their dependence on soil properties. Soil Biol Biochem 84, 107-115.

Heil, J., Vereecken, H. and Brüggemann, N. (2016) A review of chemical reactions of nitrification intermediates and their role in nitrogen cycling and nitrogen trace gas formation in soil. European Journal of Soil Science 67, 23-39.

Hofer, C. and Schlosser, D. (1999) Novel enzymatic oxidation of Mn^{2+} to Mn^{3+} catalyzed by a fungal laccase. FEBS Let 451, 186-190.

Holland, K. and Walker, J. (1996) Crystal structure modeling of a highly disordered potassium birnessite. Clay Clay Miner 44, 744-748.

Hollibaugh, J., Gifford, S., Sharma, S., Bano, N. and Moran, M. (2011) Metatranscriptomic analysis of ammonia-oxidizing organisms in an estuarine bacterioplankton assemblage. ISME 5, 866-878.

Hooper, A., Arciero, D. and Hendrich, M. (2004) The oxidation of ammonia as an energy source in bacteria, in: Zannoni, D. (Ed.), Respiration in Archaea and Bacteria. Springer, Dordrecht, The Netherlands, pp. 121-147.

Hooper, A. and Terry, K. (1979) Hydroxylamine oxidoreductase of *Nitrosomonas* production of nitric oxide from hydroxylamine. Biochem Biophys Acta 571, 12-20.

Hui, L., Szeinbaum, N., DiChristina, T. and Taillefert, M. (2012) Microbial Mn(IV) reduction requires an initial one-electron reductive stabilization step. Geochim Coscmochim Acta 99, 179-192.

Hulth, S., Aller, R. and Gilbert, F. (1999) Coupled anoxic nitrification/manganese reduction in marine sediments. Geochim Cosmochim Ac 63, 49-66.

Hussain, M., Stedman, G. and Hughes, M. (1968) Kinetics and mechanism of the reaction between nitrous acid and hydroxylamine. Part III. The formation of hyponitrous acid. J Chem Soc B, 597-603.

Hynes, M., Wurm, K. and Moloney, A. (1993) Reduction of the bis(pentane-2,4-dionato)diaquo manganese(III) complex by hydroxylamine and L-ascorbic acid in aqueos solution. Inorg Chim Acta, 5-10.

IPCC (2007) Climate Change 2007: The physical science basis, in: Change, W.G.I.C.t.t.F.A.R.o.t.I.P.o.C. (Ed.), Cambridge.

IPCC (2014) Climate change 2014: Synthesis report. Contribution of Working Groups I, II and III to the fifth assessment report of the Intergovernmental Panel on Climate Change, in: Pachauri, R., Meyer, L. (Eds.). IPCC, Geneva, Switzerland.

Jackson, M., Han, T., Serbulea, L., Dutton, A., Ford, E., Miranda, K., Houk, K., Wink, D. and Fukuto, J. (2009) Kinetic feasibility of nitroxyl reduction by physiological reductants and biological implications. Free Radic Biol Med 47, 1130-1139.

Javanaud, C., Michotey, V., Guasco, S., Garcia, N., Anschutz, P., Canton, M. and Bonin, P. (2011) Anaerobic ammonium oxidation mediated by Mn-oxides: from sediment to strain level. Res Microbiol 162, 848-857.

Ji, Q., Babbin, A., Jayakumar, A., Oleynik, S. and Ward, B. (2015) Nitrous oxide production by nitrification and denitrification in the Eastern Tropical South Pacific oxygen minimum zone. Geophs Res Lett 42, 10755-10764.

Ji, Q., Buitenhuis, E., Suntharalingam, P., Sarmiento, J. and Ward, B. (2018) Global nitrous oxide production determined by oxygen sensitivity of nitrification and denitrification. Global Biogeochem Cy 32, 1790-1802.

Ji, Q. and Ward, B. (2017) Nitrous oxide production in surface waters of the mid-latitude North Atlantic Ocean. J Geophys Res: Oceans 122, 2612-2621.

Johnson, K., Gordon, R. and Coale, K. (1997) What controls dissolved iron concentrations in the world ocean? Mar Chem 57, 137-161.

Jones, M., Luther III, G., Mucci, A. and Tebo, B. (2019) Concentrations of reactive Mn(III)-L and MnO_2 in estuarine and marine waters determined using spectrophotometry and the leuco base, leucoberbelin blue. Talanta 200, 91-99.

Kampschreur, M.J., Kleerebezem, R., de Vet, W.W.J.M. and van Loosdrecht, M.C.M. (2011) Reduced iron induced nitric oxide and nitrous oxide emission. Water Research 45, 5945-5952.

Kartal, B., Maalcke, W., de Almeida, N., Cirpus, I., Gloerich, J., Geerts, W., Op den Camp, H., Harhangi, H., Janssen-Megens, E., Francoijs, K., Stunnenberg, H., Keltjens, J., Jetten, M. and Strous, M. (2011) Molecular mechansims of anaerobic ammonium oxidation. Nature 479, 127-132.

Kim, I.-N. (2018) Estimating "mean-state" July (1986-2007) N_2O fluxes in the Northern Gulf of Mexico hypoxic region: Variation, distribution, and implication. Front Marine Sci 5, 249.

Kitzinger, K., Padilla, C.C., Marchant, H.K., Hach, P.F., Herbold, C.W., Kidane, A.T., Könneke, M., Littmann, S., Mooshammer, M. and Niggemann, J. (2019) Cyanate and urea are substrates for nitrification by *Thaumarchaeota* in the marine environment. Nature Microbiol. 4, 234.

Klinkhammer, G. and Bender, M. (1980) The distribution of manganese in the Pacific Ocean. Earth Planet Science Letters 46, 361-384.

Koch, A. and Bange, H. (2013) Nitrite removal improves hydroxylamine analysis in aqueous solution by conversion with iron(III). Environ Chem 10, 64-71.

Komarov, A., Wink, D., Feelisch, M. and Schmidt, H. (2000) Electron-paramagnetic resonance spectroscopy using N-methyl-D-glucamine dithiocarbamate iron cannot discriminate between nitric oxide and nitroxyl: Implications for the detection of reaction products for nitric oxide synthase. Free Radic Biol Med 28, 739-742.

Korth, F., Koch, A., Arévalo-Martínez, D. and Bange, H. (2019) Hydroxylamine as a potential indicator of nitrification in the open ocean. Geophs Res Lett 46, 2158-2166.

Kostka, J., Luther, G. and Nealson, K. (1995) Chemical and biological reduction of Mn(III) pyrophosphate complexes: Potential importance of dissolved Mn(III) as an environmental oxidant. Geochim Coscmochim Acta 59, 885-894.

Kozlowski, J., Kits, K. and Stein, L. (2016a) Comparison of nitrogen oxide metabolism among diverse ammonia-oxidizing bacteria. Front Microbiol 7, 1090.

Kozlowski, J., Steiglmeier, M., Schleper, C., Klotz, M. and Stein, L. (2016b) Pathways and key intermediates required for obligate aerobic ammonia-dependent chemolithotrophy in bacteria and Thaumarchaeota. ISME, 1-10.

Kozlowski, J.A., Price, J. and Stein, L.Y. (2014) Revision of N_2O-producing pathways in the ammonia-oxidizing bacterium *Nitrosomonas europaea* ATCC 19718. Appl Environ Microbiol 80, 4930-4935.

Krumbein, W. (1971) Manganese oxidizing fungi & bacteria in recent shelf sediments of the Bay of Biscay and the North Sea. Naturwissenschaften 58, 56-57.

Krumbein, W. and Altmann, H. (1973) A new method for the detection and enumeration of manganese oxidizing and reducing microorganisms. Helgoländer wiss. Meeresunters. 25, 347-356.

Kuyper, M., Marchant, H. and Kartal, B. (2018) The microbial nitrogen-cycling network. Nat Reviews Microbio 16, 263-276.

Lam, P., Lee, J.-M., Heller, M., Mehic, S. and Xiang, Y. (2018) Size-fractionated distributions of suspended particle concentration and major phase composition from the U.S. GEOTRACES Eastern Pacific Zonal Transect (GP16). Mar Chem 201, 90-107.

Lam, P., Ohnemus, D. and Auro, M. (2015) Size-fractionated major particle composition and concentrations from the US GEOTRACES North Atlantic Zonal Transect. Deep-Sea Research II 116, 303-320.

Lancaster, K., Caranto, J., Majer, S. and Smith, M. (2018) Alternative bioenergy: Updates to and challenges in nitrification metalloenzymology. Joule 2, 421-441.

Latimer, W. (1952) The oxidation states of the elements and their potentials in aqueous solution, 2nd edn. Prentice-Hall, Englewood Cliffs.

Law, C.S. (2008) Predicting and monitoring the effects of large-scale ocean iron fertilization on marine trace gas emissions. Mar Ecol Prog Ser 364, 283-288.

Learman, D., Voelker, B., Madden, A. and Hansel, C. (2013) Constraints on superoxide mediated formation of manganese oxides. Front Microbiol 4, 262.

Learman, D., Voelker, B., Vasquez-Rodriguez, A. and Hansel, C. (2011a) Formation of manganese oxides by bacterially generated superoxide. Nat Geosci 4, 95-98.

Learman, D., Wankel, S., Webb, S., Martinez, N., Madden, A. and Hansel, C. (2011b) Coupled biotic-abiotic Mn(II) oxidation pathway mediates the formation and structural evolution of biogenic Mn oxides. Geochem Cosmochim Ac 75, 6048-6063.

Lee, Y. and Tebo, B. (1994) Cobalt(II) oxidation by the marine manganese(II)-oxidizing *Bacillus* sp. strain SG-1. Appl. Environ. Microbiol. 60, 2949-2957.

Lian, L. and Hunter, K. (1986) The dynamic balance of manganese transport and diagenesis in the Otago Harbour, New Zealand. Marine Chemistry 19, 175-192.

Lin, H. and Taillefert, M. (2014) Key geochemical factors regulating Mn(IV)-catalyzed anaerobic nitrification in coastal marine sediments. Geochem Cosmochim Ac 133, 17-33.

Liu, S., Berns, A., Vereecken, H., Wu, D. and Brüggemann, N. (2017a) Interactive effects of MnO_2, organic matter and pH on abiotic formation of N_2O from hydroxylamine in artificial soil mixtures. Scientific Reports 7, 39590.

Liu, S., Han, P., Hink, L., Prosser, J., Wagner, M. and Brüggemann, N. (2017b) Abiotic conversion of extracellular NH_2OH contributes to N_2O emission during ammonia oxidation. Environ Sci Technol 51, 13122-13132.

Liu, S., Herbst, M., Bol, R., Gottselig, N., Pütz, T., Weymann, D., Wiekenkamp, I., Vereecken, H. and Brüggemann, N. (2016) The contribution of hydroxylamine content to spatial variability of N_2O formation in soil of a Norway spruce forest. Geochim Cosmochim Ac 178, 76-86.

Liu, S., Vereecken, H. and Brüggemann, N. (2014) A highly sensitive method for the determination of hydroxylamine in soils. Geoderma 232-234, 117-122.

Löscher, C., Kock, A., Könneke, M., LaRoche, J., Bange, H. and Schmitz, R. (2012) Production of oceanic nitrous oxide by ammonia-oxidizing archaea. Biogeosciences 9, 2419-2429.

Lovley, D. (1991) Dissimilatory Fe(III) and Mn(IV) reduction. Microbiol Rev 55, 259-287.

Lovley, D., Giovannoni, S., White, D., Champine, J., Phillips, E., Gorby, Y. and Goodwin, S. (1993) *Geobacter metallireducens* gen. nov. sp. nov., a microogranism capable of couling the complete oxidation of organic compounds to the reduction of iron and other metals. Arch Microbiol 159, 336-344.

Lovley, D., Holmes, D. and Nevin, K. (2004) Dissimilatory Fe(III) and Mn(IV) reduction. Adv Microb Physiol 49, 219-286.

Lovley, D. and Phillips, E. (1988) Novel mode of microbial energy metabolism: Organic carbon oxidation coupled to dissimilatory reduction of iron and manganese. Appl Environ Microbiol 54, 1472-1480.

Lovley, D., Phillips, E. and Lonergan, D. (1989) Hydrogen and formate oxidation coupled to dissimilatory reduction of iron and manganese by *Alteromonas putrefaciens*. Appl Environ Microbiol 55, 700-706.

Lunau, M., Lemke, A., Walther, K., Martens-Habbena, W. and Simon, M. (2005) An improved method for counting bacteria from sediments and turbid environments by epifluorescence microscopy. Environmental Microbiology 7, 961-968.

Luther, G. (2010) The Role of one- and two-electron transfer reactions in forming thermodynamically unstable intermediates as barriers in multi-electron redox reactions. Aqua Geochem 16, 395-420.

Luther, G., Sundby, B., Lewis, B., Brendel, P. and Silverberg, N. (1997) Interactions of manganese with the nitrogen cycle: Alternative pathways to dinitrogen. Geochem Cosmochim Ac 61, 4043-4052.

Luther III, G. (2005) Manganese(II) oxidation and Mn(IV) reduction in the environment--Two one-electron transfer steps versus a singel two-electron step. Geomicrobio J 22, 195-203.

Luther III, G., de Chanvalon, A., Oldham, V., Estes, E., Tebo, B. and Madison, A. (2018) Reduction of manganese oxides: Thermodynamic, kinetic and mechanistic considerations for one- versus two-electron transfer steps. Aquatic Geochem, 1-21.

Ma, X., Bange, H., Eirund, G. and Arévalo-Martínez, D. (2018) Nitrous oxide and hydroxylamine measurements in the Southwest Indian Ocean. J Mar Syst, 103062.

Mallik, T. (1980) Macro- and micromorphology of some manganese nodules from the Indian Ocean. Marine Geology 34, M45-M56.

Mandernack, K. and Tebo, B. (1993) Manganese scavenging and oxidation at hydrothermal vents and in vent plumes. Geochim Coscmochim Acta 57, 3907-3923.

Martens-Habbena, W., Berube, P.M., Urakawa, H., De la Torre, J.R. and Stahl, D.A. (2009) Ammonia oxidation kintics determine niche separation of nitrifying Archaea and Bacteria. Nature 461, 976-981.

Martens-Habbena, W., Qin, W., Horak, R., Urakawa, H., Schauber, A., Moffett, J., Armburst, E., Ingalls, A., Devol, A. and Stahl, D. (2014) The production of nitric oxide by marine ammonia-oxidizing archaea and inhibition of archaeal ammonia oxidation by a nitric oxide scavenger. Environ Microbiol, 1-14.

Martí, M., Bari, S., Estrin, D. and Doctorovich, F. (2005) Discrimination of nitroxyl and nitric oxide by water-soluble Mn(III) porphyrins. J Am Chem Soc 127, 4680-4684.

Miyata, N., Maruo, K., Tani, Y., Tsuno, H., Seyama, H., Soma, M. and Iwahora, K. (2006a) Production of biogenic manganese oxides by anaorphic ascomycete fungi isolated from streambed pebbles. Geomicrobio J 23, 63-73.

Miyata, N., Tani, Y., Iwahora, K. and Soma, M. (2004) Enzymatic formation of manganese oxides by an *Acremonium*-like hyphomycete fungus, strain KR21-2. FEMS Microb Ecol 47, 101-109.

Miyata, N., Tani, Y., Maruo, K., Tsuno, H., Sakata, M. and Iwahora, K. (2006b) Manganese(IV) oxide production by *Acremonium* sp. strain KR21-2 and extracellular Mn(II) oxidase activity. Appl Environ Microbiol 72, 6467-6473.

Moews, P., Jr. and Audrieth, L. (1959) The autoxidation of hydroxylamine. J Inorg Nucl Chem 11, 242-246.

Moffett, J. (1997) The importance of microbial Mn oxidation in the upper ocean: A comparison of the Sargasso Sea and equatorial Pacific. Deep-Sea Res 44, 1277-1291.

Mogollón, J., Mewes, K. and Kasten, S. (2016) Quantifying manganese and nitrogen cycle coupling in manganese-rich, organic carbon-starved marine sediments: Examples from the Clarion-Clipperton fracture zone. Geophysical Research Letters 43, 7114-7123.

Moraghan, J. and Buresh, R. (1977) Chemical reduction of nitrite and nitrous oxide by ferrous iron. Soil Sci Soc Am J 41, 47-50.

Morel, F., Rueter, J., Anderson, D. and Guillard, R. (1979) Aquil: a chemically defined phytoplankton culture medium for trace metal studies. Journal of Phycology 15, 135-141.

Murray, J. (1974) The surface chemistry of hydrous manganese dioxide. Journ of Colloid and Interface Sci 46, 357-371.

Myers, C. and Nealson, K. (1988) Bacterial manganese reduciton and growth with manganese oxide as the sole electron acceptor. Science 240.

Nameroff, T., Balistrieri, L. and Murray, J. (2002) Suboxic trace metal geochemistry in the Eastern Tropical North Pacific. Geochim Coscmochim Acta 66, 1139-1158.

Naqvi, S.W.A., Jayakumar, D.A., Narvekar, P.V., Naik, H., Sarma, V.V.S.S., D'Souza, W., Joseph, S. and George, M.D. (2000) Increased marine production of N_2O due to intensifying anoxia on the Indian continental shelf. Nature 408, 346-349.

Nealson, K., Myers, C. and Wimpee, R. (1991) Isolation and identification of manganese-reducing bacteria and estimates of microbial Mn(IV)-reducing potential in the Black Sea. Deep-Sea Res 38, S907-S920.

Nealson, K. and Saffarini, D. (1994) Iron and manganese in anaerobic respiration: Environmental significance, physiology, regulation. Annu Rev Microbiol 49, 311-343.

Neretin, L., Pohl, C., Jost, G., Leipe, T. and Pollehne, F. (2003) Manganese cycling in the Gotland Deep, Baltic Sea. Marine Chemistry 82, 125-143.

Newell, S., Babbin, A., Jayakumar, A. and Ward, B. (2011) Ammonia oxidation rates and nitrification in the Arabian Sea. Global Biogeochem Cy 25, GB4016.

Nickel, M., Vandieken, V., Bruchert, V. and Jørgensen, B. (2008) Microbial Mn(IV) and Fe(III) reduction in northern Barents Sea sediments under different conditions of ice cover and organic carbon deposition. Deep-Sea Res II 55, 2390-2398.

Nitahara, S., Kato, S., Urabe, T., Usui, A. and Yamagishi, A. (2011) Molecular characterization of the microbial community in hydrogenetic ferromanganese crusts of the Takuyo-Daigo Seamount, northwest Pacific. FEMS Microbiol Lett 321, 121-129.

Nitahara, S., Kato, S., Usui, A., Urabe, T., Suzuki, K. and Yamagishi, A. (2017) Archaeal and bacterial communities in deep-sea hydrogenetic ferromanganese crusts on old seamounts of the northwestern Pacific. PLoS ONE 12, e0173071.

Oshiki, M., Ali, M., Shinyako-Hata, K., Satoh, H. and Okabe, S. (2016) Hydroxylamine-dependent anaerobic ammonium oxidation (anammox) by "*Candidatus* Brocadia sinica". Environ Microbiol 18, 3133-3143.

Ostrom, N., Sutka, R., Ostrom, P., Grandy, A., Huizinga, K., Gandhi, H., von Fischer, J. and Robertson, G. (2010) Isotopologue data reveal bacterial denitrification as the primary source of N_2O during a high flux event following cultivation of a native temperate grassland. Soil Biol Biochem 42, 499-506.

Overnell, J., Brand, T., Bourgeois, W. and Statham, P. (2002) Manganese dynmanics in the water column of the upper basin of Loc Etive, a Scottish fjord. Estuarine and Coastal Marine Science 55, 481-492.

Picardal, F. (2012) Abiotic and microbial interactions during anaerobic transformations of Fe(II) and NO_x^-. Front Microbiol 3, 112.

Poth, M. and Focht, D. (1985) ^{15}N Kinetic analysis of N_2O production by *Nitrosomonas europaea*: an examination of nitrifier denitrfication. Appl Environ Microbiol 49, 1134-1141.

Potter, R. and Rossman, G. (1979) The tetravalent maganese oxides: identification, hydration, and structural relationships by infrared spectroscopy. Am Mineral 64, 1199-1218.

Ravishankara, A., Daniel, J. and Portmann, R. (2009) Nitrous oxide (N_2O): The dominant ozone-depleting substance emitted in the 21st century. Science 326, 123-125.

Remucal, C. and Ginder-Vogel, M. (2014) A critical review of the reactivity of manganese oxides with organic contaminants. Environ Sci: Processes Impacts 16, 1247-1266.

Riley, J. (1953) The spectrophotometric determination of ammonia in natural waters with particular reference to sea-water. Anal Chim Acta 9, 575-589.

Rönner, U. and Sörensson, F. (1985) Denitrification rates in the low-oxygen waters of the stratified Baltic Proper. Appl Environ Microbiol 50, 801-806.

Rose, A. (2012) The influence of extracellular superoxide on iron redox chemistry and bioavailability to aquatic microorganisms. Front Microbiol 3, 124.

Rue, K., Rusevova, K., Biles, C. and Huling, S. (2018) Abiotic hdyroxylamine nitrification involving manganese- and iron-bearing minerals. Sci Total Environ 644, 567-575.

Salem, I. (1995) A kinetic study of the homogeneous oxidation of hydroxylamine by manganese(III)-*bis*(salicylaldimine) complexes. Transition Met Chem 20, 312-315.

Samuni, Y., Goldstein, S., Dean, O. and Berk, M. (2013) The chemistry and biological activities of N-acetylcysteine. Biochem Biophys Acta 1830, 4117-4129.

Santoro, A., Buchwald, C., McIlvin, M. and Casciotti, K. (2011) Isotopic signature of N_2O produced by marine ammonia-oxidizing archaea. Science 333, 1282-1285.

Schleper, C. and Hofer, C. (2002) Laccase-catalyzed oxidation of Mn^{2+} in the presence of natural Mn^{3+} chelators as a novel source of extracellular H_2O_2 production and its impact on manganese peroxidase. Appl Environ Microbiol 68, 3514-3521.

Schweiger, B., Hansen, H. and Bange, H. (2007) A time series of hydroxylamine (NH_2OH) in the southwestern Baltic Sea. Geophysical Research Letters 34.

Shafirovich, V. and Lymar, S. (2002) Nitroxyl and its anion in aqueous solutions: Spin states, protic equilibria, and reactivities toward oxygen and nitric oxide. PNAS 99, 7340-7345.

Shiller, A. and Gieskes, J. (1985) Particulate iron and manganese in the Santa Barbara Basin, California. Geochim Cosmochim Ac 49, 1239-1249.

Shiraishi, F., Mitsunobu, S., Suzuki, K., Hoshino, T., Morono, Y. and Inagaki, F. (2016) Dense microbial community on a ferromanganese nodule from the ultra-oligotrophic South Pacific Gyre: Implications for biogeochemical cycles. Earth Planet Sci Lett 447, 10-20.

Soler-Jofra, A., Stevens, B., Hoekstra, M., Picioreanu, C., Sorokin, D., van Loosdrecht, M. and Pérez, J. (2016) Importance of abiotic hydroxylamine conversion on nitrous oxide emissions during nitrification of reject water. Chem Eng J 287, 720-726.

Solórzano, L. (1969) Determination of ammonia in natural waters by the phenolhypochlorite method. Limnol Oceanogr 14, 799-801.

Soni, V. and Mehrotra, R. (2003) Kinetics and mechanism of oxidation of hydroxylamine by tetrachloroaurate(III) ion. Transition Met Chem 28, 893-898.

Spiro, T.G., Bargar, J.R., Sposito, G. and Tebo, B.M. (2009) Bacteriogenic manganese oxides. Acc. Chem. Res 43, 2-9.

Steiglmeier, M., Moosammer, M., Kitzler, B., Wanek, W., Zechmeister-Boltenstern, S., Richter, A. and Scleper, C. (2014) Aerobic nitrous oxide production through N-nitrosating hybrid formation in ammonia-oxidizing archaea. ISME J 8, 1135-1146.

Stein, L. (2011) Surveying N_2O-producting pathways in bacteria, in: Klotz, M.G. (Ed.), Methods in Enzymology. Elsevier, San Diego, USA, pp. 131-152.

Stein, L. (2019) Insights into the physiology of ammonia-oxidizing microorganisms. Curr Opin Chem Biol 49, 9-15.

Strickland, J. and Parsons, T. (1972) A practical handbook of seawater analysis.

Sunda, W. and Huntsman, S. (1994) Photoreduction of manganese oxides in seawater. Marine Chemistry 46, 133-152.

Sutherland, K., Wankel, S. and Hansel, C. (2018) Oxygen isotope analysis of bactreial and fungal manganese oxidation. Geobiol 16, 399-411.

Sutka, R.L., Ostrom, N.E., Ostrom, P.H., Breznak, J.A., Gandhi, H., Pitt, A.J. and Li, F. (2006) Distinguishing nitrous oxide production from nitrification and denitrification on the basis of isotopomer abundances. Appl Environ Microbiol 72, 638-644.

Takeda, M., Kawasaki, Y., Umezu, T., Shimura, S., Hasegawa, M. and Koizumi, J. (2012) Patterns of sheath elongation, cell proliferation, and manganese(II) oxidation in *Leptothrix cholodnii*. Arch Microbiol 194, 667-673.

Tebo, B. (1991) Manganese(II) oxidation in the suboxic zone of the Black Sea. Deep-Sea Research 38, 5883-5905.

Tebo, B. and Emerson, S. (1985) Effect of oxygen-tension, Mn(II) concentration, and teperature on the microbially catalyzed Mn(II) oxidation rate in a marine fjord. Appl Environ Microbiol 50, 1268-1273.

Tebo, B., Johnson, H., McCarthy, J. and Templeton, A. (2005) Geomicrobiology of manganese(II) oxidation. Trends Microbiol 13, 421-428.

Tebo, B., Nealson, K., Emerson, S. and Jacobs, L. (1984) Microbial mediation of Mn(II) and Co(II) precipitation at the O_2/H_2S interfaces in two anoxic fjords. Limnol Oceanogr 29, 1247-1258.

Templeton, A. and Knowles, E. (2009) Microbial transformations of minerals and metals: recent advances in geomicrobiology derived from synchrotron-based X-ray spectroscopy and X-ray microscopy. Annual Review of Earth and Planetary Sciences 37, 367-391.

Terada, A., Sugawara, S., Hojo, K., Takeuchi, Y., Riya, S., Harper, W., Yamamoto, T., Kuroiwa, M., Isobe, K., Katsuyama, C., Suwa, Y., Koba, K. and Hosomi, M. (2017) Hybrid nitrous oxide production from a partial nitrifying bioreactor: hydroxylamine interactions with nitrtite. Environ Sci Technol 51, 2748-2756.

Thamdrup, B. (2000) Bacterial manganese and iron reduction in aquatic sediments, in: Schink, B. (Ed.), Advances in microbial ecology. Springer, Boston, MA, pp. 41-84.

Thamdrup, B. and Dalsgaard, T. (2000) The fate of ammonium in anoxic manganese oxide-rich marine sediment. Geochimica et Coscmochimica Acta 64, 4157-4164.

Thamdrup, B., Rosselló-Mora, R. and Amann, R. (2000) Microbial manganese and sulfate reduction in Black Sea shelf sediments. Appl Environ Microbiol 66, 2888-2897.

Thanabalasingam, P. and Pickering, W.F. (1985) Sorption of mercury(II) by manganese(IV) oxide. Environmental Pollution Series B, Chemical and Physical 10, 115-128.

Thiel, G. (1925) Manganese precipitated by microorganisms. Econ Geol 20, 301-310.

Toner, B., Fakra, S., Villalobos, M., Warwick, T. and Sposito, G. (2005) Spatially resolved characterization of biogenic manganese oxide production within a bacterial biofilm. Appl Environ Microbiol 71, 1300-1310.

Trefry, J., Presley, B., Keeney-Kennicutt, W. and Trocine, R. (1984) Distribution and chemistry of manganese, iron, and suspended particulates in Orca Basin. Geo-Marine Letters 4, 125-130.

Tully, B. and Heidelberg, J. (2013) Microbial communities associated with ferromanganese nodules and the surrounding sediments. Front Microbiol 4, 161.

Turk, T. and Hollocher, T. (1992) Oxidation of dithiothreitol during turnover of nitric oxide redutase: Evidence for generation of nitroxyl with the enzyme from *Paracoccus denitrificans*. Biochem Biophys Research Comm 183, 983-988.

Twining, B., Rauschenberg, S., Morton, P. and Vogt, S. (2015) Metal contents of phytoplankton and labile particulate material in the North Atlantic Ocean. Prog Oceanogr 137, 261-283.

Vajrala, N., Martens- Habbena, W., Sayavedra-Soto, L., Schauer, A., Bottomley, P., Stahl, D. and Arp, D. (2013) Hydroxylamine as an intermediate in ammonia oxidation by globally abundant marine archaea. PNAS 110, 1006-1011.

Van Waasbergen, L., Hildebrand, M. and Tebo, B. (1996) Identification and characterization of a gene cluster involved in manganese oxidation by spores of the marine *Bacillus* sp. SG-1. J Bacteriol 178, 3517-3530.

Vandieken, V., Finke, N. and Thamdrup, B. (2014) Hydrogen, acetate, and lactate as electron donors for microbial manganese reduction in a manganese-rich coastal marine sediment. FEMS Microb Ecol 87, 733-745.

Vilbert, A., Caranto, J. and Lancaster, K. (2018) Influences of the heme-lysine crosslink in cytochrome P460 over redox catalysis and nitric oxide sensitivity. Chem Sci 9, 368-379.

Villalobos, M., Toner, B., Bargar, J. and Sposito, G. (2003) Characterization of the manganese oxide produced by *Pseudomonas putida* strain MnB1. Geochem Cosmochim Ac 67, 2649-2662.

von Breymann, M., de Angells, M. and Gordon, L. (1982) Gas chromatography with electron capture detection for determination of hydroxylamine in seawater. Anal Chem 54, 1209-1210.

Walker, C., de la Torre, J., Klotz, M., Urakawa, H., Pinel, N., Arp, D., Brochier-Armanet, C., Chain, P., Chan, P., Gollabgir, A., Hemp, J., Hügler, M., Karr, E., Könneke, M., Shin, M., Lawton, T., Lowe, T., Martens- Habbena, W., Sayavedra-Soto, L., Lang, D., Sievert, S., Rosenzweig, A., Manning, G. and Stahl, D. (2010) *Nitrosopumilus maritimus* genome reveals unique mechanisms for nitrification and autotrophy in globally distributed marine crenarchaea. PNAS 107, 8818-8823.

Wang, X., Gan, L., Wiens, M., Schloßmacher, U., Schröder, H. and Müller, W. (2012) Distribution of microfossils within polymetallic nodules: Biogenic clusters within manganese layers. Mar Biotechnol 14, 96-105.

Webb, S., Dick, G., Bargar, J. and Tebo, B. (2005a) Evidence for the presence of Mn(III) intermediates in the bacterial oxidation of Mn(II). PNAS 102, 5558-5563.

Webb, S., Tebo, B. and Bargar, J. (2005b) Structural characterization of biogenic Mn oxides produced in seawater by the marine *Bacillus* sp. strain SG-1. Am Mineral 90, 1342-1357.

Weiss, R. and Price, B. (1980) Nitrous oxide solubility in water and seawater. Marine Chemistry 8, 347-359.

Wrage, N., Velthof, G., van Beusichem, M. and Oenema, O. (2001) Role of nitrifier denitrification in the production of nitrous oxide. Soil Biology & Biochemistry 33, 1723-1732.

Xia, Y., Cardounel, A., Vanin, A. and Zweier, J. (2000) Electron paramagnetic resonance spectroscopy with N-methyl-D-glucamine dithiocarbamate iron complexes distinguishes nitric oxide and nitroxyl anion in a redox-dependent manner: Applications in identifying nitrogen monoxide products from nitric oxide synthase. Free Radic Biol Med 29, 793-797.

Yoshida, T. and Alexander, M. (1964) Hydroxylamine formation by *Nitrosomonas europaea*. Can J Microbiol 10, 923-926.

Zhou, Y., Toupin, M., Bélanger, D., Brousse, T. and Favier, F. (2006) Electrochemical preparation and characterization of birnessite-type layered manganese oxide films. J Phys Chem Solids 67, 1351-1354.

Zhu-Barker, X., Cavazos, A., Ostrom, N., Horwarth, W. and Glass, J. (2015) The importance of abiotic reactions for nitrous oxide production. Biogeochemistry 126, 251-267.

Zhu, X., Burger, M., Doane, T. and Horwarth, W. (2013) Ammonia oxidation pathways and nitrifier denitrification are significant sources of N_2O and NO under low oxygen availability. PNAS 110, 6328-6333.

Zhu, Y., Liang, X., Zhao, H., Yin, H., Liu, M., Liu, F. and Feng, X. (2017) Rapid determination of the Mn average oxidation state of Mn oxides with a novel two-step colorimetric method. Anal Methods 9, 103-109.